Chemical Science

ROYAL SOCIETY OF CHEMISTRY

REVIEW

View Article Online
View Journal | View Issue

Cite this: *Chem. Sci.*, 2026, **17**, 1423

Converting natural biopolymers to sustainable bioplastics *via* structure engineering

Xinlei Ji, [ab] Keyi Zhou,[a] My Ha Tran,[b] Xi Chen *[a] and Ning Yan *[bc]

Sustainable bioplastics have attracted considerable attention as alternatives to conventional petroleum-based plastics in response to growing concerns about resource depletion and environmental pollution. Natural biopolymers, such as starch, cellulose, and chitin/chitosan, are emerging as promising candidates for bioplastic production due to their widespread availability and biodegradability. This review conducts a comprehensive examination of recent advances in polymer-level structural engineering of natural biopolymers into bioplastics, with a focus on strategies that introduce intermolecular interactions, including permanent covalent bonds, dynamic covalent linkages, and noncovalent interactions, to reconstruct intrinsic hydrogen-bonded networks. This reconstruction provides the basis for converting natural biopolymers into bioplastics with permanent covalent, dynamic covalent, and physically crosslinked architectures, and the ways in which these architectures affect material properties, processability, and overall performance are systematically assessed. Additionally, the review discusses the direct utilization of raw lignocellulosic biomass as a potential approach to enhance the cost-effectiveness and scalability of bioplastic production. Finally, the challenges in developing high-performance bioplastics are examined, along with future perspectives for advancing bioplastics in alignment with circular economy principles and carbon neutrality objectives.

Received 30th September 2025
Accepted 23rd December 2025

DOI: 10.1039/d5sc07592k

rsc.li/chemical-science

1. Introduction

Plastics are indispensable and prevalent commodities which are important for our modern life.[1–6] It is estimated that annual plastic production will reach ~1.2 billion tons by 2060,[7] with essential applications[8–10] in packaging, construction, textiles, electronics, transportation, *etc.*, driven by the versatility, processability, durability and cost-effectiveness of plastic materials.[11–14] While the plastic industry has provided notable economic benefits and contributed to high standards of living, it has also raised critical environmental concerns,[15] including white pollution, resource depletion and global warming.[16–18] The conventional production of petroleum-derived plastics proceeds through a linear, fossil resource-intensive pathway (Scheme 1, top): crude oil is refined into naphtha, cracked into

[a]*State Key Laboratory of Green Papermaking and Resource Recycling, China-UK Low Carbon College, Shanghai Jiao Tong University, Shanghai 201306, China. E-mail: chenxi-lcc@sjtu.edu.cn*

[b]*Department of Chemical & Biomolecular Engineering, National University of Singapore, Singapore 117585, Singapore. E-mail: ning.yan@nus.edu.sg*

[c]*Centre for Hydrogen Innovations, National University of Singapore, Singapore 117580, Singapore*

Xinlei Ji

Xinlei Ji received her Bachelor's Degree from the China University of Petroleum (East China). She is currently a PhD candidate at Shanghai Jiao Tong University under the supervision of Prof. Xi Chen. She is also a visiting PhD student in Prof. Ning Yan's group at the National University of Singapore. Her research mainly focuses on biomass valorization into functional materials and high-value chemicals.

Keyi Zhou

Keyi Zhou is a graduate student at the China-UK Low Carbon College, Shanghai Jiao Tong University, under the supervision of Prof. Xi Chen. Her major is resources and the environment.

monomers, and polymerized into plastic products.[19–21] The production stage alone is estimated to account for ~3.8% of global greenhouse gas (GHG) emissions.[17] Post-consumer handling further exacerbates environmental burdens:[22–26] incineration contributes additional CO_2 and co-emitted toxic species, while landfilling perpetuates persistent white pollution and induces indirect GHG release associated with waste degradation.

To mitigate the climate impact of conventional plastic production, governments worldwide have implemented policy initiatives to promote bioplastics derived from renewable resources. Notable examples include the European Union's Circular Economy Action Plan,[27] Japan's Biomass Nippon Strategy,[28] and China's Plastic Pollution Control Policy.[29] Biomass resources such as agricultural wastes and oceanic wastes offer distinct advantages for bioplastic production due to their carbon neutrality, abundance, wide availability, and cost-effectiveness.[30–35]

My Ha Tran

My Ha Tran is a researcher specializing in biomass conversion and sustainable materials development. She obtained her PhD from the Department of Chemical Engineering, Kyung Hee University, in 2023. After a one-year postdoctoral stay there, she joined the National University of Singapore as a Research Fellow in Prof. Ning Yan's group. Her current research focuses on transforming low-value biomass and waste into value-added bioproducts, including biochemicals, bioplastics, functional biomaterials, and biocomposites for sustainable and circular manufacturing.

Xi Chen

Xi Chen received her Bachelor's (2010) and Master's (2012) degrees from Wuhan University in China. She then obtained her PhD in Chemical Engineering from the National University of Singapore under the supervision of Prof. Ning Yan in 2016, where she stayed as a postdoc. After that, she joined the China-UK Low Carbon College at Shanghai Jiao Tong University in 2018 and is now an Associate Professor. Her group focuses on the chemical utilizations of various waste resources including biomass, plastics and CO_2.

Generally, there are two main approaches to utilize these biomass feedstocks for bioplastic production: (1) the biomass resources are first converted into building block monomers and then re-polymerized into bioplastics[36–38] with new structures such as polylactic acid (PLA)[39] or identical structures to conventional ones such as bio-polyethylene terephthalate (PET);[40] (2) the macromolecular structures of biomass materials are largely preserved, which avoids the energy-intensive depolymerization of biomass into monomers and the subsequent repolymerization steps, thereby offering a reduced carbon footprint.[41–43] In this review, we mainly focus on the second strategy which converts natural resources into bioplastics through polymer-level structural engineering. Polymer-level structural engineering differs significantly from passive side-chain derivatizations or physical blending. It provides a more comprehensive design for network reconstruction to alter the original topology of the natural resources. For instance, it achieves this by transforming the native hydrogen-bonded matrix into tailored architectures through permanent covalent bonds, dynamic covalent linkages, or noncovalent interactions, to enable precise tuning of material characteristics. Consequently, this tailored network reconstruction (Scheme 1, down) may provide a more sustainable and structurally controllable pathway for developing bioplastics that can meet, or even surpass, the performance benchmarks of conventional plastics, compared to the fossil-based route.

Among various biomass feedstocks, starch has been successfully commercialized for bioplastic production, primarily because it is inexpensive and readily available.[44] Nevertheless, the material properties (such as the mechanical strength) require further improvement.[45] Non-edible biomass, especially cellulose, as the most abundant biomass on Earth derived from agricultural and forestry wastes, has shown exceptional promise and drawn considerable attention for bioplastic production with inherently higher mechanical strength and thermal stability.[46–49] Besides, chitin/chitosan from oceanic wastes (such as shrimp shells) sharing a similar skeleton of cellulose but bearing organonitrogen in the side chain, is also

Ning Yan

Ning Yan received his BSc and PhD degrees in chemistry from Peking University in China (supervisor: Prof. Yuan Kou). Then he joined the École Polytechnique Fédérale de Lausanne in Switzerland with a Marie Curie Fellowship (collaborator: Prof. Paul Dyson). After that, he worked in the Department of Chemical and Biomolecular Engineering at the National University of Singapore. His group focuses on the catalytic transformation of renewable resources and heterogeneous catalysis.

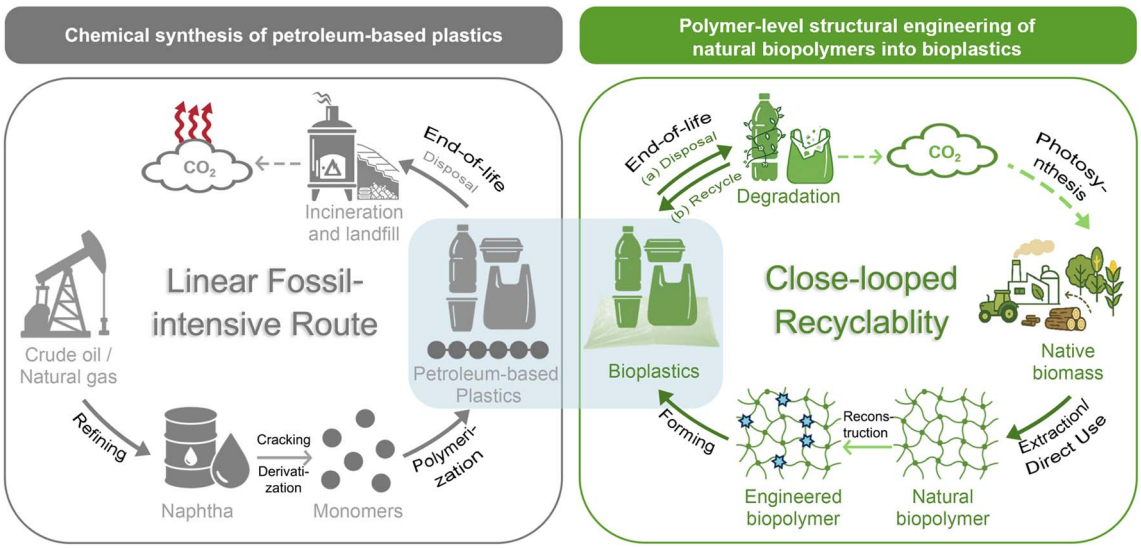

Scheme 1 Comparison of petroleum-based plastic synthesis and polymer-level structural engineering of natural biopolymers into bioplastics.

regarded as a potential alternative.[50] In particular, the amino groups in chitosan provide reactive sites for chemical modifications, enhancing its versatility.[51–53] Beyond single-component feedstocks, the direct valorization of raw lignocellulosic biomass (*e.g.*, corn stalk, eucalyptus, wood, bagasse, and peanut shells) has also been reported.[54–56] This could further reduce bioplastic production costs and facilitate large-scale production.

Recent efforts have been made by rational structure engineering at the polymer level to adjust and enhance the performances. In this review, progress over the past five years on the bioplastic production from key biomass resources including starch, cellulose, chitin/chitosan and raw lignocellulosic biomass through polymer-level structure engineering is summarized. Scheme 2 outlines the integrated valorization pathway: renewable plant- and animal-derived feedstocks (*e.g.*, agricultural crops, forestry residues, and crustacean shells) are used either as native matrices or fractionated to isolate natural biopolymers (starch, cellulose and chitin/chitosan) with hydrogen-bond-dominated architectures; through reconstruction of these native hydrogen-bonded networks *via* targeted modulation of interchain molecular interactions, the macromolecules acquire plasticity and functionality and are subsequently processed into bioplastics for diverse applications.

Excellent reviews on the depolymerization–repolymerization strategy,[57] life-cycle assessments[58,59] or with other focuses (such as chemical modifications, applications, *etc.*)[60,61] could be found elsewhere. In contrast, this review introduces and systemizes polymer-level structural engineering as a primary approach for developing advanced bioplastics. The review details the recent advances under this paradigm, focusing on how this engineering strategy is used to reconstruct natural biopolymers into sustainable bioplastics by forming permanent crosslinked networks, dynamic crosslinked networks, and physical crosslinked networks. Permanent crosslinked networks are constructed *via* irreversible covalent bonds (*e.g.*, ether, ester and amine bonds) between biopolymer chains (Scheme 3), imparting superior mechanical strength and chemical resistance but somehow sacrificing toughness, reprocessability and recyclability due to their stable crosslinking architecture. Dynamic crosslinked networks are achieved by reversible or exchangeable covalent bonds (*e.g.*, imine, hydroxyl ester and borate ester bonds) (Scheme 3) that can be cleaved and reformed in response to external stimuli (*e.g.*, temperature and pH),

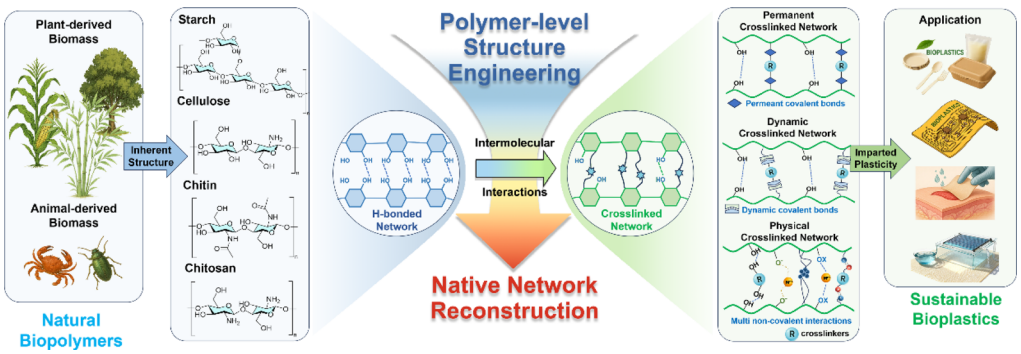

Scheme 2 An overview of polymer-level structural engineering in this review.

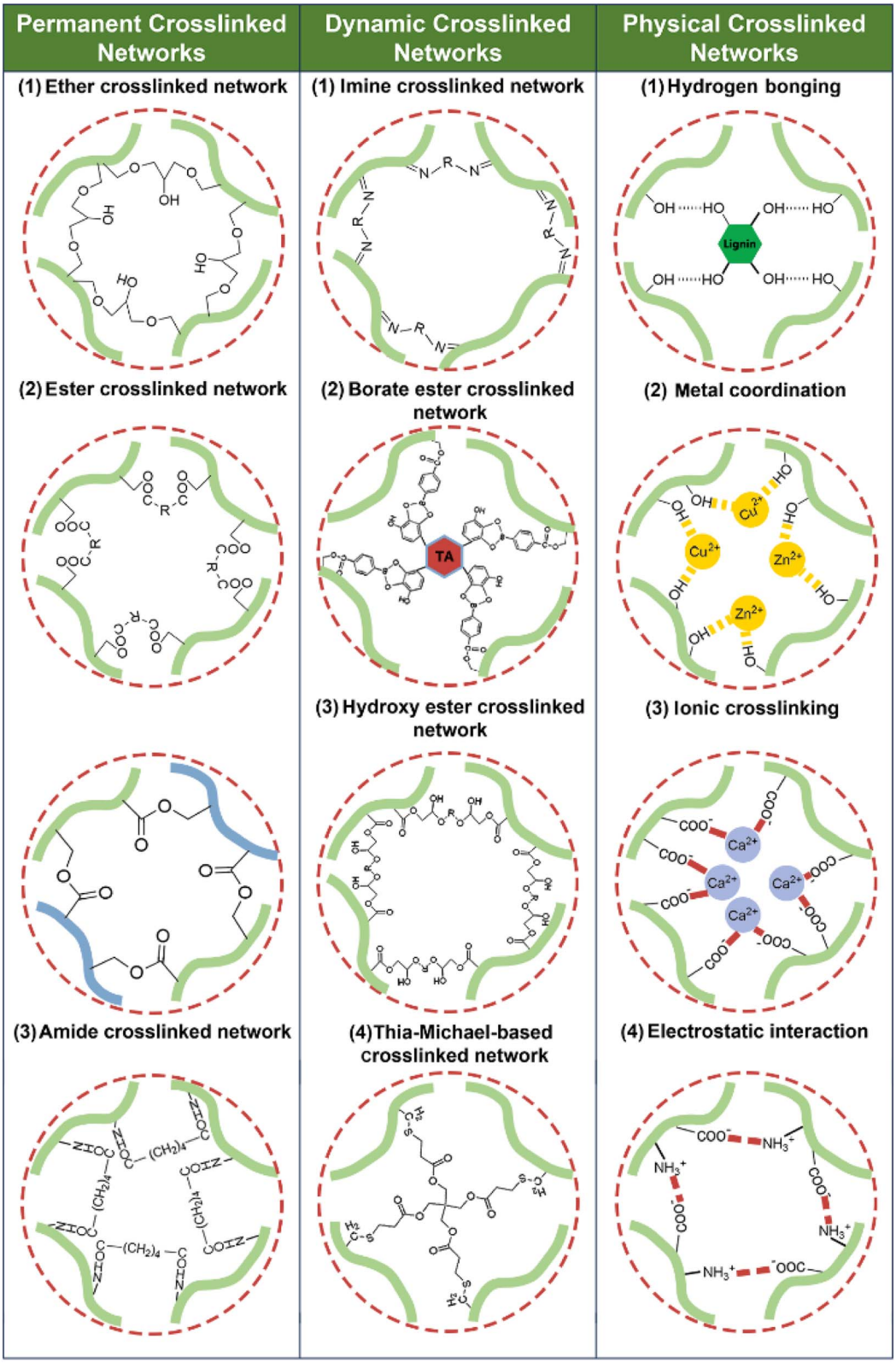

Scheme 3 Representative bonding modes of permanent, dynamic, and physical crosslinked bioplastic networks.

enabling tunable toughness and self-adaptive properties such as self-healing, weldability and reprocessability. However, they typically exhibit lower stability compared to permanent networks. Physical crosslinked networks are organized by non-covalent interactions (*e.g.*, hydrogen bonding, metal coordination, ionic crosslinking, and electrostatic interactions) (Scheme

3), affording low-energy processing, recyclability, tunable viscoelasticity, and sacrificial-bond toughening. On the down side, their strength and thermal-endurance ceilings are typically below those of covalent networks, and their properties are the most susceptible to environmental stimuli. According to the different network types, the relevant modification approaches will be described in detail to illustrate how the methods are designed and developed to adjust the network structures and correspondingly influence the material properties. The analysis of structure–property–function relationships is beneficial for purpose-oriented strategy development for bioplastic production. Besides, the challenges and future prospects for producing sustainable bioplastics from natural biopolymers are discussed at the end of the review.

2. Starch-based bioplastics

Starch is an abundant polysaccharide consisting of two distinct glucose polymers, the linear, helical-structured amylose and the branched amylopectin. Starch serves as the primary energy reserve in numerous photosynthetic organisms and represents a fundamental component of nutritional carbohydrates consumed by humans. Owing to its low cost and broad availability, thermoplastic starch (TPS) bioplastics have currently dominated the commercial bioplastic market.[44] In conventional processing, TPS materials are prepared by thermoforming native starch in the presence of plasticizers such as water, sorbitol, or glycerol.[62] However, they still suffer from critical problems such as insufficient mechanical strength, pronounced moisture sensitivity and retrogradation, a narrow thermal-processing window, and plasticizer migration, which limit broader adoption.

Against this background, various enhancement strategies have been explored. Given that starch is an edible resource with food-competing concerns, this review focuses specifically on the construction of dynamic crosslinked networks, arguably the most intensively investigated starch-structure engineering route recently, to exemplify how polymer-level structure engineering strategy addresses the corresponding technical challenges through network reconstruction, instead of providing a comprehensive account.

Chen *et al.* developed two fully bio-based hydroxyester (BHE) vitrimers by crosslinking epoxidized soybean oil (ESO) with acetylated starch succinate monoesters derived from amylose and amylopectin.[63] As shown in Fig. 1(a), starch was first esterified *via* acetylation and succinic mono-esterification to introduce carboxyl groups along the chains. ESO was then reacted with the modified starch to build a dynamical hydroxyester crosslinked network. The network comprised crosslinked domains and ESO-rich plasticized segments, with excess ESO chains serving as internal plasticizers. The resulting solids were hot-pressed at 130 °C to produce ABHE (from amylose) and PBHE (from amylopectin) films with uniform morphology and excellent ductility. PBHE (Table 1, entry 1), benefiting from the branched architecture of amylopectin, enabled a higher crosslinking density upon esterification, resulting in enhanced ductility with an elongation at break of 230%. In comparison, ABHE (Table 1, entry 2) showed an elongation at break of 140%, tensile strength of 0.9 MPa, and modulus of 1.2 MPa, reflecting the limited chain mobility of its linear amylose backbone. Both vitrimers displayed extremely lower glass transition temperatures (−5.88 °C for PBHE and −12.81 °C for ABHE) compared to traditional starch-based materials, attributed to internal plasticization from residual ESO segments, and showed good

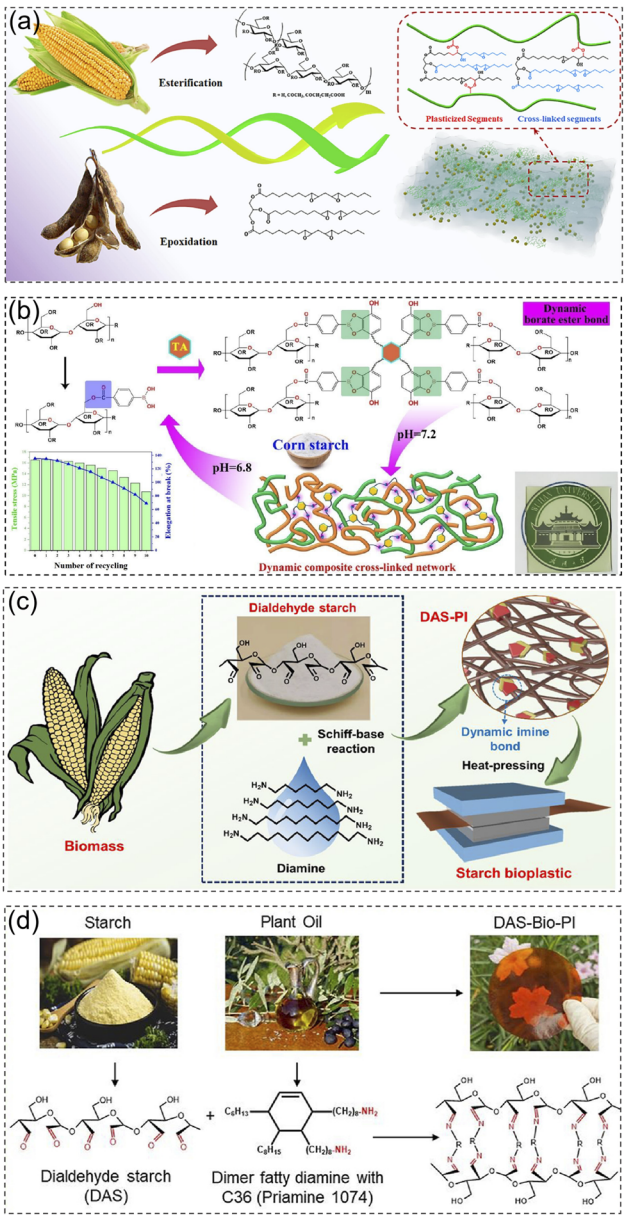

Fig. 1 (a) Construction of a dynamic hydroxyl ester crosslinked network to synthesize BHE vitrimers. Reprinted from ref. 63 with permission from Elsevier, copyright 2023. (b) Construction of a dynamic borate ester crosslinked network and its pH-responsive recyclability. Reprinted from ref. 64 with permission from Elsevier, copyright 2024. (c) Construction of a dynamic imine crosslinked network (DAS-PI) and processing into bioplastic *via* hot-pressing. Reprinted from ref. 65 with permission from American Chemical Society, copyright 2022. (d) Construction of a full bio-based dynamic imine crosslinked network (DAS-Bio-PI). Reproduced from ref. 66 with permission from Elsevier, copyright 2024.

Table 1 Dynamic crosslinked network construction, performance metrics, and practical demonstration of starch-based bioplastics[a]

Name	Network bonding type	Forming tech.	TS (MPa)	YM (MPa)	EB (%)	E_a (kJ mol^{-1})	T_g (°C)	T_{max} (°C)	WCA (°)	S	R/R	Practical potential	Ref.
PBHE	Hydroxyl ester bond	HP at 130 °C	1.8	6	230	78.1	−5.9	375	83	✓	✓	Rubber materials	63
ABHE		HP at 130 °C	0.9	1.2	140	60.27	−12.8	375	78	✓	✓		
CBT-1-2	Borate ester bond	Solution casting	16	N/A	135	N/A	N/A	∼300	78.8	N/A	✓	Recyclable materials	64
DAS-PI-C8	Imine bond	HP at 90 °C	40.6	1480	6.8	122.3	172	470	79.27	✓	✓	Packaging materials	65
DAS-Bio-PI	Imine bond	HP at 70 °C	5.4	21.5	45.2	23.9	20.2	466	109.2	✓	N/A	Petroleum-based plastic substitutes	66
DAS–TA	Imine bond	HP at 90 °C	44	1200	12	N/A	136.4	366	67.7	✓	N/A	Food & pharmaceutical packaging	67
DAS–YD	Imine bond	HP at 90 °C	26.7	220	16	49.9	73.9	356	76.8	N/A	✓		
DAS–DA-41%	Imine bond	HP at 110 °C	27.8	N/A	8.8	70.7	132.6	462	63	✓	✓	TPS & PLA plastic replacement	68

[a] HP: hot-pressing; TS: tensile strength; YS: Young's modulus; EB: elongation at break; E_a: activation energy of the bond exchange reaction; T_g: glass transition temperature from DMA; T_{max}: temperature at the maximum decomposition rate; WCA: water contact angle; S: self-healing; R/R: reprocessing/recycling.

solvent resistance in dimethyl sulfoxide (DMSO) at 25 and 80 °C, owing to the hydrophobic nature of ESO chains. PBHE demonstrated self-healing capability, with surface fracture marks repaired within 12 min at 140 °C. Furthermore, both vitrimers could be reprocessed by hot pressing at 130 °C for 15 min, retaining over 90% of their mechanical strength after three recycling cycles, underscoring their potential as sustainable and recyclable rubber materials.

Besides hydroxyl ester linkages, borate ester bonds have also been employed as reversible crosslinkers in starch-based materials. As illustrated in Fig. 1(b), 4-carboxyphenylboronic acid (CPBA) was grafted onto hydroxyethyl cellulose (HEC) to introduce boronic-acid groups. The modified HEC was then mixed with native corn starch and tannic acid (TA), and a dynamic borate ester crosslinked network was formed between boronic-acid moieties and *cis*-diols under mildly alkaline conditions. After solution casting, a corn starch/B-HEC/TA crosslinked film (CBT) was obtained.[64] The CBT-1-2 (Table 1, entry 3) film exhibited a tensile strength of 16 MPa, an elongation at break of 135% (9.5-fold increase compared to control starch films), and enhanced surface hydrophobicity (1.9-fold increase compared to control starch films). In addition, the catechol groups of TA imparted multifunctionality to the film, including antioxidant activity and UV-shielding ability. Notably, the dynamic borate ester network exhibited pH-dependent reversibility (Fig. 1(b)). Accordingly, the CBT films could be dissolved in weakly acidic water (pH 6.8) and re-casted at neutral pH (7.2), retaining over 94% of their original tensile strength after five recycling cycles.

Dynamic imine crosslinked networks have been fabricated through reversible Schiff-base reactions between aldehyde-functionalized starch and diamine crosslinkers in solution. As shown in Fig. 1(c), Wang's group established such networks within dialdehyde starch (DAS) by reacting it with a series of aliphatic diamines (C6–C12) in DMSO solvent.[65] The resulting starch-based polyimine (DAS-PI) networks exhibited excellent thermal malleability and could be readily heat-pressed into films at 90 °C without requiring any plasticizer. Mechanical properties of DAS-PI films were tunable *via* diamine chain length. Increasing the chain length led to reduced stiffness and enhanced ductility. Among the tested variants, DAS-PI-C8 (Table 1, entry 4) achieved the best strength–flexibility balance, with a tensile strength of 40.6 MPa, Young's modulus of 1.48 GPa, and elongation at break of 6.8%. Dynamic mechanical analysis (DMA) stress relaxation tests further demonstrated that the reversible nature of the imine bonds facilitated efficient stress dissipation, supporting heat-induced network rearrangement and self-healing. When subjected to 15 min of heat pressing, films with extensive surface damage could self-heal with high recovery rates (>90%) of the mechanical properties. The DAS-PI films also exhibited outstanding water and chemical resistance. Meanwhile, the materials show complete degradation under specific stimuli, such as 5% acetic acid (to promote C=N bond hydrolysis) or *via* transamination reactions with 1,8-octanediamine at 80 °C. To enhance ductility and sustainability, the same group developed a fully bio-based variant by introducing Priamine 1074 (a C36 dimer fatty diamine derived from plant oils) into the imine network, which reacted with DAS to yield a DAS-Bio-PI (Fig. 1(d)).[66] The resulting material could be easily processed into transparent, smooth films by hot pressing at 70 °C due to its depressed glass transition temperature (20.15 °C), wide thermal processing window (>230 °C before decomposition), and rapid stress relaxation dynamics (activation energy = 23.9 kJ mol^{-1}). Compared to DAS-PI films constructed with shorter-chain aliphatic diamines, DAS-Bio-PI (Table 1, entry 5) not only exhibited significantly enhanced flexibility with a tensile strength of 5.4 MPa, Young's modulus of 21.5 MPa, and elongation at break of 45.2%, but also demonstrated improved hydrophobicity (water contact angle of 109.2°), making it more suitable for packaging applications. Like its DAS-PI counterparts, the bio-based films retained key features of thermal self-healing and chemical

degradability. Upon mild heating, surface damage was fully repaired *via* imine bond exchange, while complete degradation could be achieved under acidic or amine-rich conditions.

To better understand the structure–property relationships in dynamic imine networks, Huang's group examined the effect of the diamine side-chain structure by comparing two crosslinkers: tris(2-aminoethyl)amine and a C12-functionalized hydrophobic diamine showing long alkyl side chains, for constructing DAS-based polyimine networks.[67] Their mechanical and water-resistance properties varied markedly due to differences in side-chain architecture. The introduction of long alkyl side chains in DAS–YD enhanced the flexibility and hydrophobicity of the polymer network. Compared to the DAS–TA (Table 1, entry 6) film, the DAS–YD (Table 1, entry 7) film demonstrated a more balanced mechanical profile, with a tensile strength of 26.7 MPa, Young's modulus of 220 MPa, and elongation at break of 16%. The C12 segment also reduced water uptake to 15.5% and improved foldability and dimensional stability under humid conditions. Following this study, Wang's group further investigated the influence of the starch oxidation degree on network formation by reacting DAS samples with varying aldehyde contents (15% to 80%) with 1,10-diaminodecane in water.[68] As the oxidation level increased, the molecular weight and crystallinity of DAS decreased markedly, resulting in shortened polymer chains and a transition from crystalline to amorphous structures. The mechanical performance, thermal stability, and environmental resistance of DAS–DA are highly dependent on the oxidation degree of the DAS. DAS with a moderate aldehyde content (41.1%) (Table 1, entry 8) yielded optimal film properties, in terms of mechanical strength, thermal stability and water/solvent resistance.

Overall, the above studies summarized in Table 1 demonstrate that polymer-level structural engineering, specifically the reconstruction into dynamic crosslinked networks, can markedly enhance the performance of starch-based materials. Converting starch into dynamic crosslinked networks increases tensile strength and, in particular, elongation at break by promoting more effective energy dissipation. It also increases chain mobility, thereby widening the processing window between glass transition temperature and thermal decomposition and reducing dependence on external plasticizers. Enhanced moisture resistance was frequently observed, attributed to the formation of dynamic crosslinked domains. In addition, dynamic bond exchange imparts stimuli-responsiveness and reprocessability. Among the reported dynamic crosslinked networks, hydroxyl ester and borate ester networks are exchangeable under mild conditions and highly compatible with the hydroxyl-rich starch backbone. They typically yield high flexibility (*e.g.*, PBHE achieved an elongation at break of 230%) but comparatively lower strength (<16 MPa). In contrast, imine-based networks provide broader structural tunability and robust mechanical properties; using DAS as a reactive matrix enables tensile strengths to reach ~40–44 MPa (*e.g.*, DAS–TA and DAS-PI-C8), while the diamine structure modulates flexibility and hydrophobicity. In terms of dynamic behavior, hydroxyl ester and imine networks support heat-induced bond exchange, allowing thermal self-healing and hot-press reprocessing even from ground powders. Borate ester networks provide complementary advantages through pH-triggered recyclability. Beyond the inherent biodegradability of starch feedstocks, imine networks are also chemically degradable under acidic or amine-rich conditions. Consequently, these findings indicate that careful selection of the dynamic bond type, crosslinker structure, and degree of starch modification allows fine-tuning of material performance, thereby expanding the application space of starch-derived bioplastics in packaging and engineering contexts.

3. Cellulose-based bioplastics

Cellulose, the most abundant biopolymer on Earth, comprises linear β(1→4)-linked D-glucose chains stabilized by extensive intra- and intermolecular hydrogen bonding.[69] This dense network endows cellulose with superior structural robustness[70] compared to starch for fabricating bioplastics with enhanced mechanical strength. Moreover, as cellulose is predominantly derived from agricultural residues (*e.g.*, straw and husks) and forestry byproducts, its utilization supports sustainability while avoiding competition with food supplies.[69,71,72] Nonetheless, the hydrogen bonding network that imparts rigidity and crystallinity also leads to inherent brittleness and poor thermal processability. To address these limitations, polymer-level structural engineering modulates the native hydrogen-bonded lattice and introduces additional intermolecular linkages to reconstruct cellulose into targeted network architectures. Implementations span permanent crosslinked networks, dynamic crosslinked networks, and physical crosslinked networks architectures; representative designs are detailed below.

3.1 Permanent crosslinked networks

Qian *et al.* developed a carboxymethyl cellulose (CMC)-based composite bioplastic (Table 2, entry 1) formed by citric acid (CA) crosslinking, along with 12 wt% walnut shell (WS) reinforcement and glycerol plasticization.[73] The CA-mediated covalent network had dual structural functions: (1) forming covalent ester bonds to disrupt excessive hydrogen bonding and increase chain mobility; (2) establishing multiple esterification and hydrogen bonding interactions with both CMC and WS. These modifications led to significant flexibility enhancement, including a 195% increase in elongation at break to 78% and a tensile strength of 18.53 MPa. Such bioplastics can have two end-of-life pathways: alkaline dissolution (pH ~ 13, 60 °C) enabled chemical recycling into new films, or soil burial led to complete biodegradation within 9 days. Building on bio-based diacids, Chen *et al.* employed maleic acid to fabricate chemically crosslinked cellulose films through a hydronium ion-triggered dissociation and esterification strategy in a mixed sulfuric acid/maleic acid aqueous solution.[74] The protons disrupted cellulose hydrogen bonding and enable rapid cellulose dissolution at 0 °C, while sulfuric acid catalyzed esterification between cellulose hydroxyls and maleic acid carboxyls. The synthesized MHA-0 film (Table 2, entry 2) exhibited optical transparency (~90%), and good tensile strength (~122 MPa),

Table 2 Permanent crosslinked network construction, performance metrics, and practical demonstration of cellulose-based bioplastics[a]

Name	Network bonding type	Forming tech.	TS (MPa)	YM (MPa)	EB (%)	T_{max} (°C)	WCA (°)	R/R	Practical potential (P)/application (A)	Ref.
CWGA-12	Ester bond	Solution casting	18.5	1.2	78	300	42	✓	P: disposable packaging & UV shielding	73
MHA-0	Ester bond	Solution casting	122	6120	5.2	N/A	91.6	N/A	P: packaging, mulch, and biomaterials	74
WCF–$TA_{0.4}$	Ester bond Ca^{2+} coordination	Solution casting	126	2600	20	280	99.7	N/A	A: food packaging	75
FPB2-30	Ether bond	Solution casting	58.2	1650	15	349	93.2	N/A	A: paper/plastic replacement	77
DCRC	Ether bond & hydrogen-bonding	HP at 110 °C	174	4400	33.9	340	62	✓	P: disposable tableware, degradable flexible devices & packing materials	76
TEMPO-CNF	Ether bond & Ca^{2+} coordination	Vacuum filtration	303	23 800	2.6	350	N/A	N/A	P: biodegradable packaging, flexible optoelectronics & lightweight automobiles	78

[a] CN: crosslinked network; HP: hot-pressing; TS: tensile strength; YS: Young's modulus; EB: elongation at break; T_{max}: temperature at maximum decomposition rate; WCA: water contact angle; R/R: reprocessing/recycling.

modulus (6120 MPa), and hydrophobicity (contact angle 91.6°). Besides, the material demonstrated good environmental compatibility, with 94.6% mass loss after six weeks in soil and 92% seed germination in degraded soil, making it promising for biodegradable transparent packaging application.

Thioctic acid offers multifunctional crosslinking through esterification with cellulose hydroxyls and concurrent disulfide-mediated ring-opening polymerization. Gao *et al.* dissolved softwood kraft pulp-derived cellulose in a $ZnCl_2/CaCl_2$ aqueous medium and introduced thioctic acid as a crosslinker *via* solution casting.[75] The WCF–$TA_{0.4}$ film (Table 2, entry 3) demonstrated superior performance to uncrosslinked controls: the tensile strength increased by 61.7%, elongation at break improved by 150%, the initial decomposition temperature increased by ~23 °C, and the water contact angle increased from 56.1° to 99.7°, along with remarkable solvent resistance after 30 days in various organic solvents. In packaging tests, these films reduced water evaporation from tomatoes, extending shelf life comparably to polyethylene.

Li *et al.* employed 1,4-butanediol diglycidyl ether (BDDE) as a crosslinker to initiate one-pot dissolution and co-crosslinking processes, where the $AlCl_3/ZnCl_2$ aqueous solution partially

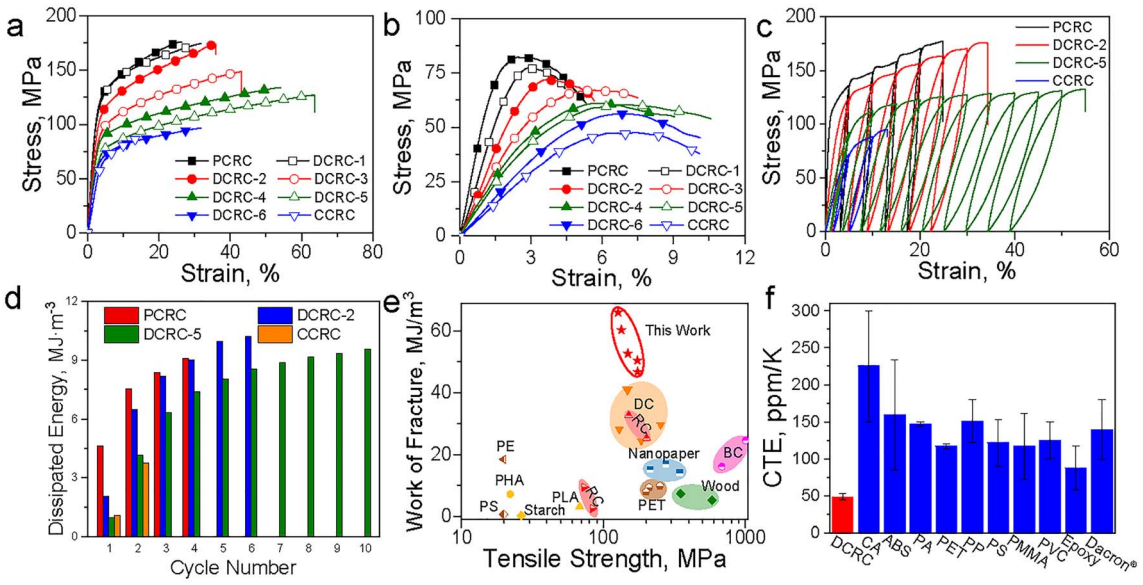

Fig. 2 Mechanical properties and thermal expansion of the DCRC. Representative tensile (a) and flexural (b) stress–strain curves of the samples with different ECH : AGU molar ratios at 58% RH. (c) Tensile stress–strain curves during loading–unloading cycles. (d) Dissipated energies of each loading–unloading cycle. (e) Comparison of the tensile strength and fracture work of the samples prepared in this study with those of the cellulose materials and common biobased plastics and synthetic polymer plastics reported previously. (f) Comparison of the CTE of the DCRC with those of the commonly used plastics. Reprinted from ref. 76 with permission from Elsevier, copyright 2021.

dissolved cellulose fibers and catalyzed the ether bond formation between BDDE epoxide rings and cellulose hydroxyls.[77] The resulting paper-derived plastics retained two types of intermolecular interactions including the covalent ether linkages and residual hydrogen bonding networks. Crosslinker content was pivotal. Excess BDDE suppressed effective dissolution and drives high crystallinity, while insufficient BDDE compromised the integrity of the microscale fiber skeleton. An optimal 2 wt% BDDE yielded FPB2-30 (Table 2, entry 4) films with outstanding wet/dry performance with the tensile strengths of 24.2 MPa (wet) and 58.2 MPa (dry). Ecologically, the films fully degraded within 21 days in soil without suppressing seed germination. Cai *et al.* further advanced the etherification-based strategy by designing hybrid networks of covalent scaffolds and secondary noncovalent interactions.[76] The dual-crosslinked cellulose hydrogels were prepared through epichlorohydrin (ECH) crosslinking coupled with ethanol-induced gelation, which was subsequently transformed into densified regenerated cellulose (DCRC) films (Table 2, entry 5) by planar hot pressing at 110 °C under different pressures (from 0.1 to 60 MPa). During this process, water removal promoted cellulose recrystallization and in-plane nanofibril alignment. Multimodal structural analyses resolved a well-defined dual-network architecture and anisotropic semicrystalline organization. The DCRC films delivered tunable mechanical performance dependent on the ECH : AGU molar ratio, achieving tensile strengths of 87–176 MPa, and flexural stresses of 48–82 MPa (Fig. 2(a and b)). As further revealed by the cyclic loading–unloading tests (Fig. 2(c)) and dissipated-energy analysis (Fig. 2(d)), the DCRC exhibited larger hysteresis loops and higher energy dissipation compared to its single-network physical (PCRC) or chemical (CCRC) counterparts. This behavior was consistent with the synergistic dual-network design, in which reversible hydrogen bonds acted as sacrificial domains to dissipate energy during deformation, while permanent covalent crosslinks preserved structural integrity. Consequently, as summarized in the Ashby plot (Fig. 2(e)), the DCRC achieved a work of fracture (34–62 MJ m^{-3}) that surpassed not only that of neat cellulose films but also that of commercial synthetic plastics such as PET and PLA. Moreover, the film demonstrated superior dimensional stability with a very low thermal expansion coefficient (CTE) of ~50 ppm K^{-1} (Fig. 2(f)). Additionally, the physical crosslinked hydrogen-bond network operated as a humidity-switchable "soft phase", leading to reversible remoldability in response to relative humidity (RH) adjustments by water-assisted 3D shaping without plasticizer addition or heating. The DCRC films are biocompatible (>95% cell viability) and completely biodegraded in soil within 52 days. Following a similar rationale, Lee *et al.* engineered dual-crosslinked TEMPO-cellulose nanofibril (CNF) films (Table 2, entry 6) *via* sequential covalent crosslinking and electrostatic interaction: robust permanent ether bonds were first formed among nanofibrils, followed by Ca^{2+}–carboxylate coordination introduced after wet-film formation.[78] The synergy between the covalent scaffold and ionic coordination yields exceptional performance (tensile strength of 303 MPa, Young's modulus of 23.8 GPa, thermal degradation onset at ~350 °C and water swelling suppression).

Across the above studies summarized in Table 2, permanent covalent crosslinking, whether by esterification (citric, maleic, and thioctic acids) or etherification (BDDE and ECH), significantly enhances structural integrity compared to native cellulose; for instance, maleic acid-crosslinked films achieved a robust tensile strength of 122 MPa, while functional crosslinkers like thioctic acid balanced a robust strength of 126 MPa with hydrophobicity (water contact angle of ~99.7°), introducing hydrophobic domains and strong solvent resistance. Crucially, the mechanical performance is further improved by "permanent + physical" dual-crosslinked network architectures. By integrating a robust permanent covalent scaffold (ether bonds) with a reversible physical network (sacrificial hydrogen bonds in DCRC or ionic Ca^{2+} coordination in TEMPO-CNF), these systems unlock efficient energy dissipation mechanisms, delivering tensile strengths of 174 MPa and 303 MPa, respectively.

3.2 Dynamic crosslinked networks

Dynamic imine networks are among the most widely explored dynamic crosslinked systems. Wang and Chen designed dynamic imine networks in cellulose plastics *via* two complementary pathways based on the Schiff base reaction.[79,80] In the "amine-first, aldehyde-second" strategy, tosylated cellulose was first aminated into amino-cellulose (AC), which was then crosslinked with terephthalaldehyde (TPA).[79] The incorporation of dynamic C=N bonds at the C6 position partially replaced hydrogen bonding and disrupted crystallinity, resulting in dense and dynamic networks with excellent thermal malleability, which allowed AC–TPA powders to be hot-pressed into smooth and flexible films at 100 °C. The film with a 1 : 1 aldehyde-to-amine molar ratio (Table 3, entry 1) showed optimal mechanical performance, achieving a tensile strength of 66.9 MPa but an elongation at break of 3.0%, attributed to the maximized imine linkage density and residual hydrogen bonding. In addition, the material displayed thermal stability, with a high glass transition temperature of 240 °C and an initial decomposition temperature near 300 °C. It also exhibited good waterproofing and strong chemical resistance in common organic solvents. In the "aldehyde-first" strategy, cellulose was oxidized by $NaIO_4$ into dialdehyde cellulose (DAC) and then crosslinked with a plant-derived diamine (Pramine).[80] Compared to the previous AC–TPA networks, DAC–Pramine networks exhibited accelerated imine bond exchange (bond exchange activation energies as low as 29.5–41.4 kJ mol^{-1}) and hydrogen bond dissociation, reducing the thermal processing temperature from 100 °C to 70 °C. The films (Table 3, entry 2) displayed tunable tensile strengths (3.0–33.5 MPa), Young's moduli (4.7–1320 MPa), elongation at break (2.5–108%), and toughness (43–321 kJ m^{-2}), depending on the oxidation degree and aldehyde/amine stoichiometry. DAC–Pramine systems also exhibited superior thermal stability above 400 °C, a CTE below 0.2 ppm K^{-1}, and good solvent resistance.

The same group further prepared vitrimeric cellulose polyimine networks by crosslinking DAC with aliphatic diamines (C6–C10). Heat-activated transamination promoted rapid imine

Table 3 Dynamic crosslinked network construction, performance metrics, and practical demonstration of cellulose-based bioplastics[a]

Bioplastics	Network bonding type	Forming tech.	TS (MPa)	YM (MPa)	EB (%)	E_a (kJ mol^{-1})	T_g (°C)	T_{max} (°C)	WCA (°)	S	R/R	Practical potential (P)/application (A)	Ref.
AC–TPA-1	Imine bond	HP at 100 °C	66.9	3000	3	74	240	350	82.3	✓	✓	P: paper & some traditional plastic replacement	79
Cellulosic plastic DS = 0.1–0.4	Imine bond	HP at 70 °C	3.0–33.5	4.7–1320	2.5–108	29.5–41.4	25–105	350–473	81–93	✓	✓	P: fossil-plastic replacement	80
Cel-PI-C6	Imine bond	HP at 70 °C	46.3	2900	2.2	84.8	192	N/A	N/A	✓	✓	P: cellulose-based plastic replacements	81
ALDC10	Imine bond	Solution casting	164.8	12 100	3.3	N/A	N/A	290	97.5	N/A	N/A	A: sustainable food packaging & photothermal applications	82
ACC-2	Acetals & hemiacetal bond	Thermal casting at 130 °C-5 h, 150 °C-1 h	35	N/A	10.5	115.6	124.4	313	N/A	✓	✓	P: petroleum-based plastic substitution	83
$DACNF_{0.2}$–$ESO_{0.8}$	Borate ester bond	Casting & HP at 85 °C	41	829	24.3	~39	101.3	N/A	92.1	✓	✓	A: flexible electronic substrates	84
H-HEC 1.0	Thia-Michael-based bond	HP at 140 °C	28.8	486.1	6.5	~119	135	360	101	N/A	N/A	P: petroleum-based plastic substitution	85
PDIGM(1)-*c*-AcCMC(1.2)	Ester bond	Twin-screw extruding at 130 °C	3.8	17.5	155	77.4	37.5	350	N/A	N/A	✓	P: 3D printing, insulating materials, shape memory materials	86

[a] HP: hot-pressing; TS: tensile strength; YS: Young's modulus; EB: elongation at break; E_a: activation energy of the bond exchange reaction; T_g: glass transition temperature from DMA; T_{max}: temperature at the maximum decomposition rate; WCA: water contact angle; S: self-healing; R/R: reprocessing/recycling.

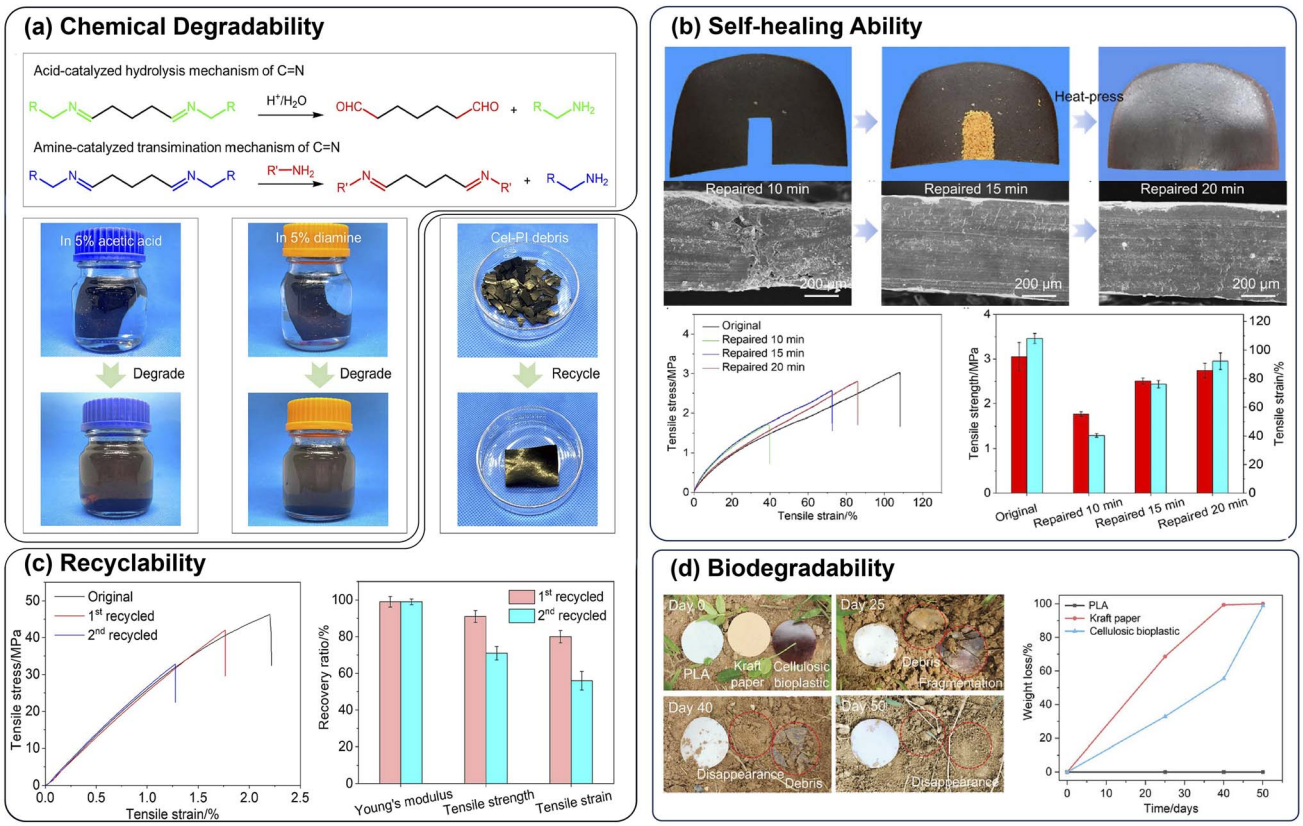

Fig. 3 The (a) chemical degradability, (b) self-healing ability, (c) recyclability and (d) biodegradability of dynamic imine crosslinked cellulosic bioplastics. Reproduced from ref. 79–81 with permission from American Chemical Society, Wiley-VCH and Elsevier, copyright 2023.

exchange, disrupting dense hydrogen-bonded structures into amorphous networks with enhanced chain mobility.[81] These vitrimers (denoted as Cel-PIs) exhibited efficient stress relaxation ($E_a \approx 84.8$ kJ mol^{-1} for Cel-PI-C6 (Table 3, entry 3)), tunable glass transition temperatures (192–153 °C), ultralow thermal expansion (0.1 ppm K^{-1} for Cel-PI-C6), and excellent solvent resistance. With increased diamine chain length, tensile strength and modulus decreased while ductility improved. Notably, beyond tunable mechanical, thermal, and solvent-resistant properties, dynamic imine chemistry also endows cellulose plastics with full lifecycle versatility. For service-life extension, as shown in Fig. 3(b), heat-activated imine exchange enables efficient self-healing, allowing fractured surfaces to be repaired with the retention of mechanical integrity. The material fragments can also be readily remolded into new films through simple hot-pressing for recycling (Fig. 3(c)). For end-of-life management, the chemical degradability of the C=N linkages is demonstrated by their selective cleavage in mildly acidic or amine-rich media (Fig. 3(a)). Finally, soil-burial tests verify environmental compatibility, indicating that the materials retain the inherent biodegradability of cellulose (Fig. 3(d)).

He *et al.* expanded imine chemistry into hybrid systems by combining DAC with aminated lignin (AL).[82] The positively charged AL crosslinked with DAC through dynamic imine bonds, while residual hydroxyl groups facilitated additional hydrogen bonding formation. The optimized ALDC10 (10 wt% AL) films (Table 3, entry 4) exhibited a superior tensile strength of 164.8 MPa and Young's modulus of 12.1 GPa. Beyond this mechanical robustness, the multifaceted advantages afforded by aminated lignin incorporation are highlighted in Fig. 4. Digital photographs (Fig. 4(a and b)) revealed that despite the lignin incorporation, the film retained high optical transparency and flexibility, overcoming the aggregation-induced opacity often observed in lignin composites. This hybrid film also showed improved water resistance (hydrophobicity) and barrier performance alongside UV shielding and antibacterial activity compared to pure cellulose controls (Fig. 4(c)). These multifunctional features translated into practical benefits. In food preservation tests, the ALDC10 films effectively suppressed oxidative browning (Fig. 4(d)) and significantly reduced moisture loss, limiting apple weight reduction to 0.1 g *versus* 0.3 g for the control (Fig. 4(f)). This improvement was attributed to the dense film structure and the tortuous path effect, which restrict the diffusion of water vapor and gases (Fig. 4(e)). In addition, the ALDC10 film exhibited a rapid temperature increase and high photothermal conversion efficiency under solar irradiation as shown in Fig. 4(g–i). When applied in a model indoor environment, the film restricted temperature increase to only 0.9 °C, whereas commercial glass led to a 2.8 °C increase (Fig. 4(j and k)). Such a performance demonstrated the potential of ALDC10 films for energy-efficient building and packaging applications.

Beyond imine-based networks, a diverse range of dynamic covalent chemistries has been employed including acetal/

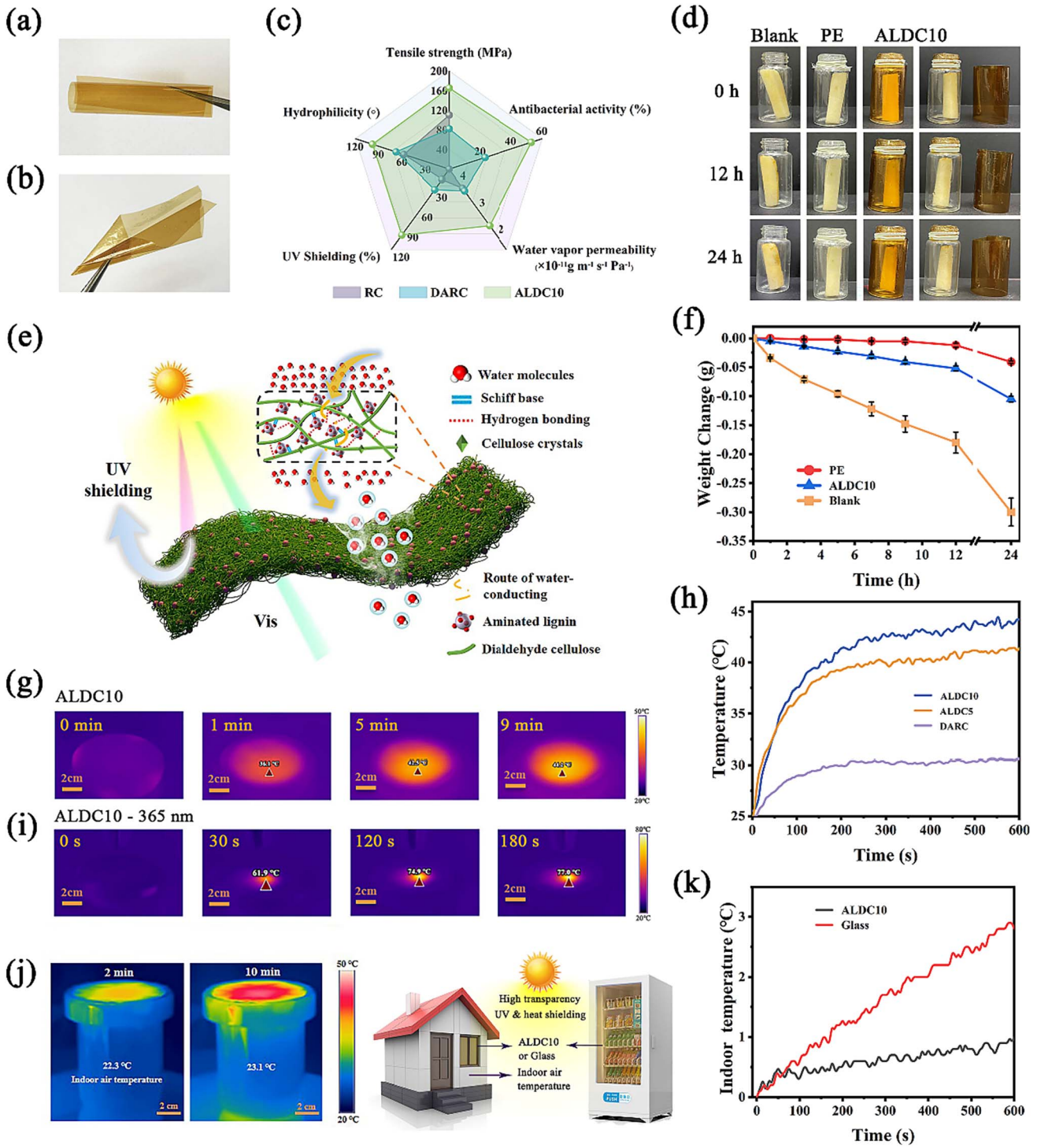

Fig. 4 Overall performance, food packaging and photothermal applications of ALDC10 bioplastics. Photos show the flexibility of ALDC10 films with (a) curly, (b) folding style, and (c) multifunctionality. (d) The color change of apple recorded at 0, 12 and 24 h, respectively, (e) Water vapor barrier and UV shielding. (f) Apple weight change over time, (g) Representative IR images of ALDC10 after exposure to simulated solar radiation (100 mW cm^{-2}) for 1, 5, and 9 min. (h) Temperature variation with time for DARC, ALDC5, and ALDC10. (i) Representative IR images of ALDC10 before UV irradiation and after UV irradiation for 30, 120, and 180 s with 40 mm distance between the membranes and the UV sources. (j) Experimental setup for measuring indoor air temperature with glass covered with ALDC10 film as ceiling and infrared images of coated glass irradiated under simulated solar irradiation (100 mW cm^{-2}) after 2 and 10 min. (k) Indoor air temperature change curves under simulated solar irradiation (100 mW cm^{-2}) with glass covered with ALDC10 film or glass as a ceiling. Reprinted from ref. 82 with permission from Elsevier, copyright 2024.

hemiacetal, borate ester, β-hydroxy ester, and thia-Michael linkages. Han *et al.* demonstrated the use of DAS as a renewable crosslinker to form dynamic acetal and hemiacetal bonds with hydroxypropyl cellulose (HPC) *via* condensation reactions.[83] Following thermal casting, the fully bio-based material ACC-2 (Table 3, entry 5) was obtained with a tensile strength of 35 MPa and elongation at break of 10.5%, while stress–relaxation analysis revealed an activation energy of 115.6 kJ mol^{-1}. These films could be reprocessed *via* hot-pressing at 150 °C. The acid-labile acetal bonds provided closed-loop recyclability: ACC-2 was completely degraded in 0.5 M H_2SO_4, regenerating DAS and HPC feedstocks. This study highlights the potential of acetal chemistry for combining bio-based feedstocks with dynamic recyclability. Targeting greater toughness and multifunctionality, Zhang *et al.* engineered boronic ester linkages by reacting phenylboronic acid-modified cellulose nanofibers (DACNF-B) with epoxidized soybean oil (ESO-B).[84] Following casting and hot-pressing at 85 °C, the $DACNF_{0.2}$–$ESO_{0.8}$ bioplastic (Table 3, entry 6) with "reinforced-concrete" architecture delivered enhanced tensile strength (∼41 MPa), Young's modulus (∼820 MPa), and ductility (elongation: ∼24%), coupled with good thermal stability (maintained integrity at 180 °C, CTE: 31 ppm K^{-1}) and waterproofness (contact angle: 92.1°). The borate ester bonds enabled ethanol/heat-triggered reversibility, yielding 95.4% welding strength retention *via* hot-pressing and near-complete mechanical recovery after five cycles. Moreover, it can be fully biodegraded in soil within 80 days. The films have been tested as food packaging and substrates for flexible electronic circuits, exhibiting high potential for market uses. Complementary to the above chemistries, Li *et al.* introduced dynamically reversible thia-Michael crosslinked networks by grafting acrylate groups onto HEC, followed by crosslinking with a thiol-based crosslinker.[85] The modified HEC could be processed into transparent films (H-HECs) at 140 °C (Table 3, entry 7). The general properties of the films include water hydrophobicity, mechanical robustness (tensile strength of 22–29 MPa, elongation at break of 6–11%, and Young's modulus of 457–626 MPa), and a toughness of 10–17 MJ m^{-3}. Besides, they also exhibited superior UV-shielding ability, shape memory and remolding capabilities.

To address the challenge of continuous processing, Li *et al.* introduced ester bonds into acetylated carboxymethyl cellulose (AcCMC) using poly(diglycidyl methacrylate) (PDIGM) under catalysis.[86] This approach enabled twin-screw extrusion to produce cellulose vitrimers continuously. The incorporation of entangled PDIGM chains provided enhanced chain mobility enabling melt-processability at 130 °C. The PDIGM(1)-*c*-AcCMC(1.2) formulation (Table 3, entry 8) exhibited toughness-dominated mechanical performance, achieving an elongation at break of 155% and a tensile strength of 3.8 MPa. Owing to the dynamic nature of β-hydroxy ester linkages, the material retained >90% of its properties after three reprocessing cycles and exhibited reliable shape-memory with a fixity ratio of 97% and recovery ratio of 89%.

As illustrated in Table 3, among dynamic crosslinked cellulose bioplastics, imine networks represent the most frequently reported network architectures. It offers a desirable combination of melt-processability, self-healing, and chemical recyclability, and medium to high mechanical strength. Two primary strategies dominate the design of these imine networks: the amine-first method, which introduces C=N linkages by reacting aminated cellulose with dialdehydes, and the aldehyde-first method, which constructs imine networks directly from dialdehyde cellulose through its reaction with multifunctional amines. By tuning strength–ductility *via* the crosslinker structure and crosslinking density, the materials with tensile strengths ranging from 3 to 67 MPa and elongations of 3–108% were achieved. The introduction of lignin to form a lignin–cellulose hybrid imine network further enhanced the mechanical strength to 165 MPa, alongside added UV-shielding and antibacterial properties. While other dynamic linkages generally exhibit comparatively lower mechanical strength (typically 28–41 MPa) relative to imine networks, they provide property profiles tailored for specific needs. For instance, acetal/hemiacetal and borate ester networks provide acid-triggered closed-loop recyclability, while borate esters additionally enable reversible welding and balance strength and ductility. Thia-Michael crosslinking imparts thermal flexibility and shape-memory capabilities, and hydroxy ester vitrimers stand out for their exceptional flexibility, achieving an elongation at break of 155%, enabling continuous processing *via* twin-screw extrusion. From these, the selection of bond type allows for precise optimization: imine networks are well suited for high-strength applications, while systems like hydroxy esters address the need for highly processable, flexible bioplastics.

3.3 Physical crosslinked networks

In contrast to permanent or dynamic crosslinked networks, which rely on covalent bond formation, physical crosslinked cellulose networks are assembled *via* reversible non-covalent interactions—including hydrogen bonding, hydrophobic association, ionic crosslinking, metal–ligand coordination, and electrostatic interactions—between cellulose chains (and external crosslinkers). Leveraging cellulose's hydroxyl-rich backbone, the construction of physical crosslinked networks either enables low-energy processing, water/solvent-assisted reprocessing, recycling, and stimuli-responsive behavior, or achieves enhanced mechanical and thermal properties, depending on the specific non-covalent interaction dominating and network design.

Hydrogen-bonding mediated hydroplastics (with hydrophobic modification). Hydrogen bonding is the predominant non-covalent interaction in cellulose-based bioplastics. Owing to cellulose's intrinsic hydrophilicity, water acts as a dynamic switch, reversibly disrupting and re-forming inter- and intrachain hydrogen bonds.[87] This water-mediated plasticization converts an otherwise rigid hydrogen-bonded network into a reconfigurable matrix in the hydrated state, affording temporary flexibility for shaping or programming, followed by fixation upon drying.[88] A hydroplastic herein denotes a biopolymer whose mechanical state and processability are reversibly governed by water content/activity rather than temperature alone: absorbed water transiently replaces native hydrogen-bonds and increases segmental mobility, whereas

Table 4 Physical crosslinked network construction, performance metrics, and practical demonstration of cellulose-based bioplastics[a]

Bioplastics	Network bonding type	Forming tech.	TS (MPa)	YM (MPa)	EB (%)	T_{max} (°C)	WCA (°)	W	R/R	Practical potential (P)/application (A)	Ref.
Cellulose hydro-plastic	Hydrogen-bonding	Solution casting	64.8	6830	20.3	N/A	82.27	N/A	✓	P: consumer items & structural-electronics	88
CCi	Hydrogen-bonding & hydrophobic association	Solution casting	92.4	2600	15.2	N/A	91	N/A	✓	N/A	89
TCel–Cu	Hydrogen-bonding & Cu^{2+} coordination	Filtration	118.2	5080	11	N/A	121.5	N/A	✓	P: soft robotics & adaptive camouflage, A: encrypted information carrier	90
C–$TA_{0.15}$	Hydrogen-bonding with TA	Solution casting	265	7640	31.9	N/A	N/A	✓	N/A	P: medical, food, & cosmetic fields	91
TA_1–MC	Hydrogen-bonding with TA	HP at 80 °C	109.6	3100	7	N/A	52.9	✓	✓	A: substrate for flexible printed circuit boards	92
CNC/H-lignin	Hydrogen-bonding with lignin	Solution casting	32.5	9440	1	215.9	N/A	N/A	N/A	P: food packaging	93
Lignin–cellulose	Hydrogen-bonding with lignin	HP at 100–130 °C	200	10 000	1.3	453	N/A	N/A	N/A	A: substrate for flexible integrated circuit boards	94
BC/PMO-20	Hydrogen-bonding with a secondary network	Solution casting	442	11 000	9.21	430	15.19	N/A	N/A	A: ITO sputtering	95
HDBP	Hydrogen-bonding with a secondary network	Casting & HP at 70 °C	193	7000	3.3	N/A	N/A	N/A	N/A	P: packaging and coatings	96
LDBP			66	4000	32.5	N/A	N/A	N/A	N/A		
CTCaBP-2	Hydrogen bonding, ionic crosslinking & Ca^{2+} coordination	Solution casting	114	N/A	6.5	260	N/A	✓	N/A	P: lightweight & high-strength structural materials	97
Ca–CNF/LMNP1	Hydrogen bonding & ionic crosslinking	Vacuum filtration	223.8	N/A	4	350	72.5	N/A	N/A	P/A: substrate for electronic fields	98
CMF-based bioplastic	Ester bond, Al^{3+} coordination & electrostatic interactions	Papermaking process	158	N/A	N/A	310	75	N/A	✓	P: packaging material	100

[a] HP: hot-pressing; TS: tensile strength; YS: Young's modulus; EB: elongation at break; T_{max}: temperature at the maximum decomposition rate; WCA: water contact angle; W: welding; R/R: reprocessing/recycling.

dehydration restores the hydrogen-bond network and stiffness.[89] Operationally, hydroplastic behavior entails a tunable "hydration window," reversibility over wet–dry cycles, and water-enabled forming/reshaping, analogous to thermoplastic softening across thermal transitions, but with water activity as the control variable. Koh *et al.* reported cellulose hydroplastics (Table 4, entry 1) by deacetylating solution-cast cellulose acetate films to produce highly amorphous cellulose, which exhibited reversible wet–dry transitions.[88] In the hydrated state, water molecules formed extensive hydrogen bonds with cellulose chains and one another, disrupting native inter- and intra-chain hydrogen bonding networks. At a critical water content (45%), percolated hydrogen-bonded water clusters emerged, dramatically enhancing chain mobility. The hydrated films exhibited a tensile strength of 21.3 MPa, modulus of 28.1 MPa, and elongation at break of 121.4% (Fig. 5(a)), indicating high flexibility and ductility and can be programmed into various desired 2D/3D shapes, followed by ambient drying (~60% RH) to yield a rigid structure within 24 min. In the dry state (water content = 10%), the material displayed significantly improved mechanical strength with a tensile strength of 64.8 MPa, modulus of 6.8 GPa, and elongation at break of 20.3% (Fig. 5(a)). The films maintained structural integrity over 20 wet–dry cycles, remained stable at 90% RH, and were biodegradable *via* enzymatic hydrolysis. To expand its utility, functionalization with conductive carbon black enabled 3D printing of LED displays and resistive sensors, demonstrating the potential of hydroplastic cellulose for sustainable electronics.

To overcome the limitation of compromised mechanical stability of hydrophilic cellulose-based bioplastics, hydrophobic modifications have been usually employed to introduce hydrophobic moieties or coordination domains into hydrophobic cellulose matrices, thereby balancing hydrophilic and hydrophobic properties. Zhang *et al.* grafted hydrophobic cinnamoyl moieties onto cellulose chains to produce cellulose cinnamate (CCi) membranes *via* solvent casting.[89] The CCi membranes (Table 4, entry 2) balanced mechanical strength and ductility, achieving a tensile strength of 92.4 MPa, modulus of 2.6 GPa, elongation at break of 15.2%, and fracture energy of 11.9 MJ m^{-3}. Importantly, they exhibited hydrosetting shape programmability: the membranes softened upon water immersion (5 min) and could be reshaped into complex and long-term stable 2D/3D structures upon air drying (10–30 min) (Fig. 5(b)). Reprogramming was feasible for at least 15 cycles with maintained tensile strength and modulus (Fig. 5(b)). Zeng *et al.* advanced amphiphilic hydroplastics by converting TEMPO-oxidized cellulose (TCel) into TCel–Cu membranes *via* a Cu^{2+}-coordinated mercerization process.[90] The resulting membranes (Table 4, entry 3) exhibited a dual-phase structure, where Cu^{2+}-crosslinked hydrophobic domains acted as rigid net points, while the hydrophilic interior retained reversible hydrogen-bonded domains functioning as dynamic switches (Fig. 5(c)), to enable both robustness and stimuli-responsiveness. They displayed exceptional mechanical strength in dry (118.2 MPa, modulus 5.08 GPa) and wet states (94.9 MPa, modulus 3.50 GPa). Along with the water-responsive and hydrosetting behavior, the material showed a unique shape memory behavior, which presumably arises from the synergy of water-mediated hydrogen-bond rearrangements and the entropic elasticity provided by Cu^{2+} coordination, demonstrating potential in encrypted information carriers (Fig. 5(c)).

Hydrogen-bonding with supramolecular donors. Supramolecular reinforcement through external hydrogen-bond donors has also been used to solve the problem of compromised mechanical stability. Owing to the abundance of hydroxyl groups along its backbone, cellulose readily interacts with polyphenols, polyhydroxyl compounds, or polymeric binders to form dense polymer networks. Consequently, the introduction of these external donors establishes multivalent and reversible

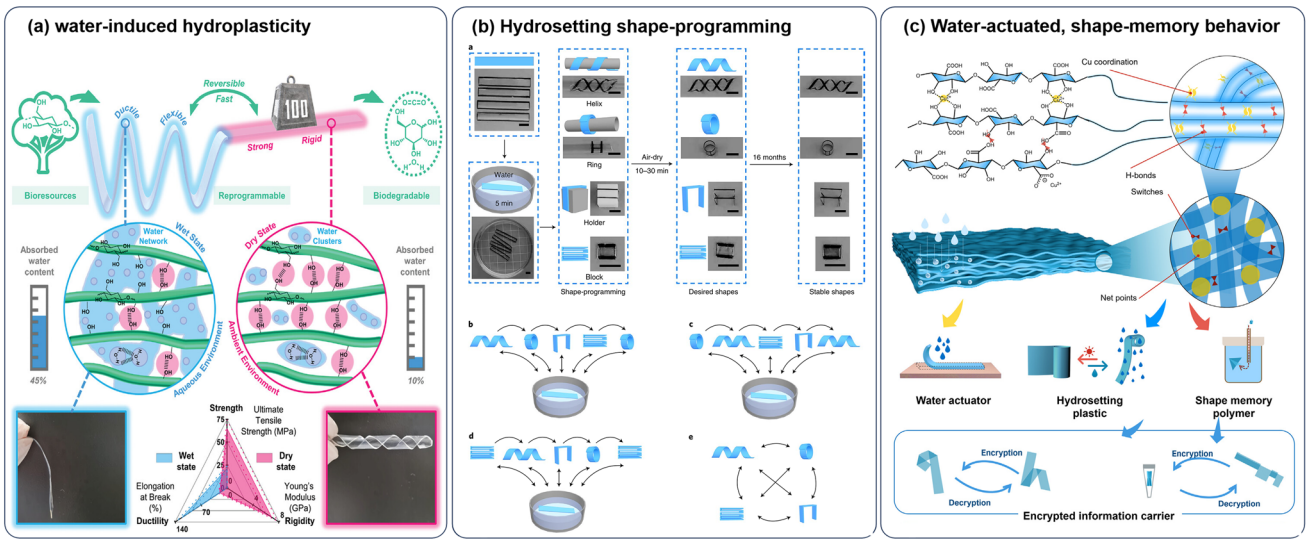

Fig. 5 (a) Overview of cellulose hydroplastics: water-induced hydroplasticity. (b) Sustainable and highly facile hydrosetting shape-programming of CCi membranes. (c) Tuning water–cellulose interactions for developing water-actuated, shape-memory cellulosic hydroplastics with potential applications as encrypted information carriers. Reprinted from ref. 88–90 with permission from Wiley-VCH, Springer Nature and Elsevier, copyright 2024, 2021 and 2024.

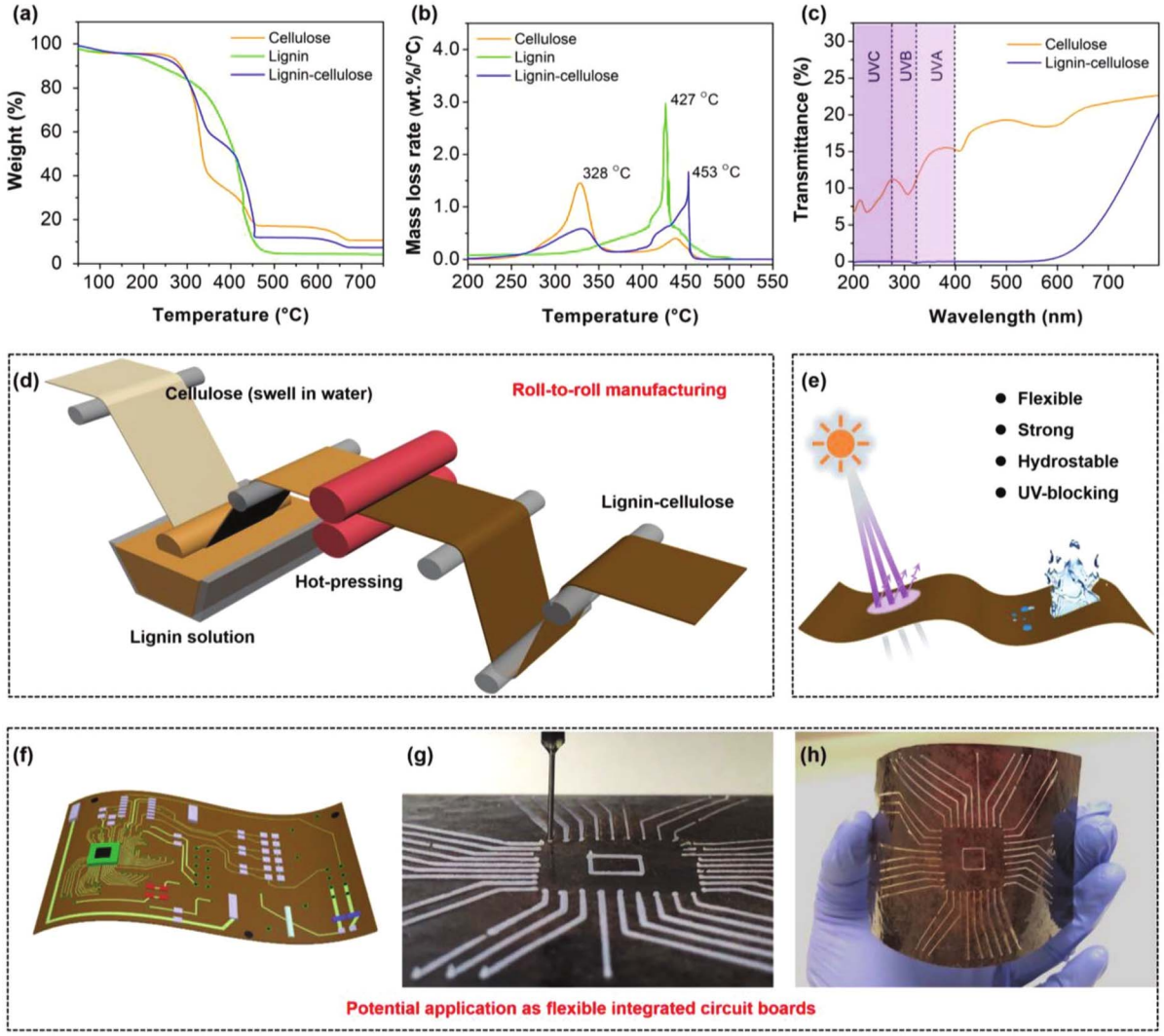

Fig. 6 The (a) weight loss and (b) mass loss rate of the cellulose paper, lignin, and lignin–cellulose. (c) UV transmittance curves of the cellulose paper and lignin–cellulose. Lignin–cellulose shows excellent UV-blocking performance. (d) Schematic showing the potential roll-to-roll fabrication of lignin–cellulose based on the processes of pulping and papermaking. (e) Schematic of the outstanding properties of the lignin–cellulose composite. (f) Schematic of the potential application of lignin–cellulose as a substrate for flexible integrated circuit boards. (g) Digital image of a 3D printed circuit (conductivity polymer with silver paste) on lignin–cellulose. (h) Lignin–cellulose featuring a printed circuit shows outstanding flexibility. Reprinted from ref. 94 with permission from WILEY-VCH, copyright 2020.

hydrogen-bonding interactions that not only enhance mechanical robustness and thermal/water resistance, but also provide reprocessability and energy-dissipative mechanisms. The Sun group reported the fabrication of fully bio-based supramolecular plastics by complexing regenerated cellulose with TA.[91] In this study, cellulose was dissolved in LiCl/DMAc with the addition of TA at various mass ratios to obtain yellowish transparent and flexible C–TA films after casting and drying. The optimized formulation containing 15 wt% TA (C–$TA_{0.15}$) (Table 4, entry 4) achieved remarkable mechanical properties, with a tensile strength of ~265 MPa, Young's modulus of 7.6 GPa, strain at break of ~31.9% and toughness of ~55 MJ m^{-3}. Importantly, the C–$TA_{0.15}$ bioplastic retained high strength under humid conditions (~166 MPa at 80% RH and ~98 MPa at 100% RH after seven days) and maintained the mechanical properties after immersion in water for 48 h. The material also exhibited good thermal resistance, reprocessability, biodegradability and biocompatibility. Molecular dynamics simulations revealed that hydrogen bonds between the hydroxyl groups of cellulose and the ester carbonyl or ester ether oxygen groups of dendritic TA molecules acted as supramolecular cross-links to enhance the mechanical strength while TA-centered hydrogen-bond clusters with cellulose chains improved the toughness by dissipating local stress. The hydrophobic aromatic rings in the TA structure further contributed to moisture resistance. Following this, the same group developed a greener and more scalable processing strategy to prepare TA–methylcellulose (TA–MC) bioplastics *via* an all-aqueous route.[92] This method eliminated the need for organic solvents and enabled large-area film production. The

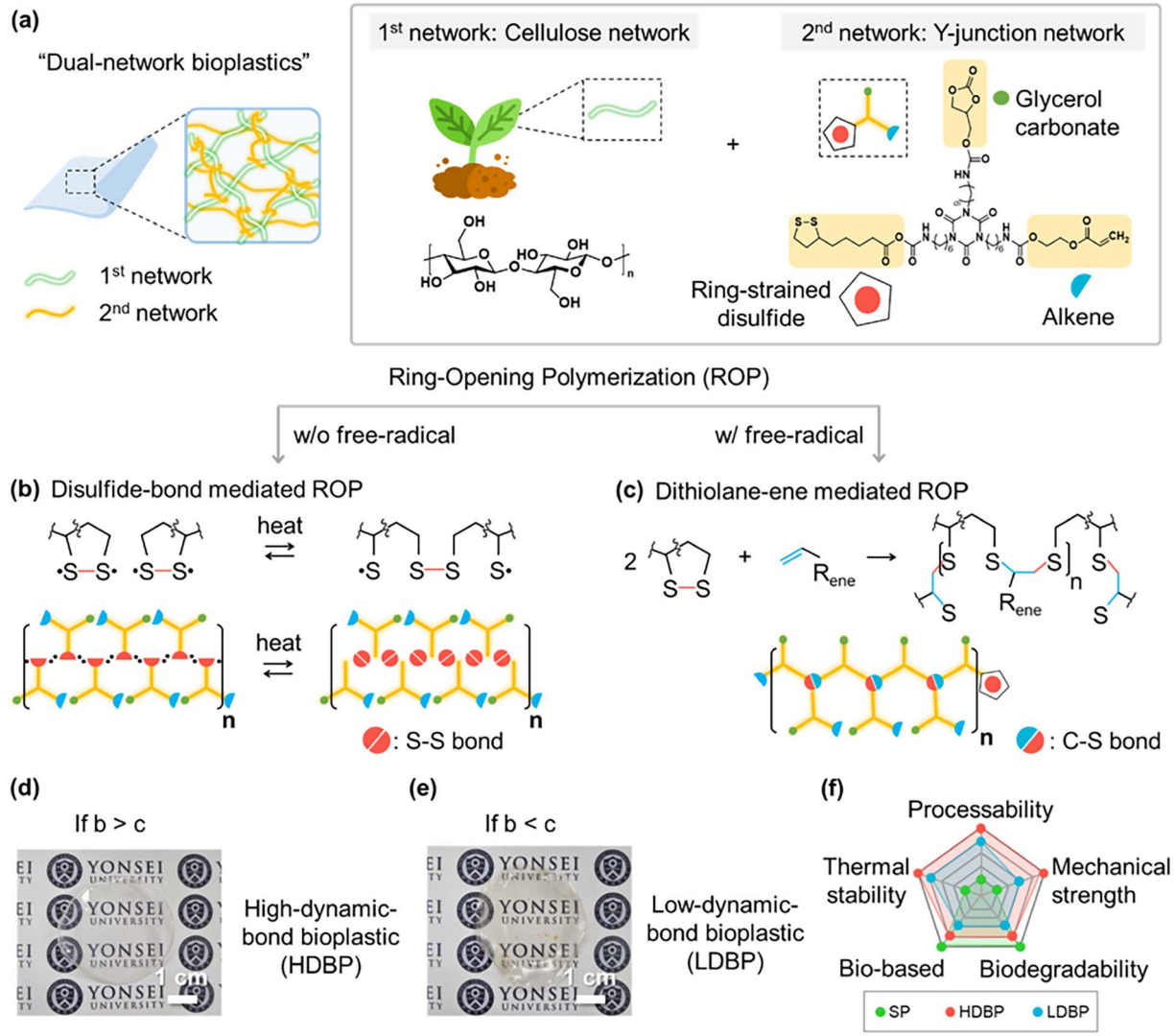

Fig. 7 Design of the dual-network bioplastics *via* ROP. (a) Dual-network bioplastics comprising cellulose and Y-junction networks. (b) Mechanism of disulfide-bond-mediated ROP. (c) Mechanism of dithiolane–ene-mediated ROP. (d) Optical photograph of the HDBP. (e) Optical photograph of the LDBP. (f) Radar chart of SP, HDBP, and LDBP corresponding to processability, mechanical strength, biodegradability, biobased materials, and thermal stability. Reprinted from ref. 96 with permission from American Chemical Society, copyright 2025.

resulting TA_1–MC (Table 4, entry 5) exhibited a tensile strength of 109.6 MPa, Young's modulus of 3.1 GPa, elongation at break of 7%, and a storage modulus of 3.1 GPa at 180 °C, while maintaining 40.4 or 34.2 MPa strength after immersion in water for 15 days or soaking in 80 °C water for 72 h, respectively. Such mechanical robustness and water tolerance were attributed to dense hydrogen-bonding networks combined with hydrophobic nanoconfinement phases introduced by TA. Solvent resistance was demonstrated by its stability in common organic solvents but dissolution in DMAc and 1 M NaOH. In addition, TA–MC was tested as a flexible printed circuit board substrate exhibiting reliable dielectric performance, high sensitivity, and mechanical durability. The material could be selectively dissolved in 75% ethanol, allowing the efficient recovery of intact electronic components.

Wei *et al.* introduced a hydrogen-bond tailoring strategy to construct multifunctional cellulose nanocrystal (CNC) composites reinforced with hyperbranched lignin (H-lignin).[93] In this work, alkali lignin was functionalized with a hyperbranched bis-MPA polyester to increase the abundance of hydroxyl groups. Compared with unmodified lignin, the self-bonding of H-lignin and its extensive interactions with CNC chains have produced a robust physical cross-linking network. As a result, the CNC/H-lignin films (Table 4, entry 6) exhibited a tensile strength of 32.5 MPa and a Young's modulus of 9.44 GPa, corresponding to 34% and 63% increases relative to pure CNC films. Beyond mechanical reinforcement, the addition of H-lignin improved crystallinity, water resistance, and thermal stability. The composites also demonstrated near-complete UV shielding attributed to the phenolic chromophores of lignin, and displayed antioxidant activity. In parallel, Jiang *et al.* reported a wood-inspired approach in which lignin was employed as a natural binder to reinforce cellulose paper with superior mechanical strength and thermal stability.[94] The

strategy mimicked the architecture of natural wood, where cellulose fibrils are embedded in a lignin–hemicellulose matrix. In the process, commercial cellulose paper was mildly alkali-swollen, infiltrated with a lignin solution, and subsequently hot-pressed. During hot-pressing, lignin melted and redistributed onto cellulose fibers. Structural analysis showed cleavage of β-O-4′ linkages and formation of new C–C bonds during hot-pressing, which, together with hydrogen bonding with cellulose hydroxyl groups and self-bonding among lignin fragments, contributed to the dense, mechanically robust network. The resulting lignin–cellulose composite (Table 4, entry 7) exhibited an isotropic tensile strength of ~200 MPa and a Young's modulus of ~10 GPa, far exceeding those of conventional cellulose paper (40 MPa, 4.7 GPa) and even outperforming many petroleum-based plastics. In this composite, lignin acted as a functional reinforcement that enhanced thermostability and UV-blocking capability. The maximum decomposition temperature increased from 328 °C to 453 °C, and the films absorbed nearly 100% of UVC and UVB radiation (Fig. 6(a–c)). Moreover, the infiltration-hot-pressing process used to fabricate the composite was compatible with roll-to-roll papermaking manufacturing (Fig. 6(d)). The excellent flexibility, strength, water stability, and UV-blocking performance of the lignin–cellulose composite (Fig. 6(e)) further enabled its integration into flexible electronics. For instance, 3D-printed circuits on the composite substrate maintained electrical continuity even under bending (Fig. 6(f–h)).

Hydrogen-bonding with secondary networks. Dual-network structures have emerged as an effective strategy to tailor the performance of cellulosic-based bioplastics. The synergy between two networks enables a dynamic balance between rigidity and flexibility, dissipating applied stress and thereby enhancing toughness and fracture resistance. Wang *et al.* developed a cellulose-based dual-network metafilm by embedding a secondary supramolecular network within a bacterial cellulose (BC) matrix.[95] The dual network originated from the *in situ* growth of a cyclotriphosphazene-bridged organosilica framework within the BC scaffold, formed *via* hydrolysis of organosiloxane and subsequent silanol polycondensation. Strong interfacial hydrogen bonding and efficient stress transfer between the two networks endowed the BC/PMO-20 composite metafilm (Table 4, entry 8) with outstanding mechanical properties, including a tensile strength of ~442 MPa, modulus of ~11 GPa, elongation at break of 9.21%, and toughness of 23.5 MJ m^{-3}, remarkably surpassing those of single-network cellulose plastics. The dual-network architecture also imparted exceptional thermal stability and superior flame retardancy, outperforming common plastics such as PET. In addition, the materials displayed good water/solvent resistance and biodegradability. The film has been applied as a flexible substrate for indium tin oxide (ITO) coatings as a demonstration. Very recently, Kim *et al.* reported a cellulose-based dual-network bioplastic film *via* ring-opening polymerization (ROP) of a Y-junction monomer comprising ring-strained disulfide at one end and alkene at another end.[96] In this design, the dual-network was established through hydrogen-bonding between the primary cellulose network and the secondary Y-junction polymer network, while the chemical structure of the latter could be tuned by ROP kinetics (Fig. 7(a)). Depending on the reaction route, the ROP proceeded either through ring-opening of the disulfides or through a dithiolane–ene mechanism with alkenes under radical conditions, yielding dynamic S–S or permanent C–S linkages (Fig. 7(b and c)). Accordingly, two materials were obtained: the high-dynamic-bond bioplastic (HDBP) (Table 4, entry 9) with reversible disulfide exchange (Fig. 7(d)) and the low-dynamic-bond bioplastic (LDBP) (Table 4, entry 10) dominated by permanent C–S linkages (Fig. 7(e)). As summarized in Fig. 7(f), the two bioplastics displayed distinct trade-offs in processability, thermal stability, mechanical strength, biodegradability, and bio-based content.

Other types of noncovalent interactions. Except for hydrogen bonding, other types of interactions such as ionic crosslinking, metal–ligand coordination and electrostatic interactions could provide stronger noncovalent forces and have been utilized. Yang *et al.* proposed a multi-physical crosslinking strategy where TA and calcium ions (Ca^{2+}) jointly reinforced carboxylated CNF films.[97] In this architecture, three noncovalent interaction networks coexisted: hydrogen bonding between CNFs and the polyphenol hydroxyl of TA, ionic bridges between Ca^{2+} and CNF carboxylates, and metal–phenol coordination between Ca^{2+} and TA hydroxyls. The CTCaBP-2 films (Table 4, entry 11) displayed remarkable mechanical reinforcement outperforming many commodity plastics of similar thickness. Xu and co-workers advanced the concept of Ca^{2+} coordination to reinforce cellulose–lignin nanocomposites.[98] Lignin nanoparticles were synthesized and blended with TEMPO-oxidized CNFs, which were vacuum-filtered into films and post-treated in $CaCl_2$ solution. In this design, strong Ca^{2+} coordination with oxygen-containing functional groups of cellulose and lignin, together with hydrogen bonding between cellulose and lignin, established a robust sacrificial network capable of dissipating stress. Mechanically, the Ca^{2+}-crosslinked composite containing 1 wt% nanolignin (Table 4, entry 12) achieved an optimal tensile strength of 223.8 MPa, more than twice that of neat CNF films (104 MPa), while maintaining a wet tensile strength of ~33.3 MPa and reducing water uptake to ~90% compared with >280% in pristine CNF films. Optical transparency remained high (88% at 800 nm), while lignin incorporation (15 wt%) imparted strong UV shielding (>99%). Soil burial tests confirmed complete biodegradation within ~30 days. Moreover, the nanocomposite films exhibited smooth surfaces, excellent electromechanical stability and enhanced thermal resistance together with flame retardancy.

Chen and colleagues developed a scalable route for producing cellulose–mineral foams by exploiting Al^{3+} coordination between cellulose chains and bentonite. The process began with dissolving cellulose in a NaOH/urea system, followed by the uniform mixing with bentonite and the addition of the 1,4-butanediol diglycidyl ether crosslinker.[99] The foams could be air-dried under ambient conditions and possess ultralow density, because Al^{3+} coordination between cellulose and bentonite stabilized the 3D network against capillary collapse. The resulting foams exhibited high mechanical properties, low thermal conductivity, improved thermal

stability, superior thermal insulation and flame-retardant performance. For end-of-life considerations, the foams could be mechanically recycled into slurry for reprocessing or completely biodegraded within three months, and life cycle analysis has been conducted. Lei *et al.* developed an efficient and scalable papermaking strategy to fabricate cellulose carboxymethylated fiber (CMF)-based bioplastic films (Table 4, entry 13) by integrating electrostatic interactions with covalent stabilization.[100] In this approach, CMFs were rapidly produced and combined with Al^{3+} ions and polyamide epichlorohydrin resin (PAE) polymers, which strongly adsorbed onto the fiber surfaces through electrostatic interactions to yield a homogeneous slurry readily processed into films *via* a classical papermaking route. Al^{3+} ions functioned as physical crosslinkers *via* ionic coordination, while flexible PAE polymers covalently crosslinked with cellulose fibers and simultaneously underwent self-crosslinking. The resulting films displayed a dense laminated structure and excellent optical properties. Mechanical robustness was markedly improved, with tensile strength reaching 158 MPa in the dry state and ~17 MPa under wet conditions. The dimensional stability in water and thermal stability have been also enhanced, with recyclability demonstrated by alkaline treatment.

From Table 4, physical crosslinked cellulose bioplastics can be classified into four design strategies, challenging the traditional view of physical networks as mechanically inferior by achieving properties which are comparable to those of covalent crosslinked networks: (i) hydrogen-bond hydroplastics (optionally reinforced by hydrophobic domains) leverage water as a switching variable for reprocessing while retaining high dry-state mechanical integrity (*i.e.*, a Cci film achieved a tensile strength of 92.4 MPa). (ii) Hydrogen-bonding with external donors (*e.g.*, polyphenols) further amplifies mechanical robustness (*i.e.*, a TA/lignin-reinforced film exhibited a remarkable tensile strength above 200 MPa). (iii) Dual-network architectures (hydrogen-bonding plus a secondary network) deliver the strongest overall balance and environmental resistance (*i.e.*, the BC/PMO-20 metafilm achieved an unprecedented tensile strength of 442 MPa). (iv) Ionic crosslinking or electrostatic interaction can be readily introduced in carboxymethylated cellulose matrices, providing stronger sacrificial links; for example, Ca^{2+}-crosslinked composites reached a tensile strength of 224 MPa.

4. Chitin/chitosan-based bioplastics

Chitin is an abundant oceanic biomass mainly extracted from waste crustacean shells such as crab and shrimp, and it is composed of *N*-acetyl-D-glucosamine units connected by β(1→4) glycosidic bonds.[101] The structure of chitin closely resembles cellulose but naturally carries nitrogen functionalities, which have been recently utilized as a renewable feedstock for producing organonitrogen compounds.[102–105] For polymer chemistry, chitin possesses a higher degree of crystallinity and stronger intermolecular hydrogen-bonding, which impart greater intrinsic rigidity and stiffness (usually high mechanical strength) to chitin-based bioplastics. But chitin has poor solubility, limited flexibility, and extremely low processability, making it significantly more difficult to process than cellulose. Chitosan, the deacetylated derivative of chitin, inherits biodegradability, biocompatibility, and antimicrobial activity, making it particularly attractive for sustainable plastic alternatives,[106,107] but it likewise suffers from brittleness and hydrophilicity. Accordingly, to address these limitations while leveraging their advantages, this section—consistent with the cellulose framework—organizes construction strategies for chitin/chitosan into three network architectures: permanent crosslinked, dynamic crosslinked, and physical crosslinked networks.

4.1 Permanent crosslinked networks

Sole *et al.* developed a covalent crosslinked chitosan film using adipic acid and 4-(4,6-dimethoxy-1,3,5-triazin-2-yl)-4-methylmorpholinium chloride (DMTMM) as the crosslinking agents.[108] The reaction between adipic acid carboxyl groups and chitosan amino groups formed a stable amide crosslinked network. Unlike conventional crosslinkers, DMTMM acted as a zero-length crosslinker, promoting only the desired reaction and eliminating the need for aldehyde-based crosslinkers. This approach enabled the production of homogeneous, compact films (Table 5, entry 1) *via* solution casting. Mechanical properties were significantly enhanced, with tensile strength increasing to 83 MPa (*vs.* <40 MPa for neat chitosan); however, the material remained less ductile, showing an elongation at break of only 1.8%. Upon the incorporation of glycerol, the elongation at break was dramatically improved to 39.7%. The thermal stability and barrier properties such as water vapor

Table 5 Permanent crosslinked network construction, performance metrics, and practical demonstration of chitosan/chitin-based bioplastics[a]

Name	Network bonding type	Forming tech.	TS (MPa)	YM (MPa)	EB (%)	T_{max} (°C)	WCA (°)	Practical potential (P)/application (A)	Ref.
AACHTC30	Amine bond	Solution casting	83	2674	1.8	258	N/A	P: food packaging	108
CS/FF	Imine & amide bond	Solution casting	11.2	3000	13	~370	N/A	A: smart food packaging	109
4% chitin bioplastic	Ether bond & hydrogen-bonding	Gelation	107	N/A	10	~300	103	A: containers (straws and cups)	110

[a] HP: hot-pressing; TS: tensile strength; YS: Young's modulus; EB: elongation at break; T_{max}: temperature at the maximum decomposition rate; WCA: water contact angle.

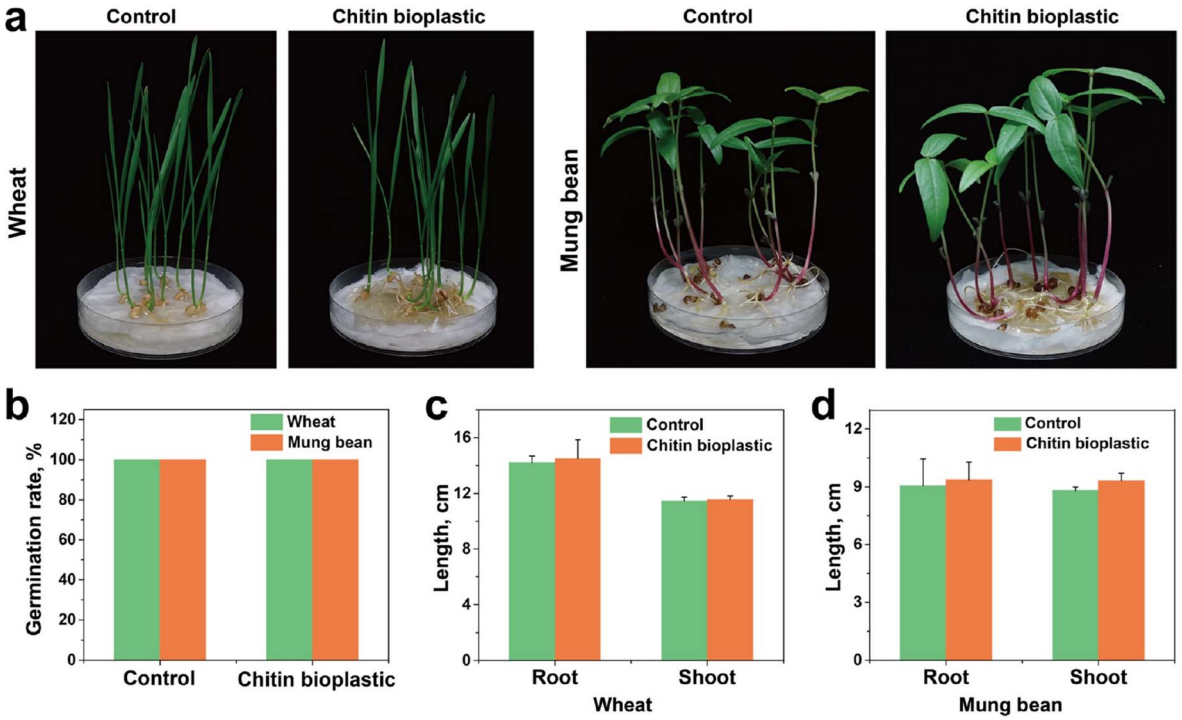

Fig. 8 Biotoxicity of the chitin bioplastic (day 10). The growth situation (a) and the germination rate (b) of wheat and mung bean. The root and shoot lengths of wheat (c) and mung bean (d). Reprinted from ref. 110 with permission from American Chemical Society, copyright 2022.

permeability and moisture uptake have been notably improved, and the film was biodegradable with negligible cytotoxicity, which is suitable for food packaging applications. Chumpon *et al.* reinforced genipin-crosslinked chitosan bio-resins with a sorbitol plasticizer and flax fibers to create a sustainable packaging material *via* solution-casting.[109] Genipin established permanent imine and amide bonds within the chitosan matrix, while sorbitol interacted with hydroxyl groups *via* hydrogen bonding and flax fibers provided effective matrix enhancement and stress transfer. Although the resulting composites (Table 5, entry 2) exhibited relatively modest mechanical performance (tensile strength: 11.2 MPa), they demonstrated exceptional functionality: the UV-blocking efficiency reached 98%, antibacterial performance exceeded 90% reduction of both Gram-positive and Gram-negative bacteria, and complete biodegradation was observed within 90 days in soil. Packaging trials using bananas further demonstrated superior weight retention (99.5% of the original weight) and delayed spoilage compared with polyethylene wraps.

Zhou *et al.* introduced ECH-mediated covalent crosslinking to fabricate high-performance chitin-based bioplastics,[110] adopting the dual-network strategy previously used by Hu *et al.* for cellulose.[76] Chitin was first dissolved in NaOH/urea and reacted with ECH to construct a robust permanent covalent network; subsequent ethanol treatment induced additional hydrogen-bonded physical crosslinking. The crosslinked 4% chitin films (Table 5, entry 3) exhibited outstanding mechanical performance (tensile strength reached 107.1 MPa) and high thermal stability. Besides, the film exhibited functional performances including good flame-retardant behavior, barrier properties, photoprotective ability and biodegradability. Straws and cups made from the films retained integrity in water, peanut oil, milk, and coffee, which indicates the practical application in food areas. The biological safety of the chitin-based bioplastic was confirmed as shown in Fig. 8. Wheat and mung bean seedlings grown with the bioplastic showed healthy development comparable to the untreated controls (Fig. 8(a)). Quantitative analysis further supported this observation, as the germination rate, root length, and shoot length remained essentially unchanged (Fig. 8(b–d)).

Across the studies in Table 5, permanent crosslinked networks have been leveraged to deliver chitin/chitosan bioplastics with packaging-relevant properties under defined processing conditions. Mechanistically, two distinct pathways drive this enhancement. For chitosan, the reactive $-NH_2$ groups facilitate the formation of stable amine/amide crosslinked networks; for instance, adipic acid-crosslinked films achieved a tensile strength of 83 MPa, while chitin possesses higher crystallinity. When effectively dissolved (*e.g.*, in NaOH/urea) and crosslinked *via* etherification, its rigid backbone translated into exceptional robustness, reaching a tensile strength of 107 MPa. However, practical application remains constrained by solubility; achieving these high-performance metrics requires overcoming the recalcitrance of chitin to dissolution.

4.2 Dynamic crosslinked networks

Dynamic covalent chemistry, chiefly imine exchange, has emerged as a versatile handle to overcome chitosan's high crystallinity and poor melt processability, enabling self-healing and reprocessing ability while preserving relatively high

Table 6 Dynamic crosslinked network construction, performance metrics, and practical demonstration of chitosan-based bioplastics[a]

Name	Network bonding type	Forming tech.	TS (MPa)	YM (MPa)	EB (%)	E_a (kJ mol^{-1})	T_g (°C)	T_{max} (°C)	WCA (°)	S	R/R	Practical potential	Ref.
CP1-40%	Imine bond & hydrogen bonding	HT at 110 °C	47	2850	4	67.7	124	N/A	N/A	✓	✓	Plastic substitutes	111
CS–PI (1 : 1)	Imine bond & hydrogen bonding	HT at 130 °C	38.7	3200	2.4	128	284	~300	86.6	✓	✓	Plastic replacement	112
CHB/PA@ZnNF-0.30	Imine bond, hydrogen bonding & metal coordination	Thermal casting	45.3	N/A	42.5	N/A	123.7	306.8	115.7	N/A	N/A	Antibacterial adhesives & UV resistant coating	113

[a] HP: hot-pressing; TS: tensile strength; YS: Young's modulus; EB: elongation at break; E_a: activation energy of the bond exchange reaction; T_g: glass transition temperature; T_{max}: temperature at the maximum decomposition rate; WCA: water contact angle; S: self-healing; R/R: reprocessing/recycling.

strength. Wang *et al.* developed a thermo-mechanically processable chitosan-based plastic substitute (CP) by incorporating polyimine (PI) powders into chitosan.[111] The PI powders were synthesized through a non-catalyzed Schiff base reaction between TPA, tris(2-aminoethyl)amine, and diamines at room temperature. The PI and chitosan mixtures were processed using stepwise hot-pressing at 110 °C. During this process, the amino groups of chitosan reacted with the PI network through dynamic imine exchange to form C=N linkages. Additionally, the abundant hydroxyl and *N*-acetyl groups on chitosan reinforced the interface through hydrogen bonding with the PI network, and therefore the as-synthesized film (Table 6, entry 1) showed excellent interfacial compatibility. After modifications, the tensile strength reached 47.0 MPa with a Young's modulus of 2.85 GPa, while the elongation at break remained low at 4%. The mechanical performance was influenced by the chain length and structure of the diamines: the secondary amine groups were unable to form hydrogen bonds with chitosan, which resulted in increased flexibility but reduced rigidity. Longer diamine chains also led to greater elongation at break and decreased tensile strength. DMA revealed that the incorporation of the PI network lowered the glass transition temperature from 316 °C for neat chitosan to 124 °C, imparting thermoplasticity and enabling stress relaxation during thermal processing. The dynamic imine network also endowed the CPs with self-adaptive capabilities, and the films could be reprocessed by cutting and hot-pressing. In addition, seamless multilayer lamination resulted in a 109% increase in tensile

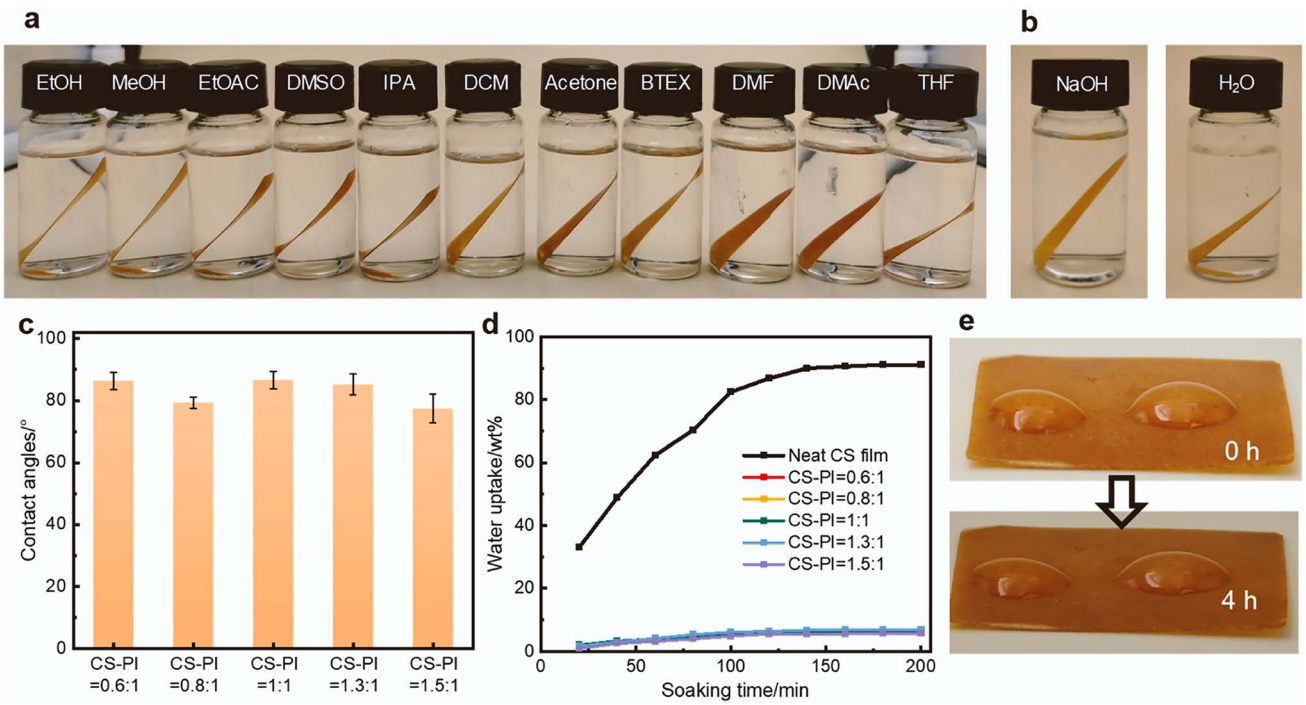

Fig. 9 Stability of CS–PI films. Chemical stability of CS–PI (a) in organic solvents after 15 d, (b) in 10% (w/v) NaOH solution after 15 d, and in water after 10 d; (c) water contact angle of CS–PI films; (d) water uptake curves of the chitosan film and CS–PI films over time; (e) waterproof performances of CS–PI films in 4 h. Reprinted from ref. 112 with permission from Elsevier, copyright 2024.

strength compared to single-layer films. The closed-loop chemical recycling was also demonstrated by immersing the films in a diluted diamine solution in ethanol to regenerate the monomers and oligomers.

Following this, the same group developed an all-natural chitosan–polyimine (CS–PI) vitrimer through Schiff base formation using dialdehyde vanillin as the crosslinker.[112] The introduction of dynamic imine linkages partially replaced native hydrogen bonds, leading to the formation of an amorphous structure that allowed melt-like flow above the exchange temperature. The optimal dynamic covalent crosslinking density was achieved with a 1 : 1 ratio of –CHO to NH_2, resulting in a tensile strength of 38.72 MPa, an elongation at break of 2.35, and a Young's modulus of 3.25 GPa. The CS–PI films (Table 6, entry 2) exhibited excellent thermal processability, with a high glass transition temperature of 284 °C and a bond exchange activation energy of 127.6 kJ mol^{-1}. The films could also be reprocessed by hot-pressing at 130 °C, with a strength recovery of 93.9% and modulus recovery of 89.8%, and blade-scratched films were able to self-heal. The UV shielding ability was improved, and the end-of-life pathway by acid depolymerization was conducted. The CS–PI films also showed better environmental stability compared with neat chitosan (Fig. 9). They retained their shape and structural integrity after 15 days in 11 organic solvents, 10% NaOH, and water (Fig. 9(a and b)). Surface wettability tests further supported this stability. The films exhibited higher water contact angles of 77.4–86.6° (Fig. 9(c)) and greatly reduced water uptake (~6% *vs.* 91.1% for chitosan; Fig. 9(d)). Macroscopically, water droplets remained on the film surface for extended periods without penetration (Fig. 9(e)).

Jin *et al.* engineered a hybrid system by combining hyperbranched chitosan with protocatechualdehyde (PA) and ZnO quantum dots (QDs) templated on nanofibrillated cellulose

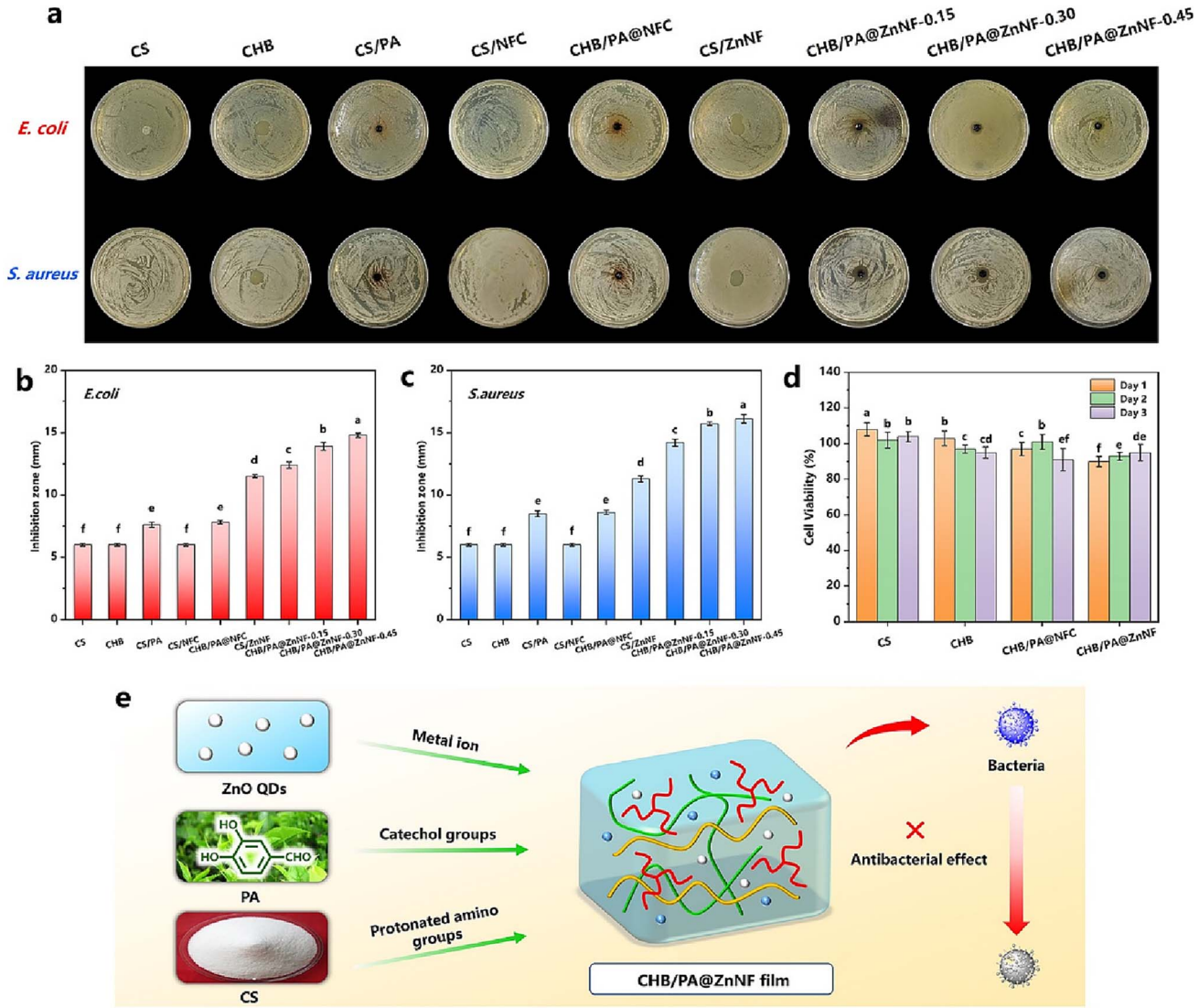

Fig. 10 (a) Antibacterial photographs, inhibition zone diameters of the composites against (b) *E. coli* and (c) *S. aureus*, (d) cell viability, and (e) antibacterial mechanism of the CHB/PA@ZnNF composites. The same letters in the column represent no significant difference ($p > 0.05$). Reprinted from ref. 113 with permission from Elsevier, copyright 2023.

(ZnNF), creating a multi-network stabilized by both the dynamic imine crosslinked network and physical crosslinked network through hydrogen bonding and metal coordination.[113] Specifically, Schiff-base reactions between amino groups in chitosan and the aldehyde groups in PA provided dynamic covalent linkages, while catechol moieties enabled reversible hydrogen bonding and metal coordination between ZnO QDs and catechol groups in PA. This architecture facilitated uniform ZnO dispersion and dense interfacial adhesion, producing films (Table 6, entry 3) with higher flexibility (elongation at break of 42.5% and a toughness of 16 MJ m^{-3}) while retaining a comparable tensile strength of 45.3 MPa. In addition, the films exhibited robust antibacterial activity, as evidenced by the inhibition zones in Fig. 10(a). The CHB/PA@ZnNF-0.45 sample showed the largest diameters (14.82 mm for *E. coli* and 16.12 mm for *S. aureus*), far exceeding those of the neat chitosan film as shown in Fig. 10(b and c). The cytotoxicity tests (Fig. 10(d)) also demonstrated that the films maintained high cell viability after 3 days of incubation. This antibacterial performance was attributed to the synergistic defense mechanism involving positively charged chitosan disrupting bacterial membranes, PA's catechol groups inhibiting microbial protein production, and ZnO QDs generating reactive oxygen species and releasing Zn^{2+} to damage DNA/respiratory enzymes (Fig. 10(e)).

In the current literature, dynamic covalent networking is predominantly demonstrated in chitosan (rather than chitin) matrices, because chitosan's primary amines enable Schiff-base (imine) formation and thereby establish a dynamic imine network within the polysaccharide matrix. Through imine–imine exchange, these systems can partially overcome crystallinity-driven limitations in melt processability while retaining tensile strength ranging from 38 to 47 MPa. As summarized in Table 6, a chitosan–PI (CP1-40%) blend produced by stepwise hot-pressing forms a coupled dynamic imine/hydrogen-bonding network, imparting thermoplasticity, self-healing, and hot-press reprocessability. A vitrimeric chitosan–PI (CS–PI) constructed with dialdehyde vanillin further exhibits melt-like flow above the exchange temperature together with strong solvent resistance and an acid-depolymerization end-of-life option. Incorporation of catechol groups and ZnO-templated nanofibrillated cellulose yields a multi-network that preserves strength while markedly increasing ductility (elongation of 42.5%, *vs.* ~2–4% for pure imine networks), and concurrently adds UV-shielding and antibacterial functions. Taken together, these observations indicate that dynamic imine networks impart thermoplasticity, solvent resistance, self-adaptive behavior, and chemical degradability, whereas the incorporation of additional bonding interactions can further enhance toughness and multifunctionality.

4.3 Physical crosslinked networks

Introducing external crosslinkers to establish non-covalent intermolecular interactions enables reconstruction of native chitin into physical crosslinked networks that combine high mechanical strength (~160–170 MPa) with reprocessability. Duan and co-workers realized this through an aqueous non-covalent self-assembly process using TA, followed by hot-pressing at 110 °C.[114] TA formed a dense supramolecular network with chitin *via* hydrogen bonding, ionic interactions, and hydrophobic associations. This physical crosslinked architecture not only stiffened the matrix but also introduced reversible sacrificial bonds that dissipate energy under stress, thereby simultaneously enhancing mechanical strength and processability. The hot-pressing step further promoted densification and in-plane alignment of chitin nanofibrils, resulting in anisotropic reinforcement and improved load transfer. CTBP-6 (Table 7, entry 1) possessed excellent mechanical strength (tensile strength of 168.8 MPa and Young's modulus of 6.8 GPa), thermal stability, solvent resistance, biodegradability and pronounced hydroplasticity to be remolded by a simple

Table 7 Physical crosslinked network construction, performance metrics, and practical demonstration of chitosan/chitin-based bioplastics[a]

Name	Network bonding type	Forming tech.	TS (MPa)	YM (MPa)	EB (%)	T_{max} (°C)	WCA (°)	S/W	R/R	Practical potential (P)/application (A)	Ref.
CTBP-6	Hydrogen bonding, ionic interactions & hydrophobic associations	HP at 110 °C	168.8	6800	5.5	~304	N/A	✓	✓	P: petroleum-based plastic substitution	114
CLBP-6	Hydrogen bonding, ionic interactions & hydrophobic associations	HP at 110 °C	159	8400	5	~300 (CLBP-8)	107	✓	✓	P: petroleum-based plastic substitution	115
CSC	Hydrogen bonding & ionic crosslinking	Solution casting	53	9400	38	N/A	N/A	N/A	✓	P: petroleum-based plastic substitution	116
QSCC	Hydrogen bonding & electrostatic interactions	Solution casting	11.3	6.2	182	N/A	94	N/A	✓	A: food packing	117
Chitosan/CPAP3-A1	Protein–chitosan interaction	Solution casting	90	3790	30	N/A	N/A	✓	✓	P: implantable devices A: wound dressings	118

[a] HP: hot-pressing; TS: tensile strength; YS: Young's modulus; EB: elongation at break; T_{max}: temperature at the maximum decomposition rate; WCA: water contact angle; S/W: self-healing/welding; R/R: reprocessing/recycling.

wetting–drying process. Besides, the acid-assisted modular assembly strategy is demonstrated in Fig. 11 as a significant fraction (~49.6%) of free amino groups was generated through chitin deacetylation during hot-pressing. As shown in Fig. 11(a), the introduction of a small amount of dilute acetic acid protonated exposed amino groups to induce solvation and chain entanglement, which subsequently re-established the noncovalent network upon hot-pressing. This mechanism enabled two separate CTBP-6 sheets to be tightly welded together (Fig. 11(b)). The welded material retained high mechanical strength (~150 MPa) (Fig. 11(c)) and exhibited a continuous surface in cross-sectional SEM images (Fig. 11(d and e)). Beyond simple welding, acid-assisted activation also allowed fragmented CTBP to be reprocessed into a composite sheet (Fig. 11(f)) and supported modular assembly into three-dimensional constructs, such as the load-bearing basket shown in Fig. 11(g and h). Later on, the same group advanced polyphenolic reinforcement by using alkali lignin (AL) as a mediator for chitin assembly, combined with plane hot-pressing at 110 °C.[115] A transparent chitin/AL hydrogel was first prepared and subsequent hot-pressing expelled water and compacted the gel along the thickness direction to yield a flat, uniform chitin/AL bioplastic (CLBP) sheet of ~0.1 mm thickness. Beyond hydrogen bonding with chitin, alkaline treatment increased carboxyl groups on AL that ionically interact with amino groups on chitin, while hydrophobic associations formed between AL's aromatic substructures and the pyranose ring/methyl groups of chitin. Plane compression induced in-plane orientation and anisotropic alignment of self-assembled chitin nanofibrils, which further underpinned the mechanical upshift. Owing to AL's hydrophobic aromatics, the bioplastic (Table 7, entry 2) showed excellent moisture resistance, hydrophobicity, solvent tolerance, and UV shielding.

Compared with the physical crosslinked chitin-based bioplastics, which typically exhibit ~5% elongation at break, physical crosslinked chitosan-based bioplastics with markedly enhanced ductility. Ma *et al.* extended noncovalent assembly into organic–inorganic composites by incorporating calcium phosphate oligomers (CPO) into chitosan/sodium alginate (CS/SA) matrices using an evaporation-induced self-assembly method.[116] CPO served as a molecular bridge, partially weakening the electrostatic interactions and hydrogen bonding within the CS/SA network, while establishing new ionic interactions between the calcium ions of CPO and the carboxyl

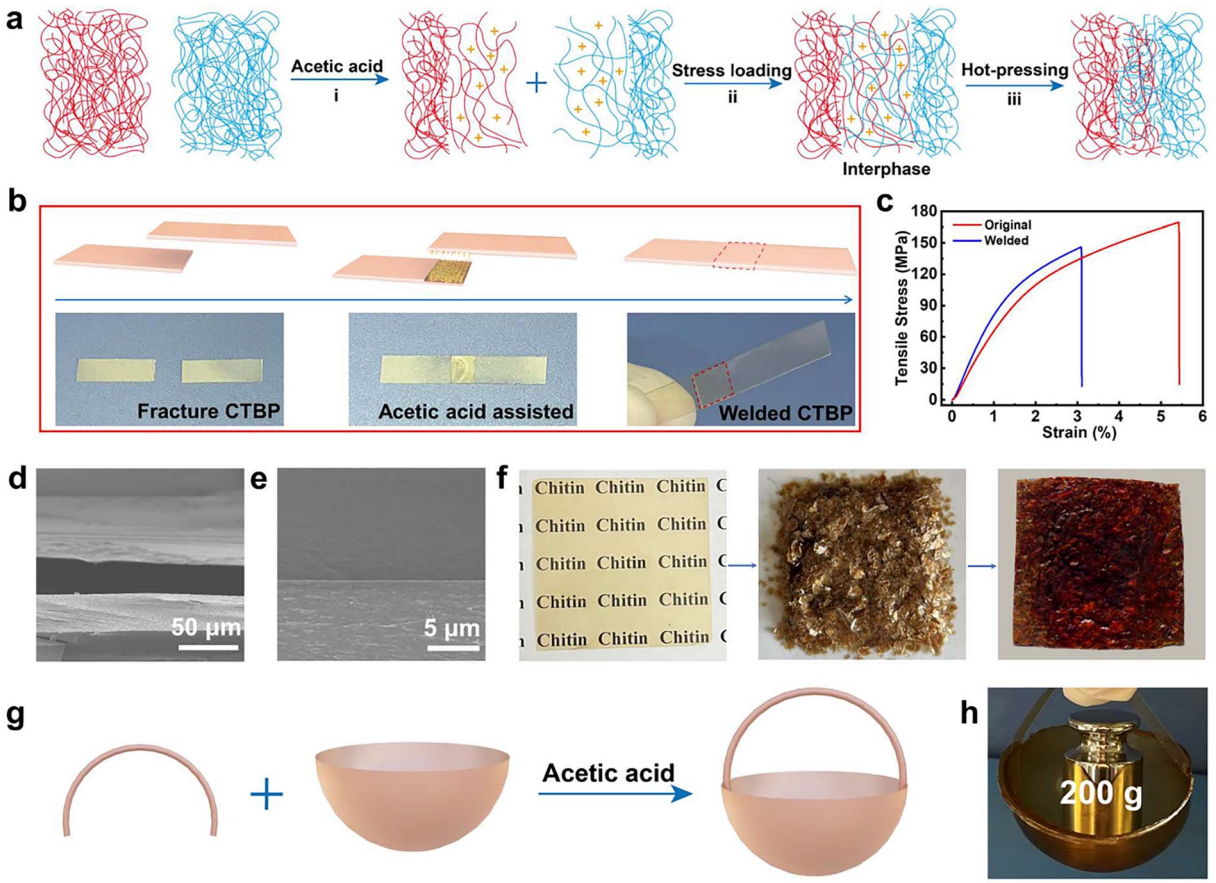

Fig. 11 Acid-assisted modular assembly strategy for CTBP-6. (a) Mechanism of acid-assisted modular assembly strategy. (b) Schematic and digital images of CTBP-6 welding process. (c) Stress-strain curves of original and welded CTBP-6. Cross-section SEM images of (d) original and (e) welded CTBP-6. (f) Digital images demonstrating the recycle process of CTBP-6. (g) Schematic and (h) digital images of CTBP-6 basket construction process which could support 200 g of weight. Reprinted from ref. 114 with permission from American Chemical Society, copyright 2024.

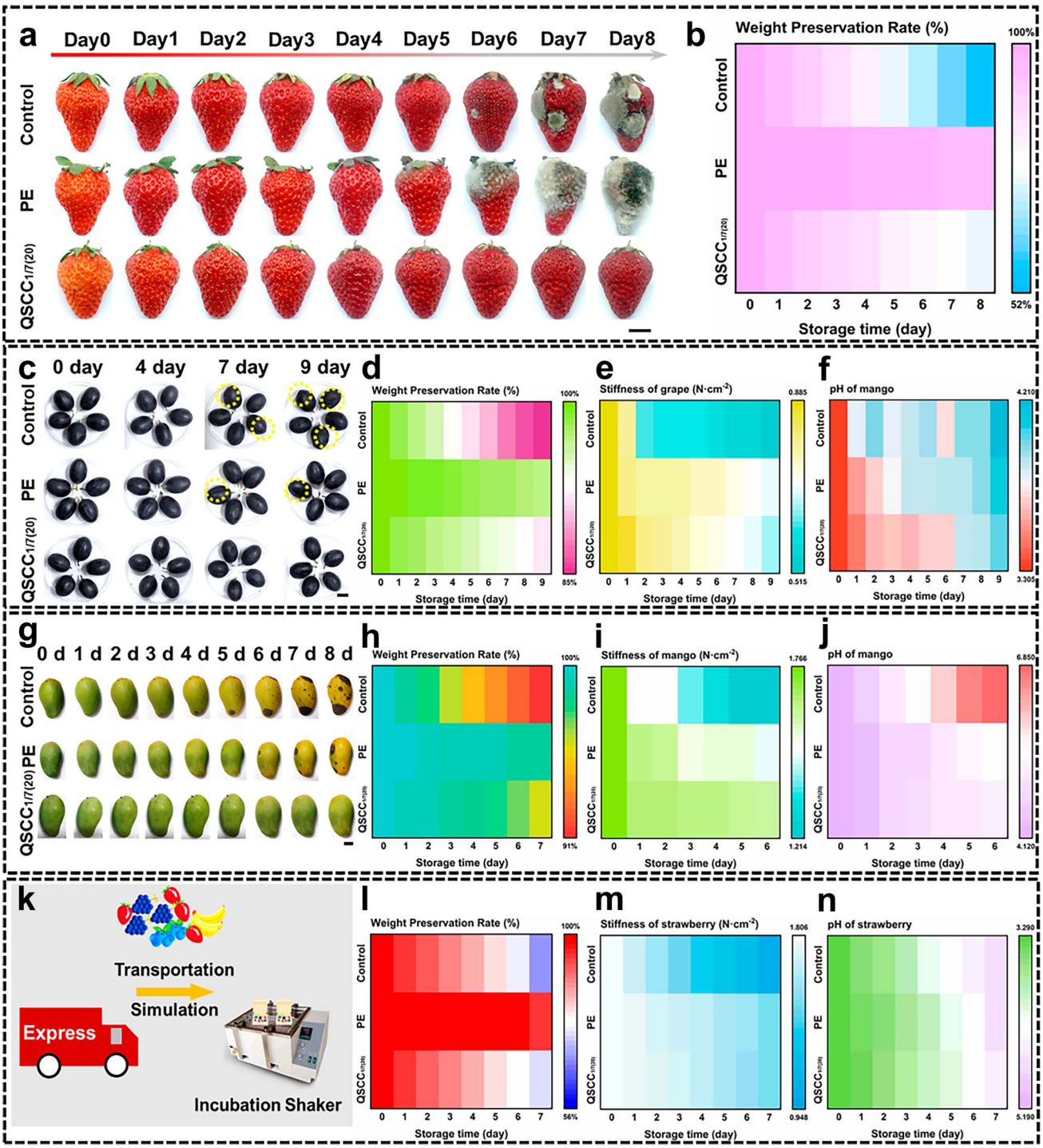

Fig. 12 Effectiveness and generalizability of QSCC bioplastics in preserving perishable fruits in a static situation and its preservation ability in a dynamic situation. (a) Appearance (scale bar: 10 mm) and (b) weight preservation rate of strawberries. (c) Appearance (scale bar: 10 mm), (d) weight preservation rate, (e) stiffness, and (f) pH of grapes. (g) Appearance (scale bar: 10 mm), (h) weight preservation rate, (i) stiffness, and (j) pH of mangoes. (k) Schematic illustration of simulated dynamic transportation. (l) Weight preservation rate, (m) stiffness, and (n) pH of strawberries during shaker simulation. Reprinted from ref. 117 with permission from American Chemical Society, copyright 2024.

groups of SA, and between the phosphate groups of CPO and the amino groups of CS. Over time, amorphous CPO polymerized into hydroxyapatite (HAP) nanolines, which were uniformly integrated with the polysaccharide chains, forming a robust organic–inorganic nanofiber network. The optimized CSC film (Table 7, entry 3) exhibited balanced mechanical properties, as well as solvent resistance, flame retardancy, water-induced processability and biodegradability. Bi *et al.* developed a dynamically electrostatic cross-linked system: quaternary ammonium chitosan (QAC) and sodium alginate (SA) were first

assembled into a polyelectrolyte complex (QS).[117] Protonated chitosan (CC), obtained by dissolution in citric acid, was then introduced, establishing a noncovalent network of electrostatic interactions between the SA anion, citrate anion, $-NH_3^+$/$-N^+(CH_3)_3$ of QAC, and hydrogen bonding to induce microcrystallization. The resulting QSCC material (Table 7, entry 4) showed a tensile strength of 11.3 MPa, extremely high elongation at break of 182%, Young's modulus of 6.2 MPa, and toughness of 8.04 MJ m^{-3}. The preservation capability of the QSCC bioplastic is shown in Fig. 12. While the unwrapped control fruits and PE-wrapped samples exhibited varying degrees of deterioration within 6–8 days (Fig. 12(a, c and g)), QSCC-wrapped fruits retained freshness throughout the observation period, showing moderate weight loss and slow, stable changes in stiffness and pH (Fig. 12(d–f and h–j)). Moreover, under simulated transportation conditions involving vibration (Fig. 12(k–n)), QSCC packaging provided better protection than commercial PE packaging, highlighting its suitability for oxygen- and humidity-sensitive fruit. Notably, the films were recyclable at room temperature by a water-assisted green process or mostly biodegraded after 20 days.

Wu *et al.* developed an insect cuticle-inspired, protein-mediated noncovalent reinforcement of chitosan using CPAP3-A1, a β-sheet-rich cuticular protein with chitin-binding domains that binds specifically to chitosan.[118] Incorporating 2.5–10 wt% CPAP3-A1 into acidic chitosan converted the precursor from a liquid-like to a gel-like form. At 10 wt% CPAP3-A1 in 6 wt% chitosan, the blend formed a viscoelastic hydrogel with a gel–sol transition near 200% strain and ∼93% self-healing after 500% strain, while shear-thinning conferred injectability, moldability, and printability. Neutralizing and dehydrating the cast gels yielded ∼50 μm chitosan/CPAP3-A1 bioplastic films (Table 7, entry 5). The films retained stiffness (Young's modulus 3.79 GPa) yet display ∼30% higher yield strength, ∼200% higher fracture strain, and ∼300% higher toughness, evidencing concurrent strengthening and toughening *via* strong but reversible protein–polysaccharide interactions. The dynamic noncovalent network also enabled closed-loop processing by acid treatment. The low immunogenicity and antibacterial activity of the material suggested potential applications in implantable devices and wound dressings.

Overall, physical crosslinked networks in this space fall into two main categories (Table 7). First, hot-pressed chitin films (*e.g.*, CTBP-6 and CLBP-6), driven by dense supramolecular hydrogen-bonding interactions, densification, and in-plane nanofibril alignment, achieve a very high strength of ∼160–169 MPa but with low ductility (∼5.5%). Moreover, exposure of active amino groups *via* deacetylation during hot-pressing enables weldability/self-healing. In contrast, solution-assembled chitosan systems prioritize ductility *via* electrostatic interactions, hydrogen-bonding or protein-mediated networks: composites like CSC and chitosan–CPAP3-A1 combine moderate–high strength (∼50–90 MPa) with significantly enhanced elongation (30–40%) and toughness up to ∼20 MJ m^{-3}. Notably, the QSCC achieved an extraordinary elongation at break of 182% while simultaneously offering excellent gas barriers. All retain recyclability and biodegradability. In

Table 8 Construction, performance metrics, and practical demonstration of lignocellulosic bioplastics[a]

Bioplastics	Network bonding type	Forming tech.	TS (MPa)	EB (%)	E_a (kJ mol^{-1})	T_g (°C)	T_{max} (°C)	WCA (°)	R/R	Practical potential (P)/application (A)	Ref.
ELCF-2	Ether bond (permanent) & hydrogen bonding (physical)	Gelation	132.5	9.8	N/A	N/A	347	95.5	N/A	P: UV protection	124
LB	Ester bond (permanent) & hydrogen bonding (physical)	Roll to roll	99	4	N/A	N/A	N/A	N/A	✓	A: TENG	125
Stalk plastics	Acetal bond (dynamic)	HP at 110 °C	2.7	33.2	63.3	57.7	N/A	62.2	✓	N/A	126
$EpP_{0.8}$	Acetal bond (dynamic)	HP at 150 °C	36	32.9	45.7	83.2	360	N/A	✓	P: solar-driven applications	127
Whole corn bioplastic	Hydrogen bonding & metal coordination (physical)	Casting & HP at 60 °C	78.5	17.2	N/A	N/A	170	71.6	✓	P: substitute for petrochemical plastics	128
Lignocellulosic bioplastics	Hydrogen bonding & metal coordination (physical)	Casting & HP at 60 °C	136	16.2	N/A	N/A	300	108.4	✓	P: substitute for petrochemical plastics	129
Lignocellulosic bioplastic	Hydrogen bonding (physical)	Casting	128	4	N/A	N/A	355	90	✓	P: agricultural mulching films, construction & automotive parts	130
Ph-bioplastic	Hydrogen bonding (physical)	Filtration	169	18	N/A	135 (DSC)	350	85.5	✓	A: food-preservation packaging	124

[a] HP: hot-pressing; TS: tensile strength; YS: Young's modulus; EB: elongation at break; E_a: activation energy of the bond exchange reaction; T_g: glass transition temperature from DMA; T_{max}: temperature at the maximum decomposition rate; WCA: water contact angle; R/R: reprocessing/recycling.

short, hot-press densification of chitin leverages its rigid, highly crystalline structure to maximize strength, whereas solution-assembled chitosan architectures inherently exhibit much higher ductility and toughness while also enabling application-specific functionalities (*e.g.*, food packaging and wound dressings).

5. Lignocellulosic biomass-derived bioplastics

Direct utilization of raw lignocellulosic biomass offers greater techno-economic feasibility and practical relevance. Unlike isolating single components *via* energy-intensive fractionation and purification, this strategy preserves multicomponent synergies while avoiding costly delignification and isolation.[119–121] Leveraging native structural features, bioplastics prepared from unrefined feedstocks can achieve tensile strengths up to 169 MPa, at reduced production cost. As summarized in Table 8, physical crosslinked lignocellulosic bioplastics typically exhibit tensile strengths of 78.5–169 MPa and elongations of 4–18%. Their performance is comparable to, and in some cases exceeds, that of many single-polymer systems. However, the use of native biomass also presents inherent challenges. The compositional heterogeneity and strong intercomponent interactions constrain molecular accessibility,[121–123] making it difficult to simultaneously disrupt native associations and selectively introduce covalent crosslinks without compromising strength. As a result, reports of permanent and dynamic crosslinked systems remain relatively few. Permanent ether/ester networks can reach strengths of 99–132.5 MPa but show only moderate ductility (4–9.8%), whereas dynamic acetal networks achieve higher deformability (~33% elongation) but at much lower strength (2.7–36 MPa).

5.1 Permanent crosslinked networks

Given these constraints, establishing durable and uniform permanent networks within lignocellulosic biomass remains challenging. The natural heterogeneity of lignin complicates controlled covalent crosslinking with cellulose, and disparities in the polarities and molecular structures further hinder interfacial compatibility. As a result, effective permanent crosslinking often requires external crosslinking agents to facilitate intermolecular interactions and stabilize the composite network. Shen *et al.* developed a permanent crosslinked network by extracting polyphenol lignin from bamboo using a green deep eutectic solvent (DES) and integrating it with cellulose. This integration was achieved through hydrogen bonding, followed by crosslinking with ECH.[124] The process formed a robust network of inter-molecular, covalent ether bonds between cellulose and lignin, which significantly improved the mechanical properties of the resulting film. The lignocellulosic film (Table 8, entry 1) displayed remarkable mechanical performance, with a tensile strength of 132.5 MPa, elongation at break of 9.8%, and toughness of 9.8 MJ m^{-3}. Moreover, the incorporation of lignin not only enhanced the mechanical strength but also significantly improved the film's durability. The ELCF-2 film demonstrated excellent resistance to water, UV light, and high temperatures. Even after 30 days of immersion in water, the film maintained a high wet strength of 68 MPa and elongation at break of 6.4%. Additionally, the film exhibited outstanding UV-blocking capabilities, effectively shielding nearly 100% of UVC and UVB, and 95.24% of UVA radiation. These properties make the ELCF-2 film a promising candidate for applications requiring high mechanical strength, environmental resistance, and UV protection. Similarly, Xue *et al.* utilized a DES composed of choline chloride and oxalic acid to deconstruct poplar wood powder, followed by water treatment to *in situ* regenerate the lignin, which rebinded with the cellulose fibers through hydrogen bonding.[125] This process resulted in the formation of a cellulose–lignin composite slurry, which was further crosslinked with citric acid (CA) and subsequently fabricated into lignocellulosic bioplastic (LB) through a roll-to-roll process. The resulting LB (Table 8, entry 2) demonstrated a notable tensile strength of 99 MPa. Moreover, LB exhibited both biodegradability and mechanical recyclability, which further enhanced its environmental sustainability. Additionally, by incorporating carbon powder into the LB, a conductive bioplastic was produced, which served as the electrode material in the triboelectric nanogenerator (TENG), expanding its applications in self-powered sensing systems.

5.2 Dynamic crosslinked networks

To overcome the major limitations of limited toughness and lack of recyclability, the construction of dynamic crosslinked networks has been employed for raw lignocellulosic biomass. When introduced into lignocellulosic feedstocks, these dynamic linkages simultaneously reorganize intrinsic interactions between cellulose, hemicellulose, and lignin while reinforcing interfacial stress dissipation, resulting in bioplastics that are both structurally flexible and reprocessable. Han *et al.* developed an innovative method to achieve the one-step plasticization of raw corn stalk, in the presence of DES with the addition of a TPA crosslinker in an internal mixer.[126] During this process, DES (composed of oxalic acid and choline chloride in a 1 : 1 molar ratio) served dual functions: the oxalic acid component breaks lignin–cellulose bonds while the chloride ion synergistically disrupts intramolecular hydrogen bonds in the native stalk. Simultaneously, the internal mixer induced a mechanical force which disrupted the regular structure of the stalk and promoted the condensation between aldehyde groups on TPA and hydroxyl groups, forming a dynamic acetal crosslinked network, which displayed stress relaxation with an activation energy of 63.3 kJ mol^{-1} for the bond exchange reaction. The resulting granular-state stalk was then hot-pressed to prepare stalk plastics (Table 8, entry 3) which exhibited a low tensile strength of 2.7 MPa and relatively high elongation at break of 33.2%. The material could be reprocessed *via* grinding and hot-pressing.

Li *et al.* developed an *in situ* plasticizing strategy for fabricating bioplastics from eucalyptus wood.[127] The process involved alkaline alcohol pretreatment to disrupt the wood's native structure, followed by propylene oxide etherification to

enhance the reactivity of lignin and cellulose. Subsequent crosslinking with divinyl ether established a dynamic covalent network while preserving a controlled density of hydrogen bonds. The resulting bioplastic (Table 8, entry 4) demonstrated impressive mechanical properties, achieving a tensile strength of 36 MPa and an elongation at break of 32.9%. The material exhibited outstanding water resistance with a swelling ratio of ~0.8%, and showed thermal stability (decomposition at 268 °C). They exhibited a shape memory effect and could be reprocessed with minimal mechanical loss after recycling. Besides, the UV resistance and photothermal effect of the bioplastics can be beneficial for solar-driven applications.

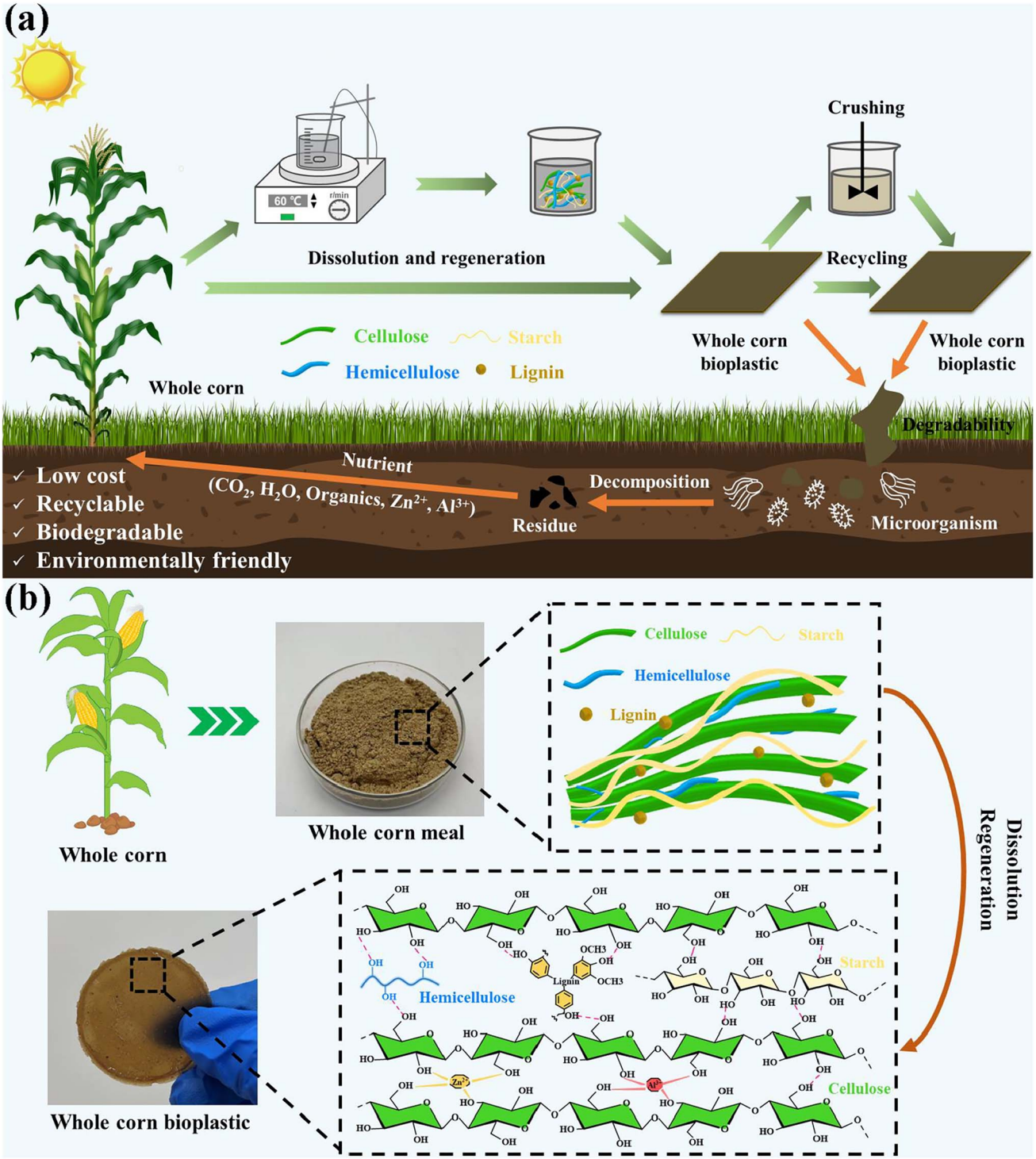

Fig. 13 (a) Schematic illustration of preparation, recycling, degradation, and closed-loop cycle of whole corn bioplastic. (b) Structural diagram of the dissolution and regeneration process of whole corn bioplastic. Reprinted from ref. 128 with permission from Elsevier, copyright 2024.

5.3 Physical crosslinked networks

To obtain physical crosslinked networks, the dissolution–regeneration method has been proven to be an efficient integrated strategy, which first fully or partially dissolves and deconstructs the raw material using appropriate solvents (*e.g.*, chloride salt solutions, or DES), followed by regeneration and noncovalent interactions. This process facilitates lignin redistribution and reinforces cellulose matrices *via* enhanced interfacial compatibility, enabling synergistic improvements in mechanical strength, thermal/water stability, and reprocessability/recyclability.

The mixed chloride salt solution has emerged as a promising and greener alternative for biomass dissolution–regeneration. Xie *et al.* utilized a $ZnCl_2/AlCl_3$ binary salt system to dissolve whole corn, which contains starch, cellulose, hemicellulose, and lignin[128] (Fig. 13(b)). Following *in situ* ethanol-induced regeneration, casting and hot-pressing (Fig. 13(a)), the biomass components reassembled through strong hydrogen bonding, ionic interactions and van der Waals force (Fig. 13(b)). The resulting material (Table 8, entry 5) demonstrated a tensile strength of 78.5 MPa, significantly outperforming both cellulose and starch-based bioplastics, which had tensile strengths of 45.0 MPa and 9.2 MPa, respectively. It also showed flexibility

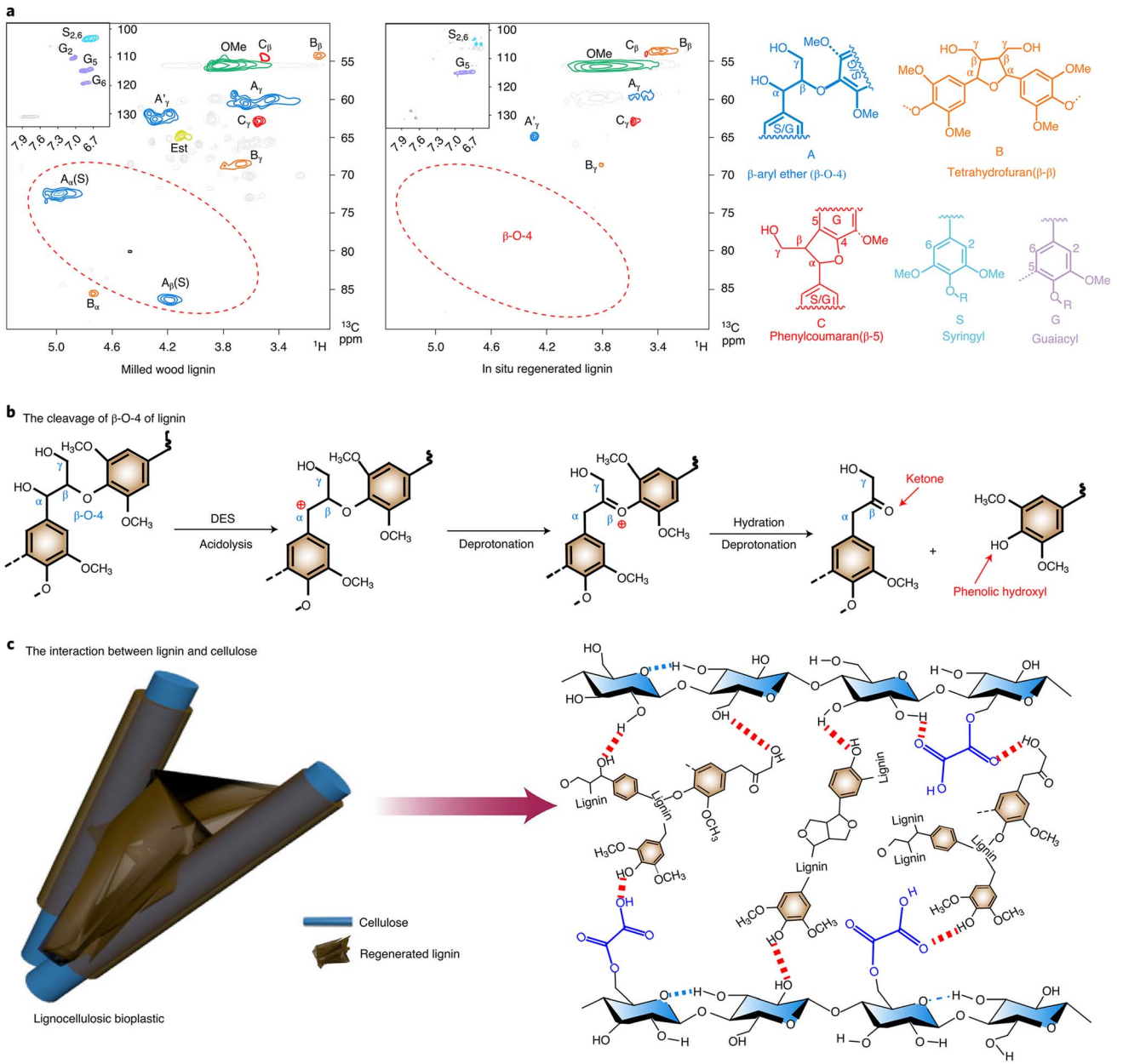

Fig. 14 The structure of the regenerated lignin and the interaction between the regenerated lignin and cellulose. (a) 2D-HSQC NMR spectra of MWL and the regenerated lignin: aliphatic regions (δ_C/δ_H 50–90/3.0–5.5) and aromatic regions (δ_C/δ_H 95–135/6.3–8.0). (b) The mechanism of cleaving the lignin β-O-4 bonds during DES treatment, resulting in the formation of a Hibbert's ketone and phenol hydroxyl group. (c) The structural linkages between regenerated lignin and cellulose. Preprinted from ref. 130 with permission from Springer Nature, copyright 2021.

with an elongation at break of 17.2% and toughness of 9.7 MJ m^{-3}. The whole corn bioplastic maintained a wet mechanical strength of 56.6 MPa, and exhibited excellent water resistance and thermal stability. At the end of life, it can be mechanically recycled or fully biodegraded in soil to return nutrients (Zn^{2+}, Al^{3+}, and organics) to the ecosystem (Fig. 13(a)). Zhou *et al.* employed another binary salt solution composed of 70 wt% $ZnCl_2/CaCl_2$ to dissolve 2.6 wt% corncob residues (CRs), followed by ultrasonic homogenization, casting, ethanol regeneration, and hot-pressing at 60 °C.[129] During dissolution and deconstruction, the exposure of lignin's phenolic hydroxyl groups enabled extensive hydrogen bond formation and entangled networks, significantly enhancing the material's mechanical properties. Residual metal ions further facilitated hydrogen bond network reconstruction. The resulting bioplastic (Table 8, entry 6) exhibited exceptional mechanical strength, with a tensile strength of 136 MPa and toughness of 9.36 MJ m^{-3}—38 and 9.8 times higher than those of pure cellulose films, respectively. It demonstrated superior water stability, maintaining structural integrity after two months of immersion and displaying a water contact angle of 108.4°. The material also showed minimal swelling (<4 wt%) in common organic solvents over 48 h at room temperature. The high thermal stability was demonstrated by the decomposition onset at approximately 310 °C. The bioplastic began degrading in soil within 18 days and fully biodegraded within four months. A closed-loop recycling process was achieved by dissolving the used material in the metal salt solution and remolding it into new sheets. LCA confirmed the bioplastic's significantly lower environmental impact compared to conventional plastics (PVF, ABS, and PET), particularly in abiotic depletion (fossil fuels), global warming potential, and eutrophication potential. The advantages stem from low-cost, sustainable raw materials and the low carbon footprint of the $ZnCl_2/CaCl_2$ dissolution–regeneration process.

Compared to chloride salt systems, DES systems enable more controlled and selective cleavage of lignin's β-O-4 ether bonds under acidic conditions, thereby efficiently dissolving lignin and exposing additional phenolic hydroxyl groups to facilitate extensive hydrogen bonding with cellulose. The Hu group demonstrated a facile *in situ* lignin regeneration strategy using a choline chloride/oxalic acid DES to process poplar wood powder at 110 °C.[130] The DES system effectively disrupted inter-fiber hydrogen bonding, promoted cellulose fibrillation, and cleaved β-O-4 linkages to solubilize lignin. This structural evolution was confirmed by 2D HSQC NMR (Fig. 14(a)), which showed that β-O-4 linkages were largely cleaved in regenerated lignin while the aromatic units were preserved. As illustrated in Fig. 14(b), the acid-catalyzed β-O-4 scission, followed by deprotonation and hydration steps, generated phenolic hydroxyl and ketone groups with higher reactivity. Upon water-induced regeneration (Fig. 14(c)), uniform lignin deposition occurred on cellulose micro/nanofibrils, forming a dense network where lignin acts as a natural binder. This interaction created a highly entangled lignin–cellulose network, enabling direct room-temperature casting of the high-solid-content slurry into continuous bioplastic films up to 360 cm^2 per batch. It was revealed that the regenerated lignin exposed its phenolic hydroxyl groups, facilitating strong hydrogen bonding with cellulose fibers to increase the mechanical and thermal performance. The coexistence of hydrophilic and hydrophobic groups in lignin further improved water resistance and mechanical performance. The resulting bioplastic (Table 8, entry 7) exhibited an exceptional tensile strength of ~128 MPa, significantly surpassing pure cellulose films, along with long-term water stability (30 days), low water absorption, and an excellent water contact angle. Thermal stability was demonstrated by decomposition at approximately 357 °C, higher than many conventional plastics. The abundant carbonyl and phenolic hydroxyl groups in the regenerated lignin endowed the bioplastic with superior UV-screening ability. The material also demonstrated full biodegradation within 3 months and mechanical recyclability, with the DES solvent being reusable across cycles. More recently, Yang *et al.* developed a ternary DES system (choline chloride/oxalic acid/resorcinol) to directly activate lignin within wood powder (*e.g.*, bagasse, peanut shells, and xylose residues) through *in situ* phenolization.[124] Under mildly acidic conditions at 120 °C, the DES facilitated β-O-4 ether cleavage and benzylic carbocation formation, enabling resorcinol to electrophilically trap lignin side chains. This process significantly increased the phenolic-OH content to 10.43 mmol g^{-1} (approximately 14 times higher than that of native milled-wood lignin), while simultaneously isolating high-purity cellulose (>99%). The phenolized lignin self-assembled into uniform nanospheres that (i) interlocked with cellulose fibrils through dense hydrogen-bond networks to dissipate fracture energy and (ii) acted as *in situ* reductants and hosts for uniformly distributed Ag nanoparticles, imparting antimicrobial properties. The resulting Ph-bioplastic (Table 8, entry 8) exhibited exceptional mechanical performance, with a tensile strength of ~160 MPa, strain of ~18% and toughness of ~20 MJ m^{-3}, surpassing conventional lignin-modified analogues. The material also demonstrated excellent UV screening, an outstanding oxygen barrier, and ~35% lower CO_2 permeability than cellulose-only films. Hydrostability improved significantly due to the aromatic, phenol-rich lignin phase restricting cellulose swelling. The bioplastic exhibited pronounced antioxidant activity and clear antimicrobial effects. The films are reprocessable and biodegradable, with excellent properties for food-preservation packaging.

Overall, for the construction of physical crosslinked networks *via* the dissolution–regeneration strategy, chloride salt and DES systems are regarded as efficient and greener media for developing bioplastics with balanced high strength, water resistance, and thermal stability. Mixed chloride salts dissolve whole biomass and, upon ethanol regeneration, yield films with substantially higher ductility, though an additional hot-pressing step is typically required. In contrast, DES systems act as multifunctional solvents that enable selective lignin depolymerization and uniform redeposition while promoting cellulose fibrillation, thereby fabricating films with the best overall performance. Furthermore, DES supports scalable production (*via* large-volume slurries and large-area sheets

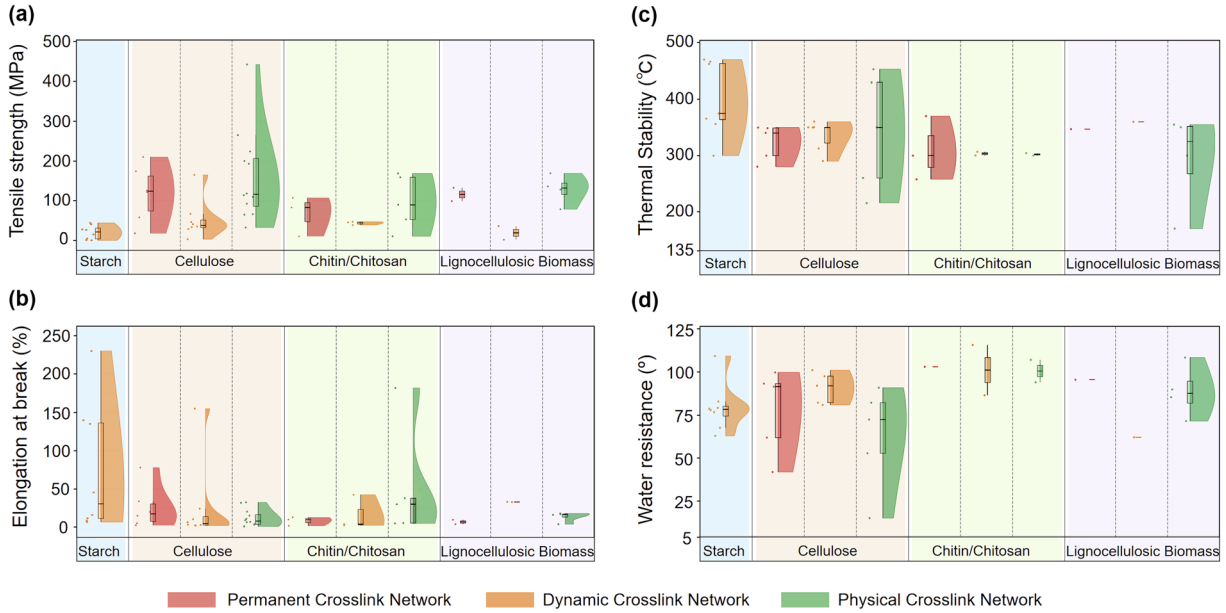

Scheme 4 Representative material properties of permanent, dynamic, and physical crosslinked bioplastic networks across various biopolymers and raw biomass. (a) Tensile strength; (b) elongation at break; (c) thermal stablity; (d) water resistance.

formed by simple casting) and closed-loop recyclability with solvent reusability.

6. Summary and outlook

6.1 Summary

The polymer-level structural engineering framework represents an important advancement from the passive blending of biopolymers to an active network design approach for bioplastic production. By modifying the native hydrogen-bonded networks of biopolymers, reducing crystallinity, and introducing controlled crosslinking domains, this strategy enhances segmental mobility, expedites viscoelastic relaxation and improves processability. These molecular-level adjustments can translate into greater ductility and toughness, while precise control over network chemistry and crosslink density contributes to the maintenance of the retention of mechanical integrity tailored to diverse application needs.

We systematically compared the key material properties summarized in Tables 1–8 and visualized them in Scheme 4, focusing on mechanical performance (tensile strength, Scheme 4(a); elongation at break, Scheme 4(b)) and environmental resistance (thermal stability, Scheme 4(c); water resistance, Scheme 4(d)), for which quantitative metrics are widely reported in the literature. Complementing these measurable properties, we also qualitatively evaluated lifecycle-related attributes, including reprocessability, recyclability, and biodegradability, to synthesize heterogeneous experimental evidence and assess the overall sustainability potential of each network architecture. Structurally, each engineered crosslinked network exhibits a distinct set of trade-offs, which determines its performance profile and application suitability.

Permanent crosslinked networks (Scheme 4, the red section) are constructed *via* irreversible covalent linkages, and they generally deliver high mechanical strength, dimensional stability, and solvent resistance, and in some cases approach the strength level of engineering plastics. For example, permanent crosslinked cellulose films reported in our dataset reach tensile strengths above 210 MPa and up to ~303 MPa, outperforming typical commodity plastics such as polyethylene (PE, ~10–30 MPa) and polypropylene (PP, ~30–40 MPa), and matching commonly reported ranges for petroleum-based products (*e.g.*, biaxially oriented PET films and PA6 grades). However, this robustness comes with a clear end-of-life trade-off: the high bond energy and stable crosslink density limit reprocessing and can slow down biodegradation. Chemical recycling can be feasible, but it often requires energy-intensive and chemically demanding conditions. As a result, their industrial potential is predominantly favored in sectors requiring long-term durability and structural integrity, where the benefits of superior performance may outweigh the challenges associated with recycling.

Dynamic crosslinked networks (Scheme 4, the orange section) feature exchangeable bonds that can partially decouple processability from performance. Such networks enable a balance between thermoset-like robustness and thermoplastic-like reprocessability. For instance, starch-based polyimine vitrimers achieve tensile strengths around ~40 MPa, comparable to commercial PP (~30–40 MPa). Cellulose-based vitrimers commonly fall in the ~40–70 MPa range, while hybrid strategies (*e.g.*, introducing aminated lignin into the dynamic network) can elevate tensile strength to >160 MPa in representative studies, allowing competition with higher-performance plastics. This self-adaptability, however, introduces a stability trade-off: faster bond exchange that

promotes healing and reprocessing may increase unwanted deformation under sustained load. Additionally, the synthesis often necessitates precise stoichiometric control, frequently relying on costly crosslinkers and organic solvents, thus potentially limiting their overall environmental profile. Furthermore, achieving efficient recyclability often relies on activating the dynamic bond exchange above a certain energetic threshold, which may involve significant energy input during reprocessing. Therefore, their industrial feasibility currently appears most viable in high-value applications requiring extended service life (*e.g.*, self-healing or smart adaptability), where the functional benefits tend to justify the higher material and processing costs.

Physical crosslinked networks (Scheme 4, the green section) rely on reversible non-covalent interactions that allow eco-efficient processing (*e.g.*, hydroplasticity) and typically preserve strong end-of-life benefits such as biodegradability. Although historically considered mechanically weaker due to the absence of covalent bonds, recent structural designs have substantially narrowed this gap. With reinforcement by external hydrogen-bonding donors or interpenetrating secondary networks, reported tensile strengths can exceed 200 MPa for lignin–cellulose composites and reach up to ~442 MPa for optimized dual-network systems, approaching or even surpassing robust petrochemical plastics in strength. The key limitation is environmental resilience. Strong stimuli-responsiveness is often associated with weaker long-term water/solvent resistance and thermal stability than that of covalent systems, which may compromise property retention during service. For example, humidity can act as a plasticizer and accelerate mechanical degradation over time. Consequently, their industrial feasibility is most promising for high-volume, short-cycle applications (such as disposable packaging or agricultural films), where their low-energy manufacturing and enhanced end-of-life options offer a distinct competitive edge over persistent plastics. This inherent advantage in low-cost, scalable processing often appears to afford the greatest near-term commercialization potential among the three structural engineering approaches.

Beyond network architecture, the intrinsic biopolymer strongly defines the performance baseline. Mechanically, starch-based bioplastics typically show the lowest tensile strength (about 0.9–44 MPa) yet can exhibit high ductility, with some dynamic networks reaching elongations >200% (Scheme 4(a and b)). Chitosan-based systems are generally intermediate (≈11–90 MPa), while chitin-based materials can reach higher robustness (≈100–170 MPa) (Scheme 4(a and b)). Cellulose-based bioplastics display the broadest window, ranging from flexible vitrimers at the low end (3 MPa) to ultra-strong films reinforced by secondary networks at the high end (up to ~440 MPa). Lignocellulosic biomass-derived materials also show strong performance (*e.g.*, ~130 MPa in representative reports), possibly benefiting from the natural binding and stiffening effect of lignin (Scheme 4(a and b)). Thermally (Scheme 4(c)), many systems exhibit comparable stability, while specific structural features, such as aromatic units from lignin or P/Si-containing secondary networks, can further increase thermal thresholds. Regarding water resistance (Scheme 4(d)), starch and cellulose are inherently hydrophilic, whereas chitin/chitosan-based networks often show higher contact angles, frequently exceeding 100°. Finally, certain biopolymers offer distinct functional value: crosslinked cellulose networks can offer excellent dimensional stability (*e.g.*, low thermal expansion), while chitin/chitosan may impart intrinsic antibacterial potential, which is attractive for food-contact and preservation-related applications.

6.2 Outlook

Despite significant advances in converting biopolymers into bioplastics through polymer-level structural engineering, future efforts are expected to focus on addressing challenges in material design, scalable manufacturing, and end-of-life management to bridge the gap between laboratory research and commercial implementation.

At the material level, single-component biopolymers have seen progress, but they still struggle to simultaneously meet the mechanical and processing requirements for high-performance applications. To address this, it is important to establish crosslinked networks between different biopolymers or directly utilize multicomponent feedstocks. Such approaches can overcome individual limitations and combine complementary advantages. However, limited interfacial compatibility due to differences in polarity, crystallinity, and hydrophilicity can hinder performance. Therefore, future research will benefit from optimizing network architectures by designing amphiphilic compatibilizers or interface-active crosslinkers to ensure structural homogeneity and prevent phase separation in multicomponent systems.

At the manufacturing level, the challenge is to scale up the production of these bioplastics while maintaining cost-effectiveness and sustainability. Bench-scale solution casting continues to be widely used in the literature; however, this approach often necessitates the use of organic solvents and energy-intensive solvent removal steps, underscoring the need for more scalable, industrially relevant processing routes. Future efforts may emphasize the development of solvent-free reactive extrusion or rapid aqueous-phase processing techniques (*e.g.*, water-assisted molding or slurry casting) that are compatible with existing infrastructure (such as roll-to-roll papermaking or thermoplastic injection molding machinery).

At the end-of-life level, one of the key challenges involves the trade-off between in-service material performance and end-of-life biodegradability. Introducing a high density of crosslinking domains significantly enhances mechanical strength and environmental resistance. At the same time, however, excessive covalent locking may impair the inherent biodegradability of the biopolymer backbone and may introduce toxicity concerns if synthetic agents are used. Future structural engineering is therefore likely to utilize or develop bio-based crosslinkers that can provide necessary structural reinforcement while ensuring biodegradability under natural conditions. This approach can potentially address the trade-off between high performance and environmental sustainability.

Accordingly, given the material-, manufacturing-, and end-of-life challenges discussed above, multicomponent-based bioplastics are increasingly desirable. Such bioplastics can be achieved by rationally integrating distinct biopolymers or, more directly, by valorizing raw lignocellulosic biomass. For example, preserving the native "cellulose–hemicellulose–lignin" matrix can reduce fractionation costs and leverage the complementary roles of rigid polysaccharide skeletons and lignin as natural binders to maximize performance. Within this context, physical crosslinked networks are particularly promising, as they can deliver high initial mechanical robustness while remaining compatible with green, low-impact processing, aligning closely with circular-economy principles. Future work may therefore focus on improving their environmental stability to extend their use from short-lived consumables to more durable, high-value products without compromising circularity.

To conclude, polymer-level structural engineering provides a powerful platform to transform natural biopolymers into sustainable bioplastics. The combination of advances in material design, scalable manufacturing, and end-of-life management will largely shape whether bioplastics can reduce reliance on petroleum-based plastics and help drive progress toward carbon neutrality, waste reduction, and a circular economy.

Author contributions

Xinlei Ji: investigation, conceptualization, visualization, and writing – original draft. Keyi Zhou: investigation, visualization, and writing – review & editing. My Ha Tran: investigation and writing – review & editing. Xi Chen: conceptualization, writing – review & editing, funding acquisition, project administration, and supervision. Ning Yan: conceptualization, writing – review & editing, funding acquisition, project administration, and supervision.

Conflicts of interest

There are no conflicts to declare.

Data availability

No primary research results, software or code have been included and no new data were generated or analysed as part of this review.

Acknowledgements

X. Chen thanks the National Natural Science Foundation of China (No. 22578269) and the Science and Technology Commission of Shanghai Municipality (Shanghai Sci-tech Co-research Program, 25HB2712100) for the financial support. M. H. Tran and N. Yan thank the Agency for Science, Technology and Research (A*STAR) MTC Programmatic Project: "Developing Liquid Wood Resin for Sustainable Specialty Polymers" for the financial support.

References

1 K. Lee, Y. Jing, Y. Wang and N. Yan, A unified view on catalytic conversion of biomass and waste plastics, *Nat. Rev. Chem.*, 2022, **6**, 635–652.
2 F. Vidal, E. R. van der Marel, R. W. F. Kerr, C. McElroy, N. Schroeder, C. Mitchell, G. Rosetto, T. T. D. Chen, R. M. Bailey, C. Hepburn, C. Redgwell and C. K. Williams, Designing a circular carbon and plastics economy for a sustainable future, *Nature*, 2024, **626**, 45–57.
3 A. Stubbins, K. L. Law, S. E. Muñoz, T. S. Bianchi and L. Zhu, Plastics in the Earth system, *Science*, 2021, **373**, 51–55.
4 J. R. Jambeck and I. Walker-Franklin, The impacts of plastics' life cycle, *One Earth*, 2023, **6**, 600–606.
5 D. Rossetto, The relative importance of carbon markets to the waste management sector's future contribution to climate change commitments under the Paris agreement: insights from Australia, *Carbon Neutrality*, 2023, **2**, 25.
6 H. Ran, S. Zhang, W. Ni and Y. Jing, Precise activation of C–C bonds for recycling and upcycling of plastics, *Chem. Sci.*, 2024, **15**, 795–831.
7 P. J. Landrigan, S. Dunlop, M. Treskova, H. Raps, C. Symeonides, J. Muncke, M. Spring, J. Stegeman, B. C. Almroth, T. C. Chiles, M. Cropper, M. Deeney, L. Fuller, R. Geyer, R. Karasik, T. Mafira, A. Mangwiro, D. M. Matias, Y. Mulders, Y. Park, C. A. Velis, R. Vermeulen, M. Wagner, Z. Wang, E. M. Whitman, T. J. Woodruff and J. Rocklöv, The Lancet Countdown on health and plastics, *Lancet*, 2025, **406**, 1044–1062.
8 N. G. Posnack, Plastics and cardiovascular disease, *Nat. Rev. Cardiol.*, 2021, **18**, 69–70.
9 T. H. Epps III, L. T. J. Korley, T. Yan, K. L. Beers and T. M. Burt, Sustainability of Synthetic Plastics: Considerations in Materials Life-Cycle Management, *JACS Au*, 2022, **2**, 3–11.
10 B. Zhao, H. Tan, J. Yang, X. Zhang, Z. Yu, H. Sun, J. Wei, X. Zhao, Y. Zhang, L. Chen, D. Yang, J. Deng, Y. Fu, Z. Huang and N. Jiao, Catalytic conversion of mixed polyolefins under mild atmospheric pressure, *Innovation*, 2024, **5**, 100586.
11 X. Chen and N. Yan, A brief overview of renewable plastics, *Mater. Today Sustain.*, 2020, **7–8**, 100031.
12 T. Yan, A. H. Balzer, K. M. Herbert, T. H. Epps and L. T. J. Korley, Circularity in polymers: addressing performance and sustainability challenges using dynamic covalent chemistries, *Chem. Sci.*, 2023, **14**, 5243–5265.
13 P. Bharmoria, S. Ghasemi, F. Edhborg, R. Losantos, Z. Wang, A. Mårtensson, M.-a. Morikawa, N. Kimizuka, Ü. İşci, F. Dumoulin, B. Albinsson and K. Moth-Poulsen, Far-red triplet sensitized Z-to-E photoswitching of azobenzene in bioplastics, *Chem. Sci.*, 2022, **13**, 11904–11911.
14 B. Zhao, Z. Hu, Y. Sun, R. Hajiayi, T. Wang and N. Jiao, Selective Upcycling of Polyolefins into High-Value Nitrogenated Chemicals, *J. Am. Chem. Soc.*, 2024, **146**, 28605–28611.

15 L. T. Hao, S. Ju, D. K. Hwang, D. S. Hwang, Y. S. Ok, S. Y. Hwang, H. J. Kim, H. Jeon, J. Park, D. X. Oh and J. M. Koo, Optimizing bioplastics translation, *Nat. Rev. Bioeng.*, 2024, **2**, 289–304.
16 M. MacLeod, H. P. H. Arp, M. B. Tekman and A. Jahnke, The global threat from plastic pollution, *Science*, 2021, **373**, 61–65.
17 S. R. Nicholson, N. A. Rorrer, A. C. Carpenter and G. T. Beckham, Manufacturing energy and greenhouse gas emissions associated with plastics consumption, *Joule*, 2021, **5**, 673–686.
18 J. Lee, E. E. Kwon, S. S. Lam, W.-H. Chen, J. Rinklebe and Y.-K. Park, Chemical recycling of plastic waste via thermocatalytic routes, *J. Clean. Prod.*, 2021, **321**, 128989.
19 E. T. C. Vogt and B. M. Weckhuysen, The refinery of the future, *Nature*, 2024, **629**, 295–306.
20 H. Li, H. A. Aguirre-Villegas, R. D. Allen, X. Bai, C. H. Benson, G. T. Beckham, S. L. Bradshaw, J. L. Brown, R. C. Brown, V. S. Cecon, J. B. Curley, G. W. Curtzwiler, S. Dong, S. Gaddameedi, J. E. García, I. Hermans, M. S. Kim, J. Ma, L. O. Mark, M. Mavrikakis, O. O. Olafasakin, T. A. Osswald, K. G. Papanikolaou, H. Radhakrishnan, M. A. S. Castillo, K. L. Sánchez-Rivera, K. N. Tumu, R. C. Van Lehn, K. L. Vorst, M. M. Wright, J. Wu, V. M. Zavala, P. Zhou and G. W. Huber, Expanding plastics recycling technologies: chemical aspects, technology status and challenges, *Green Chem.*, 2022, **24**, 8899–9002.
21 Q. Wu, Acidic and basic catalytic cracking technologies and its development prospects for crude oil to chemicals, *Fuel*, 2023, **332**, 126132.
22 M. Bachmann, C. Zibunas, J. Hartmann, V. Tulus, S. Suh, G. Guillén-Gosálbez and A. Bardow, Towards circular plastics within planetary boundaries, *Nat. Sustain.*, 2023, **6**, 599–610.
23 H. Li, H. A. Aguirre-Villegas, R. D. Allen, X. Bai, C. H. Benson, G. T. Beckham, S. L. Bradshaw, J. L. Brown, R. C. Brown, V. S. Cecon, J. B. Curley, G. W. Curtzwiler, S. Dong, S. Gaddameedi, J. E. Estela-García, I. Hermans, M. S. Kim, J. Ma, L. O. Mark, M. Mavrikakis, O. O. Olafasakin, T. A. Osswald, K. G. Papanikolaou, H. Radhakrishnan, M. A. S. Castillo, K. L. Sánchez-Rivera, K. N. Tumu, R. C. Van Lehn, K. L. Vorst, M. M. Wright, J. Wu, V. M. Zavala, P. Zhou and G. W. Huber, Correction: expanding plastics recycling technologies: chemical aspects, technology status and challenges, *Green Chem.*, 2022, **24**, 9329.
24 J. Li, H. Jiang, Q. Zhou, C. Qi, M. Palocz-Andresen, Y. Zhu, Z. Bi, W. Cao, Z. Yuan and Z. Lou, Best available technology options for the mitigation of environmental impacts in waste plastics, *Carbon Neutrality*, 2024, **3**, 29.
25 J. Song, C. Rao, Z. Zhang, X. Yang and Y. Zhang, CdS quantum dots with sulfur defects for photoreforming plastics into valuable chemicals coupled with hydrogen production, *Mol. Catal.*, 2025, **579**, 115049.
26 F. D. Bobbink, A. van Muyden, W.-T. Lee and P. J. Dyson, A Semi-Serendipitous Journey towards the Commercialisation of a Catalytic Hydrocracking Process for Polymer Waste, *ChemPlusChem*, 2022, **87**, e202200012.
27 C. Matthews, F. Moran and A. K. Jaiswal, A review on European Union's strategy for plastics in a circular economy and its impact on food safety, *J. Clean. Prod.*, 2021, **283**, 125263.
28 N. S. K. Baharin, S. Cherdkeattikul, N. Kanada, H. Hara, S. Mizuno, T. Sawai, M. Fuchihata and T. Ida, Impact and effectiveness of Bio-Coke conversion from biomass waste as alternative source of coal coke in Southeast Asia, *J. Mater. Cycles Waste Manag.*, 2023, **25**, 17–36.
29 N. Song, I. McLellan, W. Liu, Z. Wang and A. Hursthouse, The waste ban in China: what happened next? Assessing the impact of new policies on the waste management sector in China, *Environ. Geochem. Health*, 2023, **45**, 1117–1131.
30 J.-G. Rosenboom, R. Langer and G. Traverso, Bioplastics for a circular economy, *Nat. Rev. Mater.*, 2022, **7**, 117–137.
31 X. Chen, S. Song, H. Li, G. Gözaydın and N. Yan, Expanding the Boundary of Biorefinery: Organonitrogen Chemicals from Biomass, *Acc. Chem. Res.*, 2021, **54**, 1711–1722.
32 S. Feng, P. T. T. Nguyen, X. Ma and N. Yan, Photorefinery of Biomass and Plastics to Renewable Chemicals using Heterogeneous Catalysts, *Angew. Chem., Int. Ed.*, 2024, **63**, e202408504.
33 H. Cui, X. Chen, X. She, W.-X. Su, S.-C. Chen and X. Zhang, A pair of strongly reductive and oxidative photocatalysts for the general upcycling of biomass derivatives and plastic wastes, *Chem. Sci.*, 2025, **16**, 16070–16080.
34 J. Gong, N. J. English, D. Pant, G. R. Patzke, S. Protti and T. Zhang, Power-to-X: Lighting the Path to a Net-Zero-Emission Future, *ACS Sustain. Chem. Eng.*, 2021, **9**, 7179–7181.
35 Z. Sun, L. Zeng, C. K. Russell, S. Assabumrungrat, S. Chen, L. Duan, W. Xiang and J. Gong, Solar–Wind–Bio Ecosystem for Biomass Cascade Utilization with Multigeneration of Formic Acid, Hydrogen, and Graphene, *ACS Sustain. Chem. Eng.*, 2019, **7**, 2558–2568.
36 S. Yang, S. Du, J. Zhu and S. Ma, Closed-loop recyclable polymers: from monomer and polymer design to the polymerization–depolymerization cycle, *Chem. Soc. Rev.*, 2024, **53**, 9609–9651.
37 A. S. Narmon, A. Dewaele, K. Bruyninckx, B. F. Sels, P. Van Puyvelde and M. Dusselier, Boosting PLA melt strength by controlling the chirality of co-monomer incorporation, *Chem. Sci.*, 2021, **12**, 5672–5681.
38 W.-T. Lee, A. van Muyden, F. D. Bobbink, M. D. Mensi, J. R. Carullo and P. J. Dyson, Mechanistic classification and benchmarking of polyolefin depolymerization over silica-alumina-based catalysts, *Nat. Commun.*, 2022, **13**, 4850.
39 R. M. Cywar, N. A. Rorrer, C. B. Hoyt, G. T. Beckham and E. Y. X. Chen, Bio-based polymers with performance-advantaged properties, *Nat. Rev. Mater.*, 2022, **7**, 83–103.
40 C. Jehanno, J. W. Alty, M. Roosen, S. De Meester, A. P. Dove, E. Y. X. Chen, F. A. Leibfarth and H. Sardon, Critical

advances and future opportunities in upcycling commodity polymers, *Nature*, 2022, **603**, 803–814.
41 Y. Zhu, C. Romain and C. K. Williams, Sustainable polymers from renewable resources, *Nature*, 2016, **540**, 354–362.
42 X. Zhao, Y. Wang, X. Chen, X. Yu, W. Li, S. Zhang, X. Meng, Z.-M. Zhao, T. Dong, A. Anderson, A. Aiyedun, Y. Li, E. Webb, Z. Wu, V. Kunc, A. Ragauskas, S. Ozcan and H. Zhu, Sustainable bioplastics derived from renewable natural resources for food packaging, *Matter*, 2023, **6**, 97–127.
43 Z. Wang, C. Xu, L. Qi and C. Chen, Chemical modification of polysaccharides for sustainable bioplastics, *Trends Chem.*, 2024, **6**, 314–331.
44 A. Surendren, A. K. Mohanty, Q. Liu and M. Misra, A review of biodegradable thermoplastic starches, their blends and composites: recent developments and opportunities for single-use plastic packaging alternatives, *Green Chem.*, 2022, **24**, 8606–8636.
45 M. T. P. Nguyen, M. Escribà-Gelonch, V. Hessel and B. R. Coad, A Review of the Current and Future Prospects for Producing Bioplastic Films Made from Starch and Chitosan, *ACS Sustain. Chem. Eng.*, 2024, **12**, 1750–1768.
46 L. Chen, L. Yu, L. Qi, S. J. Eichhorn, A. Isogai, E. Lizundia, J. Y. Zhu and C. Chen, Cellulose nanocomposites by supramolecular chemistry engineering, *Nat. Rev. Mater.*, 2025, **10**, 728–749.
47 S. Jing, L. Wu, A. P. Siciliano, C. Chen, T. Li and L. Hu, The Critical Roles of Water in the Processing, Structure, and Properties of Nanocellulose, *ACS Nano*, 2023, **17**, 22196–22226.
48 T. Li, C. Chen, A. H. Brozena, J. Y. Zhu, L. Xu, C. Driemeier, J. Dai, O. J. Rojas, A. Isogai, L. Wågberg and L. Hu, Developing fibrillated cellulose as a sustainable technological material, *Nature*, 2021, **590**, 47–56.
49 J. Song, C. Chen, S. Zhu, M. Zhu, J. Dai, U. Ray, Y. Li, Y. Kuang, Y. Li, N. Quispe, Y. Yao, A. Gong, U. H. Leiste, H. A. Bruck, J. Y. Zhu, A. Vellore, H. Li, M. L. Minus, Z. Jia, A. Martini, T. Li and L. Hu, Processing bulk natural wood into a high-performance structural material, *Nature*, 2018, **554**, 224–228.
50 L. Bai, L. Liu, M. Esquivel, B. L. Tardy, S. Huan, X. Niu, S. Liu, G. Yang, Y. Fan and O. J. Rojas, Nanochitin: Chemistry, Structure, Assembly, and Applications, *Chem. Rev.*, 2022, **122**, 11604–11674.
51 J. Jin, B. Luo, S. Xuan, P. Shen, P. Jin, Z. Wu and Y. Zheng, Degradable chitosan-based bioplastic packaging: design, preparation and applications, *Int. J. Biol. Macromol.*, 2024, **266**, 131253.
52 X. Lin, Y. Feng, Q. Jia, K. Jiang, J. Xiang, L. Chen, P. Chen, A. Zheng and B. Duan, Competing Self-Assembly to Access Helical Chitin Nanofibers for Advanced Chitinous Materials, *Adv. Funct. Mater.*, 2025, **35**, 2503547.
53 X. Shi, X. Ye, H. Zhong, T. Wang and F. Jin, Sustainable nitrogen-containing chemicals and materials from natural marine resources chitin and microalgae, *Mol. Catal.*, 2021, **505**, 111517.
54 Y. Qiu, D. Zhang, M. Long, Z. Zhou, C. Gao, S. Ma, J. Qin, K. Chen, C. Chen, Z. Zhao and H. Deng, Coassembly of hybrid microscale biomatter for robust, water-processable, and sustainable bioplastics, *Sci. Adv.*, 2025, **11**, eadr1596.
55 C. Liu, P. Luan, Q. Li, Z. Cheng, X. Sun, D. Cao and H. Zhu, Biodegradable, Hygienic, and Compostable Tableware from Hybrid Sugarcane and Bamboo Fibers as Plastic Alternative, *Matter*, 2020, **3**, 2066–2079.
56 X. Chen, F. Chen, H. Jiang, J. Wang, Y. X. Li and G. Wang, Replacing Plastic with Bamboo: Eco-Friendly Disposable Tableware Based on the Separation of Bamboo Fibers and the Reconstruction of Their Network Structure, *ACS Sustain. Chem. Eng.*, 2023, **11**, 7407–7418.
57 P. B. V. Scholten and M. B. Figueirêdo, Back to the Future with Biorefineries: Bottom-Up and Top-Down Approaches toward Polymers and Monomers, *Macromol. Chem. Phys.*, 2022, **223**, 2200017.
58 S. Yang, Y. Li, M. Nie, X. Liu, Q. Wang, N. Chen and C. Zhang, Lifecycle Management for Sustainable Plastics: Recent Progress from Synthesis, Processing to Upcycling, *Adv. Mater.*, 2024, **36**, 2404115.
59 S. L. Nordahl and C. D. Scown, Recommendations for life-cycle assessment of recyclable plastics in a circular economy, *Chem. Sci.*, 2024, **15**, 9397–9407.
60 X. Liu, Y. Li, X. Fang, Z. Zhang, S. Li and J. Sun, Healable and Recyclable Polymeric Materials with High Mechanical Robustness, *ACS Mater. Lett.*, 2022, **4**, 554–571.
61 A. K. Mohanty, F. Wu, R. Mincheva, M. Hakkarainen, J.-M. Raquez, D. F. Mielewski, R. Narayan, A. N. Netravali and M. Misra, Sustainable polymers, *Nat. Rev. Methods Primers*, 2022, **2**, 46.
62 W. Si and S. Zhang, The green manufacturing of thermoplastic starch for low-carbon and sustainable energy applications: a review on its progress, *Green Chem.*, 2024, **26**, 1194–1222.
63 C. Li, B. Ju and S. Zhang, Fully bio-based hydroxy ester vitrimer synthesized by crosslinking epoxidized soybean oil with doubly esterified starch, *Carbohydr. Polym.*, 2023, **302**, 120442.
64 W. Zhang, T. Zhang, Y. Zhong, Y. Zhang, L. Wang, F. Zhu, X. Wang, L. Zhou and X. Zhou, Dynamic borate ester bond reinforced hydroxyethyl cellulose/corn starch crosslinked film for simple recycling and regeneration, *Int. J. Biol. Macromol.*, 2024, **279**, 135231.
65 H. Zhang, Z. Su and X. Wang, Starch-Based Rehealable and Degradable Bioplastic Enabled by Dynamic Imine Chemistry, *ACS Sustain. Chem. Eng.*, 2022, **10**, 8650–8657.
66 X. Zhang, H. Zhang, G. Zhou, Z. Su and X. Wang, Flexible, thermal processable, self-healing, and fully bio-based starch plastics by constructing dynamic imine network, *Green Energy Environ.*, 2024, **9**, 1610–1618.
67 Y. Ding, D. Liu, Y. Sun, S. Liu, P. Wang, S. Wang, D. Huang and J. Ji, Dynamic Imine Bond-Enabled Starch-Based Materials with Self-Healing and Recycling Properties, *ACS Sustain. Chem. Eng.*, 2025, **13**, 6388–6398.

68 G. Zhou, X. Zhang, Z. Lei, H. Zhou and X. Wang, Dynamic imine crosslinking for waterproof starch plastic with tunable mechanical properties, *Int. J. Biol. Macromol.*, 2024, **282**, 136872.
69 A. Etale, A. J. Onyianta, S. R. Turner and S. J. Eichhorn, Cellulose: A Review of Water Interactions, Applications in Composites, and Water Treatment, *Chem. Rev.*, 2023, **123**, 2016–2048.
70 K. S. Salem, N. K. Kasera, M. A. Rahman, H. Jameel, Y. Habibi, S. J. Eichhorn, A. D. French, L. Pal and L. A. Lucia, Comparison and assessment of methods for cellulose crystallinity determination, *Chem. Soc. Rev.*, 2023, **52**, 6417–6446.
71 W. Deng, Y. Feng, J. Fu, H. Guo, Y. Guo, B. Han, Z. Jiang, L. Kong, C. Li, H. Liu, P. T. T. Nguyen, P. Ren, F. Wang, S. Wang, Y. Wang, Y. Wang, S. S. Wong, K. Yan, N. Yan, X. Yang, Y. Zhang, Z. Zhang, X. Zeng and H. Zhou, Catalytic conversion of lignocellulosic biomass into chemicals and fuels, *Green Energy Environ.*, 2023, **8**, 10–114.
72 D. Li, Y. Yang, A. L. Elias, N. Yan and F. Guo, Biopolymer Composites Material Extrusion and their Applications: A Review, *Adv. Eng. Mater.*, 2023, **25**, 2301048.
73 Y. Qian, C. Qin, J. Zhang, B. Shi, Y. Wei, C. Wang, J. Niu, S. Kang, G. Chen and Y. Liu, Sustainable, biodegradable, and recyclable bioplastics derived from renewable carboxymethyl cellulose and waste walnut shell, *Int. J. Biol. Macromol.*, 2025, **299**, 140130.
74 Y. Chen, C. Huang, Z. Miao, Y. Gao, Y. Dong, K. C. Tam and H.-Y. Yu, Tailoring Hydronium ion Driven Dissociation-Chemical Cross-Linking for Superfast One-Pot Cellulose Dissolution and Derivatization to Build Robust Cellulose Films, *ACS Nano*, 2024, **18**, 8754–8767.
75 Y. Gao, G. Chen, C. Wu, J. Zhou, G. Jin and H.-Y. Yu, Thioctic acid driven chemical cross-linking of cellulose chains for fabricating high-performance cellulose films as food packaging, *Int. J. Biol. Macromol.*, 2025, **318**, 145076.
76 L. Hu, Y. Zhong, S. Wu, P. Wei, J. Huang, D. Xu, L. Zhang, Q. Ye and J. Cai, Biocompatible and biodegradable super-toughness regenerated cellulose via water molecule-assisted molding, *Chem. Eng. J.*, 2021, **417**, 129229.
77 X. Li, X. Li, W. Ma and J. Ma, An in-situ dissolving-co-crosslinking strategy for fabricating high-strength, wet-stable, and biocompatible multiscale cellulosic paper-based plastics, *Carbohydr. Polym.*, 2025, **355**, 123347.
78 K. Lee, Y. Jeon, D. Kim, G. Kwon, U.-J. Kim, C. Hong, J. W. Choung and J. You, Double-crosslinked cellulose nanofiber based bioplastic films for practical applications, *Carbohydr. Polym.*, 2021, **260**, 117817.
79 G. Zhou, H. Zhang, Z. Su, X. Zhang, H. Zhou, L. Yu, C. Chen and X. Wang, A Biodegradable, Waterproof, and Thermally Processable Cellulosic Bioplastic Enabled by Dynamic Covalent Modification, *Adv. Mater.*, 2023, **35**, 2301398.
80 Z. Su, L. Yu, L. Cui, G. Zhou, X. Zhang, X. Qiu, C. Chen and X. Wang, Reconstruction of Cellulose Intermolecular Interactions from Hydrogen Bonds to Dynamic Covalent Networks Enables a Thermo-processable Cellulosic Plastic with Tunable Strength and Toughness, *ACS Nano*, 2023, **17**, 21420–21431.
81 Z. Su, L. Cui, H. Zhang, L. Xiao, B. Chi, H. Xu, L. Ning, S. Jia and X. Wang, Robust, waterproof, and degradable cellulose-based polyimine vitrimer for plastic replacement, *Chem. Eng. J.*, 2023, **471**, 144501.
82 Y. He, H. Ye, H. Li, F. Cui, F. Xu and T. You, Multifunctional films with superior mechanical performance, transparency, antibacterial properties enabled by a physical and chemical dual crosslinking network construction, *Chem. Eng. J.*, 2024, **479**, 147546.
83 T. Han, Y. Huang, S. Zhang and B. Ju, Fully biomass reprocessable thermoset plastics based on acetals dynamic covalent bonds, *React. Funct. Polym.*, 2025, **214**, 106281.
84 X. Zhang, P. Li, J. Zeng, J. Su, J. Xu, J. Li, B. Wang, W. Gao and K. Chen, Dynamically Crosslinking Cellulose Nanofibers and Epoxy Soybean Oil toward Tough, Recyclable, and Degradable Bioplastics, *ACS Sustain. Chem. Eng.*, 2024, **12**, 18174–18186.
85 C. Li, X. Zhang, H. Chen, H. Wang, J. Huang, T. Li, S. Wang and W. Dong, Thermoformed, thermostable, waterproof and mechanically robust cellulose-based bioplastics enabled by dynamically reversible thia-Michael reaction, *Int. J. Biol. Macromol.*, 2025, **295**, 139567.
86 C. Li, B. Ju and S. Zhang, Twin-screw extrusion molding of a cellulose-based vitrimer containing a crosslinkable macromolecular plasticizer, *Int. J. Biol. Macromol.*, 2023, **225**, 1487–1493.
87 Z. Huang, H. Jia, A. P. v. Muyden, Z. Fei and P. J. Dyson, Sustainable, Reshapable Surfactant–Polyelectrolyte Plastics Employing Water as a Plasticizer, *ACS Appl. Mater. Interfaces*, 2019, **11**, 31311–31316.
88 J. J. Koh, X. Q. Koh, J. Y. Chee, S. Chakraborty, S. Y. Tee, D. Zhang, S. C. Lai, J. C. C. Yeo, J. W. J. Soh, P. Li, S. C. Tan, W. Thitsartarn and C. He, Reprogrammable, Sustainable, and 3D-Printable Cellulose Hydroplastic, *Adv. Sci.*, 2024, **11**, 2402390.
89 J. Wang, L. Emmerich, J. Wu, P. Vana and K. Zhang, Hydroplastic polymers as eco-friendly hydrosetting plastics, *Nat. Sustain.*, 2021, **4**, 877–883.
90 Z. Zeng, L. Yu, S. Yang, K. Guo, C. Xu, C. Chen and Z. Wang, Tuning water-cellulose interactions via copper-coordinated mercerization for hydro-actuated, shape-memory cellulosic hydroplastics, *Matter*, 2024, **7**, 3036–3052.
91 H. Sun, X. Fang, Y. Zhu, Z. Yu, X. Lu and J. Sun, Highly tough, degradable, and water-resistant bio-based supramolecular plastics comprised of cellulose and tannic acid, *J. Mater. Chem. A*, 2023, **11**, 7193–7200.
92 Z. Wang, Q. Bai, W. Wang, Y. Qing, Y. Li and J. Sun, Recyclable methylcellulose-based reversibly cross-linked hydroplastics with excellent environmental stability for use in flexible printed circuit boards capable of safe disposal, *Carbohydr. Polym.*, 2025, **359**, 123591.
93 Z. Wei, C. Cai, Y. Huang, P. Wang, J. Song, L. Deng and Y. Fu, Strong biodegradable cellulose materials with improved crystallinity via hydrogen bonding tailoring

strategy for UV blocking and antioxidant activity, *Int. J. Biol. Macromol.*, 2020, **164**, 27–36.

94 B. Jiang, C. Chen, Z. Liang, S. He, Y. Kuang, J. Song, R. Mi, G. Chen, M. Jiao and L. Hu, Lignin as a Wood-Inspired Binder Enabled Strong, Water Stable, and Biodegradable Paper for Plastic Replacement, *Adv. Funct. Mater.*, 2020, **30**, 1906307.

95 D. Wang, S. Shi, Y. Mao, L. Lei, S. Fu and J. Hu, Biodegradable Dual-Network Cellulosic Composite Bioplastic Metafilm for Plastic Substitute, *Angew. Chem., Int. Ed.*, 2023, **62**, e202310995.

96 J. Kim, W. Choi, H. Park, S. Jo, K. Park, H. Cho, Y. Oh, M. Choi, B. Choi, D. Y. Ryu, W.-G. Koh, S. Woo, S. Choi, T. Kwak, H. Kimm and J. Hong, Tunable Mechanical Properties in Biodegradable Cellulosic Bioplastics Achieved via Ring-Opening Polymerization, *ACS Nano*, 2025, **19**, 11961–11972.

97 S. Yang, D. Xie, R. Zhang, C. Zhang, S. Song, A. Yang, X. Liu and Y. Song, A multiple physical crosslinked cellulose-based bioplastics with robust mechanical and thermal stability, *Int. J. Biol. Macromol.*, 2024, **283**, 137610.

98 Y. Xu, C. Li, S. Yang, S. Wang, M. Li, J. Jin, Z. Jiang and F. Peng, Metal Ion Cross-Linked Cellulose/Lignin Nanocomposite Films: A Pathbreaking Approach toward High-Performance Sustainable Biomaterials, *ACS Nano*, 2025, **19**, 9801–9813.

99 L. Chen, S. Wang, S. Wang, C. Chen, L. Qi, L. Yu, Z. Lu, J. Huang, J. Chen, Z. Wang, X.-W. Shi, Z. Song, H. Liu and C. Chen, Scalable Production of Biodegradable, Recyclable, Sustainable Cellulose–Mineral Foams via Coordination Interaction Assisted Ambient Drying, *ACS Nano*, 2022, **16**, 16414–16425.

100 C. Lei, Y. Wei, Y. Qian, Q. Wang, P. Zhu, G. Qiu and G. Chen, Large-Scale Manufacture of Recyclable Bioplastics from Renewable Cellulosic Biomass Derived from Softwood Kraft Pulp, *ACS Appl. Polym. Mater.*, 2022, **4**, 1334–1343.

101 N. Yan and X. Chen, Sustainability: don't waste seafood waste, *Nature*, 2015, **524**, 155–157.

102 X. Ji, J. Kou, G. Gözaydın and X. Chen, Boosting 3-acetamido-5-acetylfuran production from N-acetyl-D-glucosamine in γ-valerolactone by a dissolution-dehydration effect, *Appl. Catal., B*, 2024, **342**, 123379.

103 X. Ma, G. Gözaydın, H. Yang, W. Ning, X. Han, N. Y. Poon, H. Liang, N. Yan and K. Zhou, Upcycling chitin-containing waste into organonitrogen chemicals via an integrated process, *Proc. Natl. Acad. Sci. U. S. A.*, 2020, **117**, 7719–7728.

104 H. Yang, G. Gözaydın, R. R. Nasaruddin, J. R. G. Har, X. Chen, X. Wang and N. Yan, Toward the Shell Biorefinery: Processing Crustacean Shell Waste Using Hot Water and Carbonic Acid, *ACS Sustain. Chem. Eng.*, 2019, **7**, 5532–5542.

105 X. Ji, Y. Lu and X. Chen, Catalytic conversion of chitin biomass into key platform chemicals, *Chem. Commun.*, 2025, **61**, 1303–1321.

106 J. Cheng, A. Armugam, Y. Yang, F. Jin, Y. Zhang and N. Yan, One-Pot Chitin Conversion to High-Activity Antifungal N,N-Dimethyl Chitosan Oligosaccharides, *ChemSusChem*, 2023, **16**, e202300591.

107 J. Dai, G. Gözaydın, C. Hu and N. Yan, Catalytic Conversion of Chitosan to Glucosaminic Acid by Tandem Hydrolysis and Oxidation, *ACS Sustain. Chem. Eng.*, 2019, **7**, 12399–12407.

108 R. Sole, C. Buranello, A. Di Michele and V. Beghetto, Boosting physical-mechanical properties of adipic acid/chitosan films by DMTMM cross-linking, *Int. J. Biol. Macromol.*, 2022, **209**, 2009–2019.

109 P. Chumpon, P. M. N., D. W. Lee, K. Soodpakdee and J.-I. Song, Sustainable chitosan bio-resin composites reinforced with flax fibers for high-performance food packaging, *Int. J. Biol. Macromol.*, 2025, **309**, 142990.

110 Y. Zhou, Y. He, X. Lin, Y. Feng and M. Liu, Sustainable, High-Performance, and Biodegradable Plastics Made from Chitin, *ACS Appl. Mater. Interfaces*, 2022, **14**, 46980–46993.

111 L. Lin, Z. Su, H. Zhang, G. Zhou, H. Zhou, J. Ren, X. Wang, C. Liu and X. Wang, Thermo-processable chitosan-based plastic substitute with self-adaptiveness and closed-loop recyclability, *Carbohydr. Polym.*, 2022, **291**, 119479.

112 X. Zhang, L. Lin, H. Zhou, G. Zhou and X. Wang, All-natural chitosan-based polyimine vitrimer with multiple advantages: a novel strategy to solve nondegradable plastic waste pollution, *J. Hazard. Mater.*, 2024, **465**, 133030.

113 S. Jin, L. Xiong, Y. Yu, J. Xing, J. Li, J. Han, C. Mei, K. Li and H. Xiao, Structural design of a hyperbranched chitosan-based bioplastic with excellent strength, antibacterial, and UV shielding performance, *Chem. Eng. J.*, 2023, **471**, 144687.

114 X. Ma, X. Lin, C. Chang and B. Duan, Chitinous Bioplastic Enabled by Noncovalent Assembly, *ACS Nano*, 2024, **18**, 8906–8918.

115 X. Hu, X. Ma, C. Chang and B. Duan, Alkali lignin mediated chitin self-assembly for constructing a fully naturally resourced bioplastic, *Chem. Eng. J.*, 2025, **503**, 158173.

116 Y. Ma, H. Liu, L. Zhou, Y. Yu and J. Gong, Tough, Degradable Bioplastics Enabling by Noncovalent Assembly of Polysaccharides and Inorganic Ionic Oligomers, *ACS Appl. Polym. Mater.*, 2025, **7**, 1896–1908.

117 S. Bi, S. Luo, Y. Zhang, H. Fu, Z. Lin, Y. Deng, F. Wei, J. Xin, X. Shi and B. Lin, Dynamically Electrostatic Regulated Intermolecular Cross-Linking for Preparing High-Tough Recyclable Disposable Bioplastic with Rapid Sterilization, *ACS Sustain. Chem. Eng.*, 2024, **12**, 11550–11560.

118 N. Wu, Q. Lin, F. Shao, L. Chen, H. Zhang, K. Chen, J. Wu, G. Wang, H. Wang and Q. Yang, Insect cuticle-inspired design of sustainably sourced composite bioplastics with enhanced strength, toughness and stretch-strengthening behavior, *Carbohydr. Polym.*, 2024, **333**, 121970.

119 M. Kashif, M. A. Sabri, M. Aresta, A. Dibenedetto and F. Dumeignil, Sustainable synergy: unleashing the potential of biomass in integrated biorefineries, *Sustain. Energy Fuels*, 2025, **9**, 338–400.

120 M. Saleknezhad, M. Madadi, S. Al Azad and V. K. Gupta, Harnessing the potential of biphasic solvent systems in

lignocellulosic biomass fractionation through computational insights, *Green Chem.*, 2025, **27**, 4094–4127.

121 Z. Zhong, B. M. T. Gorish, Y. Bai, W. I. Y. Abdelmula, W. Dang and D. Zhu, Predicting lignin removal efficiency in deep eutectic solvent-based biomass fractionation: an explainable machine learning approach, *Green Chem.*, 2025, **27**, 11036–11054.

122 B. Segers, P. Nimmegeers, M. Spiller, G. Tofani, E. Jasiukaitytė-Grojzdek, E. Dace, T. Kikas, J. M. Marchetti, M. Rajić, G. Yildiz and P. Billen, Lignocellulosic biomass valorisation: a review of feedstocks, processes and potential value chains and their implications for the decision-making process, *RSC Sustain.*, 2024, **2**, 3730–3749.

123 T. Wu, S. Sugiarto, U. A. Weerasinghe, R. Yang, L. Jia, P. Y. M. Yew, D. Zhang, T. Sathasivam, P. L. Chee, X. Fei and D. Kai, Deep eutectic solvent-assisted 3D printing of lignocellulosic biomass, *Chem. Eng. J.*, 2025, **523**, 168671.

124 X. Yang, J. Sun, Z. Yin, X. Lv, Y. Liu, Z. Hou, D. Sui and Q. Xia, Preparation of tough, antioxidant and antibacterial bioplastic for sustainable packaging through an in situ phenolization strategy, *Green Chem.*, 2025, **27**, 1529–1539.

125 X. Shi, P. Chen, K. Han, C. Li, R. Zhang, J. Luo and Z. L. Wang, A strong, biodegradable, and recyclable all-lignocellulose fabricated triboelectric nanogenerator for self-powered disposable medical monitoring, *J. Mater. Chem. A*, 2023, **11**, 11730–11739.

126 T. Han, S. Zhang and B. Ju, Mechanochemistry, deep eutectic solvents and dynamic cross-linking strategies are combined to achieve the one-step preparation of stalk plastics, *React. Funct. Polym.*, 2025, **216**, 106400.

127 C. Li, Q. Dai, J. Jiang, W. Wu, D. Y. Zhu and X. Qiu, Complete conversion of eucalyptus wood to dynamic covalent networks: an in-situ plasticising strategy, *Chem. Eng. J.*, 2024, **499**, 156566.

128 D. Xie, S. Yang, C. Zhang, R. Zhang, A. Yang, Y. Zhu, Q. Xia, H. Wang, S. Song and Y. Song, A robust, recyclable, and biodegradable whole corn bioplastic enabled by dissolution-regeneration strategy, *Chem. Eng. J.*, 2024, **501**, 157571.

129 H. Zhou, Y. Mao, Y. Zheng, T. Liu, Y. Yang, C. Si, L. Wang and L. Dai, Complete conversion of xylose-extracted corncob residues to bioplastic in a green and low carbon footprint way, *Chem. Eng. J.*, 2023, **471**, 144572.

130 Q. Xia, C. Chen, Y. Yao, J. Li, S. He, Y. Zhou, T. Li, X. Pan, Y. Yao and L. Hu, A strong, biodegradable and recyclable lignocellulosic bioplastic, *Nat. Sustain.*, 2021, **4**, 627–635.